Spring 2019

Understanding the Strain Localization and Progressive Damage Growth at the Free-Edge of Composite Laminates Using Digital Image Correlation

Addis Tessema

UNDERSTANDING THE STRAIN LOCALIZATION AND PROGRESSIVE DAMAGE GROWTH AT THE FREE-EDGE OF COMPOSITE LAMINATES USING DIGITAL IMAGE CORRELATION

by

Addis Tessema

Bachelor of Science,
Addis Ababa University, 2009

Master of Science,
Addis Ababa University, 2012

Submitted in Partial Fulfillment of the Requirements

For the Degree of Doctor of Philosophy in

Mechanical Engineering

College of Engineering and Computing

University of South Carolina

2019

Accepted by:

Addis Kidane, Major Professor

Micheal Sutton, Committee Member

Xiaomin Deng, Committee Member

Paul Ziehl, Committee Member

Cheryl L. Addy, Vice Provost and Dean of the Graduate School

ACKNOWLEDGEMENTS

First of all, I would like to start off by thanking the almighty God for blessing me to have the strength and patience to go through all the tough path and accomplish this work. Following, during my stay at University of South Carolina I have had the opportunity to work with many wonderful people, and their insightful advice, mentoring, help and kindness have made my work both possible and enjoyable. I would like to take this opportunity to thank each of them. I would like to offer my utmost gratitude to the professors who have principally advised me along the way, Professor Addis Kidane, certainly is owed a large debt of gratitude. He was there all the time to encourage, support, give aspiration and determined to lift my spirit whenever it is needed. He has provided me extensive personal and professional guidance and taught me a great deal about both scientific research and life in general.

It is unthinkable to plan and perform experimental works using DIC without the consult of Professor Sutton. As my teacher and mentor, he has taught me more than I could ever give him credit for. He has shown me, by his example, what a good scientist and person should be. So, I would like to take the opportunity to show my gratefulness and thank him for being in my committee. Further, I would like to thank the two remaining members of my committee, Professor Xiaomin Deng and Professor Paul Ziehl for generously offered to serve on my committee despite their busy schedule.

I also would like to express my sincere acknowledgement to my group mates at DBMML, Suraj Ravindran, Behrad Koobhor, Abigail Wohlford, Ali Fahem, Nicholas Myers, Ronak Patel and others, for their support and helpful commentaries on my research works. Here special acknowledgment for Suraj, who has been a kind, supportive, encouraging and fun friend, during my stay I have seen that it is so rare to find such generous and good-hearted colleague like Suraj. Furthermore, I want to thank profusely the Technical staffs of ME department, David Westbury, Dan Wilhelm and Bill Bradley who had given an extended hand on the technical issues I faced during my PhD stay. Further, it is my pleasure to pass my deep gratitude to Lalitha Ravi, Renee Jenkins and Misty O'Donnell for their continuous support by facilitating the office works I requested.

At last, I am grateful to my Family and Friends in Columbia, Washington DC and back in Ethiopian. As anybody who has traveled the path knows that graduate school is filled with highs and lows, and I would never have made it through some of the worst times if not for the semester breaks I spent with them to help me through the despair.

ABSTRACT

Understanding the mechanics of Fiber Reinforced Composites (FRC) that guide the design and optimization of laminate structures, have attracted numerous researchers. For the last five decades, various analytical and numerical models have been developed to understand the damage and failure mechanisms in FRC. For long, Classical laminate plate theory (CLPT) has majorly been used as a theoretical guide in the design of composite structures. The CLPT framework is developed based on the consideration of an infinitesimal wide plate that depicts a planar stress condition. Thus, as it considers only the planar stresses, the out of plane interlaminar stresses are absent from the CLPT formulation. However, for a laminate with finite width or geometrical discontinuity a complex stress condition (which includes interlaminar stresses) is expected on the free surface of the discontinuities. In such, researcher has developed models that considered a three-dimensional stress condition, and these models have revealed the great relevance of understanding the stress condition at the free-edge on the design and failure prediction of composite structures. Nevertheless, there is still a need for further experimental investigations on the free-edge stress/strains localization and their association with the damage initiated at the free-edge.

In this study a noble experimental technique is developed and applied to study the strain localization at free-edge of composite laminate under a monotonic tensile load. The technique is used to evaluate the local strain variation across the layers of the laminate

free-edge along with the applied uni-axial tensile load. The developed experimental technique has incorporated high magnification optical system for digital image correlation (DIC) in which the full field displacement and strain are measured in-situ at micro-scale. Further, based on the DIC results, the initiation and growth of cracks from the free-edge can be captured, thus, the influence of the strain localization on the formation of damage can be investigated. In overall, this dissertation is grouped in to four categories to address the various issues raised regarding free-edge effect.

In the first section, a single a quasi-isotropic (±45/ 90/ 0)s laminate is considered and the strain localization and progressive damage formation at the free-edge of the laminate is investigate. In the second part, four different laminates with varying laminas stacking arrangement are fabricated, and the influence of the relative location of laminas on the interlaminar strain localization and damage formation is studied. In the third part, by taking one stacking arrangement with different fiber angle of the off-axis plies, the effect of ply's orientation on the local intra-lamina and interlaminar strain localization and damage formation is studied. In the last section, investigation is conducted to understand the explicit correlation between local damage, material residual stiffness degradation and loss in thermal conductivity of carbon fiber composite.

TABLE OF CONTENTS

LIST OF FIGURES

CHAPTER 1

INTRODUCTION

With a tremendous growth in the usage of Fiber Reinforced Composites (FRC), numerous researchers have engaged in investigating the mechanical, electrical and thermal characteristics of structures made put of composite materials. The mechanics of the laminate composites have been under study for more than six decades. The attributions from these studies have moved the understanding of composite materials way forward and opened numerous channels to make improvements in the design and optimization mechanisms. In such journey, various analytical and numerical models have been developed to describe the deformation state, analyze the stress variation and predict the damage and failure mechanisms in composite laminates. Hence, the models are developed from various size scale approach, starting from the early classical laminate plate theory (CLPT) which deals with macro-scale stress-deformation relation, meso and micro mechanics models have been applied. For this matter, Classical laminate plate theory (CLPT) is used as a major theoretical guide in the design of composite structures [1].

Based on the stress/strain obtained from the CLPT, various failure criteria have been developed and defined the failure of a laminate [2,3]. However, the CLPT model considers an infinitesimally large laminate plate, thus, it implements plane stress condition for a given laminate plate. Hence, it accounts only the plane stresses, and the out of plane interlaminar stresses are absent from the CLPT formulation. Nevertheless, in actual/real

application laminate plates have finite size and incorporated different geometrical features, such as holes, rectangular cut-outs and edges. In such conditions, the laminate will exhibit a complex stress/traction state on the free-surfaces. Hence, the stress condition near the free-edges is much complex and completely different from the one described by the CLPT. In fact, with a consideration of the boundary effect at the free-edge and by accounting the discontinuity of elastic material properties across the different plies, researchers have found that there is a 3D stress state condition acquired at free-edge [4–9]. Moreover, stress singularity is encountered at the proximity of the free-edge. The stress singularity gradually phase out as it goes away from the free-edge and this phenomenon is known as free-edge effect.

In most cases, cracks are initiated from these free-edges, and it is presumed that these complex and high intensity stresses could be the cause for the cracking. Further, the cracks will propagate in to the laminate plate gradually and weaken the material structural integrity which in turn induce degradation in the mechanical response of the laminate. Such degradation leads to a sudden failure of the whole laminate structure. Thus, clearing the dust, which covers the stress/strain localizations and understanding the evolution of damage at the free-edge are some of the fundamental issues in the composite world. Studies at various size scales are required to articulate and address these problems. For this reason, analytical models, FEM simulations and micromechanics models has been developed and implemented. Nevertheless, these models are seen to fail in representing the actual loading and failure scenarios. Therefore, experimental works are becoming compulsory to guide and verify the virtual models. Macro scale experimental works has been performed for a

while and has brought helpful findings. Moreover, in-situ small scale experimental investigation is needed to understand and elaborate the free-edge effect.

This study is aimed to perform an in-situ experimental study on the free-edge effect using digital image correlation (DIC) at meso-scale. The study intended to obtain the strain localization on the free-edges, and these localization helps to characterize the free-edge effect. In addition, the initiation and gradual growth of cracks will captured based on the full-field strain contour. The effect of damage emergence on the mechanical response of the laminate will be investigated.

1.1 BACKGROUND

1.1.1 Free-Edge Stress/Strain Localization

Most of laminate structures are designed to have fibers aligned with the anticipated major loading directions. As well, there are plies whose fibers are off-axis from the major loading directions; such plies are required to provide shear and transverse reinforcements. For this matter, multi-directional (MD) laminates have been successful choice to account outstanding properties in the different axes of the material structure. In a material system with MD laminates, stresses are aroused by the sudden change in the elastic property between the adjacent layers at the free-edge of the laminate. However, due to the complexity of the boundary conditions and continuity of force and displacement functions between the layers, and it is challenging to find an exact solution for the stress/strain fields mathematically. Thus, there has been a significant effort to find approximate solutions which can satisfy the boundary and continuity conditions. Various efforts have been applied to evaluate the stress/strain fields at the free-edge induces from geometrical

discontinuities [4,4,7,10–13]. From earlier analytical formulations, it was found that there is stress singularity at the free-edge of a laminate. However, these stress fields are seen to last only for a short length (~nearly length equal to the thickness of the laminate) in the width of the laminate, and it decayed gradually as it goes away from the free-edge.

A vast number of studies have put forth enormous efforts to find accurate closed-form solutions. Most of the works have followed similar approaches, it started by providing an initial displacement or stress function and followed by fulfilling the boundary and continuity conditions by adjusting the parameters in the strain/stress functions. Parts of these works are made based on the consideration of equivalent single-layer theories and apply a generic displacement/stress function (where the whole laminate is taken as a single layer and the function is assumed to be continuous across the thickness). On the other hand, some other works have analyzed the problem from layer wise equilibrium formulations where each layer is considered and separate boundary conditions are set in between plies. Onwards, the continuity of the displacement fields at the interface of the layers is satisfied. In sum, the issues related with free-edge has been thoroughly studied over the past few decades, somehow, in most cases the problem is over constrained, and it is requires enormous effort to find an exact solution. For this matter, various analytical and numerical approaches had been applied to exploit the approximate solutions [6]. Based on the theory of elasticity, closed-form solutions are developed by using Lekhnitskii's stress potentials [5,6,9].

From the closed form solutions, it is found that there is exist a complex and high magnitude interlaminar stresses at the interface of angle plies. From analytical and semi numerical models, it is found that there are additional interlaminar axial and shear stresses

witnessed at the free edge of the laminate, beside the in-plane stresses described by the CLPT. For instance, under a uniaxial tensile loading, the laminate exhibited a complex 3D stress condition at the free edge and it is observed that damage is initiated from this region [14–17]. According to these studies, out of the interlaminar stress, the shear stress that existed on the plane of free edge is dominant [14–16,18–20]. These interlaminar shear stresses are suspected to influence the formation of damages at the free edge, particularly delamination of inter-ply or inter-sublaminate interfaces.

The magnitudes of interlaminar stresses are highly influenced by the relative arrangement of plies, particularly on the off-axis plies. For the quasi-isotropic laminate, higher interlaminar shear stress is observed at the plies interface with is high variation in the fiber orientation angles [21–23]. Distinction in mechanical properties of individual plies, such as Poisson's ratio, in plane shear modulus and transverse elastic modulus are the major contributors' for the rise of the interlaminar stresses. However, these free edge stresses are seen to rapidly die out at the location far from the free edge. The stress condition described by the CLT is observed to restore on the major regions of the laminate far from the free edge.

Besides the virtual models, few experimental works have been made to evaluate the deformation trends at the free-edge of a laminate [10,24,25]. Herakovich [25] used Moiré interferometry to measure the deformation on the free-edge of +Ɵ/-Ɵ laminates. These experimental works have made significant advance in capturing the sense how the displacement is varying across the thickness. However, there is still a need for high resolution in-situ experimental works that can show how the stress/strain vary across the different plies and provide a guideline for the approximate solutions. Further, an

experimental investigations on the association the free-edge stress/strains with the damage initiation and growth is demanding.

1.1.2 Damage Initiation and Growth

Beyond the concern of the approximate solutions, the presence of a 3D complex stress condition has led to the initiation of damage on the free-edges. Earlier microscopic based studies have shown that different forms of damages are initiated at the free-edge [8,26–30]. It is emphasized that the formation of these damages is not an instant event, rather it evolves gradually. In fact, the studies have reported that there are different forms of damage that appear in the laminate: fiber splitting, transverse/matrix cracking, fiber buckling (fiber kinking), fiber breakage and delamination are few [23,30–34]. The form of damage is influenced by the type of load applied and the relative arrangement of plies. For instance, under uniaxial tensile loading matrix cracking, delamination and fiber breaking are the most prominent. Moreover, the presence of a damage at a certain location in the laminate induces the stress perturbation over the surrounding; and this lead to the formation of further damage. Accumulation and growth of the damage brings a major influence on the service life of the laminate [30,35]. In general, the initiation and orientation of these damages are directly associated with the type and orientation of loading. Further, the ply thickness, stacking sequence, ply orientation and loading type have a substantial role in the matrix cracks origination and propagation [32,36]. All types of these damages may or may not appear simultaneously in the laminate; however, it is presumed that the emergence one type of damage may influence the formation of the other damage type.

Studies have indicated that the matrix cracks are the primary form of damage and it appear in the off-axis plies (mostly in the 90^{o}-plies).The presence of such higher quantity

of matric cracks induces a steady reduction in laminate stiffness [23,32,37–40]. On the other hand, when a delamination cracks advance over the interface of two adjacent laminates, which inhibits the transfer of load from one ply to another, the load will be sustained by few plies, consequently there is significant drop in the strength of the laminate [37,41–43]. Since, the whole damages initiation and growth are gradual processes and the plies that make up the laminate slowly withdraw from carrying the load. The plies that are left to carry the load before the total collapse of the laminate are known as the critical elements [37,44]. In most laminates, the 0^o-plies are critical elements and the final failure of the laminate occurs when the fibers in the critical element broke.

In light of this, numerous analytical and micromechanics models have been employed to assess the gradual growth of damages and their impact on the laminate [38,39,44–48].The impact of material structure change, due to existence of damages, on the laminate properties degradation under quasi-static and fatigue loadings have been the core for the studies revolving in the past decades. In earlier studies, for conventional laminates under quasi-static tension loading, the matrix/transverse cracking is the first and foremost form of damage. However, there is no predetermined location where these matrix cracks are initiated in the off-axis plies. Matrix cracks initiation suspected to appear at the locations where voids or pores are sited, as these presence of voids induce material discontinuity and low strength. Further, due to the presence of voids or pores there will be stress concentration at the vicinity; thus, these locations are vulnerable for the initiation of the first matrix cracks. For this sake, researchers have developed probabilistic models to speculate the locations where primary crack is expected to initiate; this prediction is based on the spatial variation in strength within the off-axis ply [49–51].

Matrix cracks are observed to initiate on the most off-axis plies of the laminate as a consequence of its lower stiffness of off-axis ply compared to the on-axis one. Masters and Reifsnider [36] have studied damage development in quasi-isotropic laminate under monotonic tension loading. A gradual crack development in the laminate was observed in a manner where the first matrix cracking was initiated in the 90^o plies, following other matrix cracks started to appear on the -45^o ply and $+45^o$ plies respectively. Tong [32] has conducted experimental investigation on matrix cracking of cross ply and quasi-isotropic laminate, from his study a similar trend of cracking is observed in the off-axis plies. O'Brien [52] has made a study on the damage evolution occurred in a cross ply and quasi-isotropic laminates. He observed that the cracks in the 90^o ply has started around 0.4% of the global strain and propagated through the laminate width, nevertheless the cracks initiated from the 45^o plies seen not to propagate further.

When delamination is initiated from a matrix crack tip, it starts to grow gradually, in parallel the stress carried by the damaged plies slowly decays. As the delamination advances the transversely cracked ply peeled off from the neighboring plies and the damaged plies are isolated from the undamaged ply. This gradual development of damage and degradation of the laminate mechanical property is described by a very well know ply discount theory [35]. Afterwards, the applied loads are sustained by the on-axis plies only (also known as critical elements), by the time when the applied stress reached the fiber ultimate stress it suddenly ruptures and brings the final failure of the laminate.

A notable change in laminate properties is recorded in the damaged laminates. Properties such as the stiffness, strength, electrical emissivity, mechanical impedance and thermal diffusivity, are shown to degrade with the damage quantity and size in the laminate.

Particularly attention was given for the degradation of modulus (axial, transverse and shear), which are experienced to decrease gradually with the different types of damages in the laminate [33,47]. In general, other mechanical properties like strength and Poisson's ratio are evidenced to degrade with the damage development. The reduction in strength is gradual with the damage growth which started from matrix cracking and followed by delamination and the final fiber breakage of the critical element [32,35,36]. As well, the Poisson's ratio is also observed to decrease at a higher rate as the matrix cracking progressed [32,36].

Different models have been developed to simulate and elaborate the mechanics behind the initiation and development of cracks, further it has been implemented to investigate the influence of damages on the mechanical properties degradation. To list some, variational method is among the well-known and it is used to describe the stress distribution around the cracks. The perturbation stress due to the presence damage on the off-axis plies are estimated from the variational analysis. Based on the evaluated perturbation stress, the critical energy release rate of the laminate is determined [50,53,54] which further applied to predict initiation damage and process of failures. Furthermore, by iteratively updating the perturbation stress at the vicinity of the crack tip as the matrix crack progress, the gradual growth of the damage/crack path is traced. Similarly, by interactively incorporating the newly formed cracks and its interaction with prior cracks (which are close by each other), is simulated. The degradation in modulus of elasticity is evaluated at various stages of damages using continuous damage mechanics (CDM) model in combined with the variational mechanics [53,54], which helped to interlink the local damages with the global laminate properties.

On the other side, synergetic approach that combines two or more analytical models with consideration of the far field load and boundary conditions, has been applied to predict the damage gradual growth. Talerja and his colleagues have developed a synergy between continuum damage mechanics (CDM) and micromechanics models [55–57], and the degradation of mechanical properties in relative to crack density has been evaluated. Moreover, by employing shear lag method, ply constitutive equations and laminate equilibrium formulations, the local stress distribution around the crack is determined in accordance with the matrix crack density and the delamination length [58,59]. It is noticed that synergetic models are more realistic in representing the actual loading constraint and boundary conditions, and appreciable prediction of the stiffness degradation along with the matrix crack density and delamination is evaluated.

1.1.3 Experimental Technique (Digital Image Correlation (DIC))

As described earlier, various experimental techniques have been applied to investigate the gradual development of damages despite the difficulty and shortage of adequate technology. In early experimental studies, the crack growth characteristics have been investigated using optical microscopic observation. The gradual growth of damages in laminates which are subjected to both static and fatigue loadings, were set under optical microscopy after a certain amount of mechanical loading [32,60–62] in order to perform visual inspection. Researchers have applied X-ray tomography to capture the damage growth (to have 3D view) at different loading stages while the load is applied in stepwise form [63,64]. However, in all cases the specimen was unloaded and taken out for microscopic observation and this makes it difficult to clearly explain how the loading and damage are interacting in the actual case.

Recently, it became familiar and convenient to use Digital Image Correlation (DIC) to capture the full-field deformation and strain distribution over the surface at macro to micro scale [51,65–67]. Digital Image Correlation (DIC) has been serving the experimental world as a non-contact deformation technique for the last few years. It was found advantageous since it helps to capture the full-field strain contour over a given surface (that could be flat or intricate), any kind of loading condition and at various size scales. In DIC, the deformation and strain of a given surface on the body is assessed by tracking the motion of artificially made speckles or the surface texture of the surface. The collective orientation of speckles is used to recognize a specific location, by acquiring raw digital images of deforming speckled surface and using numerical computation to correlate the images, the relative motion the speckles is evaluated. From the displacement functions the full-field strain is exploited. DIC can be used for different size scale range (micro to macro). Particularly, in the DBMML lab at the University of South Carolina, DIC has been used at micro scale to perform meso-scale studies that correlate the microstructure of the material with the local deformation [30,68–70]. Imaging devices are the main components of the system, depending on the size of the body, resolution of measurement and the experimental setup: thus, imaging devices such as CCD cameras, optical microscope, scanning electron microscopes (SEM) and X-ray are implemented to acquire images.

Using high magnification optical system integrated with DIC, the full-field strain of micro scale gauge area can be captured. This is found to be helpful for meso-scale studies that are focusing on formulating a correlation between the microstructural scale deformation and macro scale failure of a material [66,70]. The technique has incorporated

a camera system that captures consecutive images of the deforming body/surface and uses the images to calculate the deformation and strain.

Taking the benefit of DIC able to give both the full-field strain and the actual speckled surface images of deforming or fracturing body, it is favorable to analyze the strain distribution across the different plies, capture damage initiation and growth, quantify and perform visual analysis, and characterize the effect of damage on its surrounding environment for composite laminate. Further it is easier to compare the macro (far-field) level material degradation with micro (local) level damage formation.

In summing up, to the best of our knowledge, there is no in-situ experimental work which shows the actual the strain/stress distribution and damage formation at the laminates free edge. With the emergence of Digital image correlation (DIC), which simplified the effort to obtain the full-field strain distribution over a certain region of interest, the demand of obtaining the gradual deformation of any structure can be achieved [71].

1.2 STATEMENT OF THE PROBLEM

This study mainly focuses on capturing and understanding the characteristics of the strain/stress localizations appeared at the free-edge of composite laminates. To fulfill the main goal of the study, the research took strategic approach to address the bigger problem. The study has stepwise approach and detailed objectives to accomplish the bigger vision.

- The first issue to address is to evaluate the strain localization and progressive damage evolution in a general quasi-isotropic laminate using in-situ DIC technique. It is intended to capture the initiation and propagation of micro-cracks. The full-field local strain distribution of different plies in a laminate will be

evaluated, further the strain redistribution around the crack will be assessed at different levels of loading.

- The second stage is to extract the strain contour over the thickness of the laminate for different stacking sequences of a quasi-static laminate. Using the strain contour developed while the laminate is loaded gradually, the effect of stacking sequence on the strain/stress localization/distribution, damage initiation and growth will be investigated. Further, the local interlaminar strains at the interfaces will be emphasized. Later, the results from the experiment will be compared with the theories and assumptions developed in the analytical models.
- On the third stage, it is intended to investigate the strain localizations over the free-edge of a laminate subjected to tensile loading. From these strain (axial, transverse and shear) contours, the scale of the interlaminar stresses' influence around the free-edge on strain localization and damage formation will be explored. In addition, by using the strain localizations and visual inspection, the evolution of damage will be captured. Moreover, by changing the fiber angle of the off-axis plies the effect of fiber angle variation on the free-edge strain/stress will be investigated.

1.3 LIST OF REFERENCES

[1] Nettles AT. Basic Mechanics of Laminated Composite Plates. NASA Ref Pulication 1994:107.

[2] Kaddour AS, Hinton MJ, Smith PA, Li S. A comparison between the predictive capability of matrix cracking, damage and failure criteria for fibre reinforced composite laminates: Part A of the third world-wide failure exercise. J Compos Mater 2013;47:2749–79.

[3] Talreja R. Assessment of the fundamentals of failure theories for composite materials. Compos Sci Technol 2014;105:190–201.

[4] Tahani M, Nosier A. Free edge stress analysis of general cross-ply composite laminates under extension and thermal loading. Compos Struct 2003;60:91–103.

[5] Kassapoglou C, Lagace PA. An Efficient Method for the Calculation of Interlaminar Stresses in Composite Materials. J Appl Mech 1986;53:744.

[6] Mittelstedt C, Becker W. Free-Edge Effects in Composite Laminates. Appl Mech Rev 2007;60:217.

[7] Murthy P, Chamis C. Free-edge delamination: laminate width and loading condition effects. Nasa_Tm-100238 1987.

[8] Nailadi CL, Adams DF, Adams DO. An Experimental and Numerical Investigation of the Free Edge Problem in Composite Laminates. J Reinf Plast Compos 2002;21:3–39.

[9] Pagano NJ, Pipes RB. The Influence of Stacking Sequence on Laminate Strength. J Compos Mater 1971;5:50–7.

[10] Buczek MB, Czarnek R. Free edge strain concentrations in real composite laminates: experimental-theoretical correlation. J Appl Mech 1985;52:787.

[11] Mittelstedt C, Becker W. Free-Edge Effects in Composite Laminates. Appl Mech Rev 2007;60:217.

[12] Lecomte-Grosbras P, Réthoré J, Limodin N, Witz JF, Brieu M. Three-Dimensional Investigation of Free-Edge Effects in Laminate Composites Using X-ray Tomography and Digital Volume Correlation. Exp Mech 2015;55:301–11.

[13] Nosier A, Maleki M. Free-edge stresses in general composite laminates. Int J Mech Sci 2008;50:1435–47.

[14] Corporation D. Analysis of the Interlaminar Shear Edge Effect in Laminated Composites * 1971;5:255–9.

[15] Pipes RB. Composite Laminates Under Uniform Axial Extension 2016:538–48.

[16] Joo JWW, Sun CTT. A Failure Criterion for Laminates Governed by Free Edge Interlaminar Shear-Stress. J Compos Mater 1992;26:1510–22.

[17] Whitney JM, Browning CE, Division NM. Free-Edge Delamination of Tensile attributed 1972:300–3.

[18] Riccio A, Mozzillo G, Scaramuzzino F. Stacking sequence effects on fatigue intra-laminar damage progression in composite joints. Appl Compos Mater 2013;20:249–73.

[19] Mittelstedt C, Becker W. Interlaminar Stress Concentrations in Layered Structures: Part I - A Selective Literature Survey on the Free-Edge Effect since 1967. J Compos Mater 2004;38:1037–62.

[20] Pagano J, Pipes RB. The Influence of Stacking Sequence Laminate Strength 2016;5:50–7.

[21] Fenske MT, Vizzini AJ. The Inclusion of In-Plane Stresses in Delamination Criteria. J Compos Mater 2001;35:1325–42.

[22] Crocker LE, Ogin SL, Smith PA, Hill PS. Intra-laminar fracture in angle-ply laminates. Compos Part A Appl Sci Manuf 1997;28:839–46.

[23] Tessema A, Ravindran S, Kidane A. Experimental Study of Residual Plastic Strain and Damages Development in Carbon Fiber Composite. Fract. Fatigue, Fail. Damage Evol. Vol. 8, Springer; 2017, p. 31–6.

[24] Pipes RB. Moire analysis of the interlaminar shear edge effect in laminated composites. J Compos Mater 1971;5:255–9.

[25] Herakovich CT. Free edge effects in laminated composites.Failure in Comp. Vol. 4, 1989, 205-219.

[26] Berthelot J-M. Transverse cracking and delamination in cross-ply glass-fiber and carbon-fiber reinforced plastic laminates: Static and fatigue loading. Appl Mech Rev 2003;56:111–47.

[27] Mortell DJ, Tanner DA, McCarthy CT. An experimental investigation into multi-scale damage progression in laminated composites in bending. Compos Struct

2016;149:33–40.

[28] París F, Blázquez A, McCartney LN, Barroso A. Characterization and evolution of matrix and interface related damage in [0/90]S laminates under tension. Part II: Experimental evidence. Compos Sci Technol 2010;70:1176–83.

[29] Tong J, Guild FJ, Ogin SL, Smith PA. on Matrix Crack Growth in Quasi-Isotropic Laminates-I. Experimental Investigation. Compos Sci Technol Elsevier Sci Ltd 1997;57:1527–35.

[30] Tessema A, Mymers N, Patel R, Ravindran S, Kidane A. Experimental Investigation on the Correlation between Damage and Thermal Conductivity of CFRP. Proc. Am. Soc. Compos. Thirty-First Tech. Conf., 2016.

[31] Jamison RD, Schulte K, Reifsnider KL, Stinchcomb WW. Characterization and analysis of damage mechanisms in tension-tension fatigue of graphite/epoxy laminates. Eff. defects Compos. Mater., ASTM International; 1984.

[32] Tong J, Guild FJ, Ogin SL, Smith PA. On matrix crack growth in quasi-isotropic laminates—I. Experimental investigation. Compos Sci Technol 1997;57:1527–35.

[33] Berthelot J. Transverse cracking and delamination in cross-ply glass-fiber and carbon-fiber reinforced plastic laminates : Static and fatigue loading 2016:111–47.

[34] Li C, Ellyin F, Wharmby A. On matrix crack saturation in composite laminates. Compos Part B Eng 2003;34:473–80.

[35] Kenneth Reifsnider SC. Damage Tolerance and Durability of Material Systems. 2002.

[36] Masters J, Reifsnider K. An Investigation of Cumulative Damage Development in Quasi-Isotropic Graphite/Epoxy Laminates, Damage in Composite Materials. ASTM STP 1982;775:40–62.

[37] Reifsnider KL, Stinchcomb WW. A critical-element model of the residual strength and life of fatigue-loaded composite coupons. Compos. Mater. Fatigue Fract., ASTM International; 1986.

[38] Singh CV, Talreja R. A synergistic damage mechanics approach for composite

laminates with matrix cracks in multiple orientations. Mech Mater 2009;41:954–68.

[39] Varna J, Joffe R, Akshantala N V., Talreja R. Damage in composite laminates with off-axis plies. Compos Sci Technol 1999;59:2139–47.

[40] Tessema A, Zhao D, Kidane A, Kumar SK. Effect of micro-cracks on the thermal conductivity of particulate nanocomposite. Fract. Fatigue, Fail. Damage Evol. Vol. 8, Springer; 2016, p. 89–94.

[41] Samsur R, Rangari VK, Jeelani S, Zhang L, Cheng ZY. Fabrication of carbon nanotubes grown woven carbon fiber/epoxy composites and their electrical and mechanical properties. J Appl Phys 2013;113.

[42] Amrutharaj GS, Lam KY, Cotterell B. Delaminations at the free edge of a composite laminate. Compos Part B Eng 1996;27:475–83.

[43] Alton Highsmith KR. Stiffness-Reduction Mechanisms in Composite Laminates - Damage in Composite Materials: Basic Mechanisms, Accumulation, Tolerance, and Characterization. ASTM STP 1982;775:103–17.

[44] Reifsnider KL, Case SW. Damage tolerance and durability of material systems. WILEY; 2002.

[45] Crossman FW, Warren WJ. Initiation and Growth of Transverse Cracks and Edge Delamination in Composite Laminates Part 2. Experimental Correlation. J Compos Mater Suppl 1980;14:88–108.

[46] Katerelos DTG, Kashtalyan M, Soutis C, Galiotis C. Matrix cracking in polymeric composites laminates: Modelling and experiments. Compos Sci Technol 2008;68:2310–7.

[47] Maimi. P, Camanho PP, Mayugo JA, Turon A. Matrix cracking and delamination in laminated composites. Part II: Evolution of crack density and delamination. Mech Mater 2011;43:194–211.

[48] O'brien T. Analysis of Local Delamination and Their Influence on Composite Laminate Behavior. ASTM STP 1985;876:282–97.

[49] Asadi A, Raghavan J. Model for prediction of simultaneous time-dependent damage

evolution in multiple plies of multidirectional polymer composite laminates and its influence on creep. Compos Part B Eng 2015;79:359–73.

[50] Nairn J, Hu S. The initiation and growth of delamination induced by matrix microcracks in laminated composites. Int J Fract 1991;24:1–24.

[51] Liu S, Nairn JA. The Formation and Propagation of Matrix Microcracks in Cross-Ply Laminates during Static Loading 2016;ll:158–78.

[52] O'brien T. Damage in Composite Materials: Basic Mechanisms, Accumulation, Tolerance, and Characterization. ASTM STP 1982;775:140–67.

[53] Alter KW, Regal DM. NASA Contractor Report 4479. Control 2005.

[54] Nairn JA. Fracture mechanics of composites with residual stresses, traction-loaded cracks, and imperfect interfaces. Eur Struct Integr Soc 2000;27:111–21.

[55] Talreja R. A Continuum Mechanics Characterization of Damage in Composite Materials. Proc R Soc A Math Phys Eng Sci 1985;399:195–216.

[56] Varna J, Joffe R, Talreja R. A synergistic damage-mechanics analysis of transverse cracking [±Θ/90_4]s laminates. Compos Sci Technol 2001;61:657–65.

[57] Varna J, Talreja R. Integration of Macro- and MicroDamage Mechanics for the Performance Evaluation of Composite Materials. Mech Compos Mater 2012;48:1–16.

[58] Kashtalyan M, Soutis C. Analysis of local delaminations in composite laminates with angle-ply matrix cracks. Int J Solids Struct 2002;39:1515–37.

[59] Kashtalyan M, Soutis C. Stiffness and fracture analysis of laminated composites with off-axis ply matrix cracking. Compos Part A Appl Sci Manuf 2007;38:1262–9.

[60] Farge L, Ayadi Z, Varna J. Optically measured full-field displacements on the edge of a cracked composite laminate. Compos Part A Appl Sci Manuf 2008;39:1245–52.

[61] Farge L, Varna J, Ayadi Z. Damage characterization of a cross-ply carbon fiber/epoxy laminate by an optical measurement of the displacement field. Compos

Sci Technol 2010;70:94–101.

[62] Liu YM, Mitchell TE, Wadley HNG. Anisotropic damage evolution in a $0^o/90^o$ laminated ceramic-matrix composite. Acta Mater 2000;48:4841–9.

[63] Rask M, Madsen B, Sørensen BF, Fife JL, Martyniuk K, Lauridsen EM. In situ observations of microscale damage evolution in unidirectional natural fibre composites. Compos Part A Appl Sci Manuf 2012;43:1639–49.

[64] Lomov S V., Ivanov DS, Truong TC, Verpoest I, Baudry F, Vanden Bosche K, et al. Experimental methodology of study of damage initiation and development in textile composites in uniaxial tensile test. Compos Sci Technol 2008;68:2340–9.

[65] Koohbor B, Ravindran S, Kidane A. Meso-scale study of non-linear tensile response and fiber trellising mechanisms in woven composites. J Reinf Plast Compos 2016.

[66] Koohbor B, Ravindran S, Kidane A. Meso-scale strain localization and failure response of an orthotropic woven glass–fiber reinforced composite. Compos Part B Eng 2015;78:308–18.

[67] Pollock P, Yu L, Sutton MA, Guo S, Majumdar P, Gresil M. Full-field measurements for determining orthotropic elastic parameters of woven glass-epoxy composites using off-axis tensile specimens. Exp Tech 2014;38:61–71.

[68] Ravindran S, Tessema A, Kidane A. Local Deformation and Failure Mechanisms of Polymer Bonded Energetic Materials Subjected to High Strain Rate Loading. J Dyn Behav Mater 2016:1–11.

[69] Tessema A, Mitchell W, Koohbor B, Ravindra S, Kidane A, Van Tooren M. Effects of Nanoparticles on the Shear Properties of Polymer Composites. Am. Soc. Compos. Tech. Conf., 2015.

[70] Tessema A, Mitchell W, Koohbor B, Ravindran S, Kidane A, Van Tooren M. On the mechanical Response of Polymer fiber Composites reinforced with nanoparticles. Mech. Compos. Multi-functional Mater. Vol. 7, Springer; 2016, p. 125–30.

[71] Sutton MA, Orteu JJ, Schreier H. Image correlation for shape, motion and

deformation measurements: basic concepts, theory and applications. Springer Science & Business Media; 2009.

[72] Tamuzs V, Dzelzitis K, Reifsnider K. Prediction of the cyclic durability of woven composite laminates. Compos Sci Technol 2008;68:2717–21.

[73] Ravindran S, Tessema A, Kidane A. Note: Dynamic meso-scale full field surface deformation measurement of heterogeneous materials. Rev Sci Instrum 2016;87:1–4.

[74] Koohbor B, Mallon S, Kidane A, Sutton MA. A DIC-based study of in-plane mechanical response and fracture of orthotropic carbon fiber reinforced composite. Compos Part B Eng 2014;66:388–99.

[75] Wang SD, Palo L. Intiation and growth of transverse cracks and edge delamination in Composite laminates, Part-1. An energy method, J of Comp. Mat. Supplemnt, 2015;14:71–87.

[76] Greenhalgh E. Failure analysis and fractography of polymer composites. Elsevier; 2009.

[77] Bishop SM, McLaughlin KS. Thickness effect and fracture mechanism in notched carbon-fibre composites. 1979.

[78] Siulie Liu, Nairn JA. The Formation and Propagation of Matrix Microcracks in Cross-Ply Laminates during Static Loading. J Reinf Plast Compos 1992;11:158–78.

[79] O'Brien, T. Kevin, Hampton V, Chawan, Arun D., Demarco, Kevin, Blacksburg V, Paris, Isabelle, Hampton V., Influence of Specimen Preparation and Specimen Size on Composite Transverse Tensile Strength and Scatter. Hampton: 2001.

[80] Singh CV, Talreja R. Evolution of ply cracks in multidirectional composite laminates. Int J Solids Struct 2010;47:1338–49.

[81] Potter RT. The notch size effect in carbon fibre, glass fibre and kevlar reinforced plastics laminates. Farnborough, Hants GU146TD: 1981.

[82] Singh CV, Talreja R. International Journal of Solids and Structures Evolution of ply cracks in multidirectional composite laminates. Int J Solids Struct 2010;47:1338–

49.

[83] Naghipour P, Bartsch M, Chernova L, Hausmann J, Voggenreiter H. Effect of fiber angle orientation and stacking sequence on mixed mode fracture toughness of carbon fiber reinforced plastics: Numerical and experimental investigations. Mater Sci Eng A 2010;527:509–17.

[84] Portella EH, Romanzini D, Angrizani CC, Amico SC, Zattera AJ. Influence of Stacking Sequence on the Mechanical and Dynamic Mechanical Properties of Cotton/Glass Fiber Reinforced Polyester Composites. Mater Res 2016;19:542–7.

[85] Ball AJ, Young R, Cervenka A. The Effect of Stacking Sequence Upon the Mechanical Properties of Thermoplastic Composite Laminates. Dev. Sci. Technol. Compos. Mater., Dordrecht: Springer Netherlands; 1990, p. 1031–6.

[86] Tessema A, Ravindran S, Wohlford A, Kidane A. In-Situ Observation of Damage Evolution in Quasi-Isotropic CFRP Laminates. Fract. Fatigue, Fail. Damage Evol. Vol. 7, Springer; 2018, p. 67–72.

[87] Tessema A, Ravindran S, Kidane A. Gradual Damage Evolution and Propagation in Quasi-Isotropic CFRC under Quasi-Static Loading. Compos Struct 2017.

[88] Naik NK, Asmelash A, Kavala VR, Ch V. Interlaminar shear properties of polymer matrix composites : Strain rate effect. Aerosp Eng n.d.

[89] Rebière J-L, Gamby D. Strain Energy Release Rate Analyse of Matrix Micro Cracking in Composite Cross-Ply Laminates. Mater Sci Appl 2011;2:537–45.

[90] Katerelos DTG, Varna J, Galiotis C. Energy criterion for modelling damage evolution in cross-ply composite laminates. Compos Sci Technol 2008;68:2318–24.

[91] Canal LP, González C, Molina-Aldareguía JM, Segurado J, Llorca J. Application of digital image correlation at the microscale in fiber-reinforced composites. Compos Part A Appl Sci Manuf 2012;43:1630–8.

[92] Singh CV, Talreja R. Analysis of multiple off-axis ply cracks in composite laminates. Int J Solids Struct 2008;45:4574–89.

CHAPTER 2
GRADUAL DAMAGE EVOLUTION AND PROPAGATION IN QUASI-ISOTROPIC CFRC UNDER QUASI-STATIC LOADING

2.1 ABSTRACT

The gradual damage initiation and evolution in quasi-isotropic (±45, 90, 0)s carbon fiber laminate composites under a quasi-static tension loading is investigated experimentally. The full-field strains across the thickness of the laminate as a function of applied tensile load was acquired using high spatial resolution digital image correlation. The perturbation of strain during the initiation and growth of micro-cracks is evaluated, and the influence of strain redistribution over the surrounding layers is analyzed. The local failure mechanism is investigated and the influence of the local damage on the global mechanical response of the composite is explored. It was found that the failure is initiated as a matrix crack in the most off-axis plies, gradually grow to the nearby ply and eventually expands to a complete delamination. Further, it was found that the shear lagging induced between two adjacent plies has a significant effect in directing the matrix crack growth and inducing delamination.

A. Tessema, S. Ravindran and A. Kidane, Gradual Damage Evolution and Propagation in Quasi-Isotropic CFRC under Quasi-Static Loading. Compos Struct 2017. Reused here with permission of publisher.

2.2 INTRODUCTION

Fiber reinforced composites (FRC) have been observed to experience multi-scale forms of damage during service time. In many applications, the laminates are designed to have fibers aligned with the anticipated major loading directions. It is a common practice to have different plies whose fibers are off-axis from the major loading directions to provide shear and transverse reinforcement [68,69,71,72]. Though such arrangement gives a quasi-isotropic material system at large scale, local non-uniform stress distributions can rise due to the local inhomogeneous material structure of the laminate. This could eventually lead to formation of different damage modes like, transverse (matrix) cracking, longitudinal splitting, fiber-matrix debonding, lamina delamination, fiber buckling (fiber kinking) and fiber breakage [44,48,73,74]. In most cases, the initiation and orientation of these damage are directly associated with the type and direction of loading. In addition, the ply thickness, stacking sequence and ply orientation have a substantial role in crack initiation and propagation [32,36,75]. All damage modes may or may not appear simultaneously in the laminate; however, it is presumed that the presence of one type of damage may influence the formation of the other type.

The effect of damage on the residual strength and elastic properties of composites under quasi-static and fatigue loadings have been studied in the past decades. In earlier studies, for conventional laminates under quasi-static tension loading, the matrix/transverse cracking has been considered as the first and foremost form of damage. For example, Masters and Reifsnider [36] have studied damage development in quasi-isotropic laminate under monotonic tension loading. It was observed, the first matrix crack was initiated in the 90^o plies and consequently other matrix cracks had started to appear in the -45^o and

+45^{o} plies respectively. Tong [32] have conducted experiments and investigated matrix cracking in cross ply and quasi-isotropic laminates. A similar result in type and sequence of cracking is observed in the off-axis plies. O'Brien [52] has also conducted a study on damage evolution in cross ply and quasi-isotropic laminates. He observed that the cracks have initiated in the 90^{o} and 45^{o} plies. However, the cracks initiated in the 90^{o} plies have propagated through the laminate width while the cracks initiated in the 45^{o} plies remained at the edge of the laminate without further propagation across the width. Although such studies indicated that the matrix crack was usually initiated in the most off-axis plies (90^{o} and ±45^{o}), there was no predetermined location where these matrix cracks initiated. Researchers have developed probabilistic models, based on the spatial variation of strength within the off-axis ply, to speculate the locations where the primary matrix crack will initiate [49,50,76]. However, there is no experimental work showing the location and sequence of the formation of cracks.

Recently, in-situ observation of the gradual formation of damage in composite laminate has been a great interest in the community, with the aim of understanding when, where and how damage is initiated and propagated. It is becoming convenient to use Digital Image Correlation (DIC) to capture the full-field deformation and strain distribution over the surface of a material at macro to micro scale [65–67,76]. In DIC, the deformation and strain of a given surface are assessed by tracking the motion of artificially made speckles over the surface of the body. The recent work on the meso-scale deformation of woven composites by Koohbor et at [66], demonstrated the use of DIC on the local deformation measurement of composites. In this work, the DIC at micro-scale level is used to measure the local rotation and stretch of individual fiber bundles for different fiber orientations with

respect to the loading direction. Although such a study has been used to explain the reason behind the non-linear response of off-axis composites, these works are based on surface measurements and were not effective in identifying the initiation of cracks and propagation. Using full-field techniques, the interaction of different damage within the laminate and the influence of one damage on the formation of the succeeding damage modes, are needed to be clearly explained. Moreover, the change in the mechanical response of individual plies and its effect on the whole laminate response as a consequence of damage is still in need of an in-depth investigation.

The main focus of this paper is to evaluate the gradual evolution of damage in quasi-isotropic laminates, using an in-situ high magnification DIC technique, under a monotonic quasi-static tension loading. For this reason, eight plies, quasi-isotropic laminate composites were considered and the local deformation at the free edge of the thickness is investigated in-situ at different loading stages. To the best knowledge of the authors, this is the first comprehensive experimental work that focuses on identifying the local damage initiation and propagation mechanism of quasi-isotropic laminate. The initiation and propagation of micro-cracks were captured in–situ, the full-field local strain distribution of different plies in a laminate is evaluated, and the strain redistribution around the crack at different stages of loading is assessed. The physical reason behind the damage, beginning from the matrix crack to the final delamination is discussed.

2.3 SAMPLE PREPARATION

Specimen preparation begins from a roll of unidirectional carbon fiber Prepreg (TC350-1), that are obtained from Royal Tencate Corporate. Prepreg, IM-7 12K at FAW 150 GSM with a fiber/resin volume ratio of 64:36 is used. The resin system is TC350-1 by

Royal TenCate Corporate. The roll was stored at -18˚C to facilitate ease handling and minimizing the possibility of strand separation. From the roll, 150×150 mm2 square plies were cropped at fiber angles of 0^o, 45^o and 90^o degrees. Eight plies were stacked on top of each other in the desired stacking sequence (-45/+45/90/0)s. These stacked plies were placed in a high temperature plastic bag and taken to a vacuum seal hot press, where it was subjected to a pressure of 3.5 tons. The curing temperature was set to 107 ^{o}C for 1 hour, followed by rising it to a post curing temperature of 176.7 ^{o}C for 2.5 hrs at a rate of 2 ^{o}C/sec. After the completion of the curing cycle, the specimen was first cooled to a temperature 49 ˚C with forced convection and then allowed to cool slowly to a room temperature.

Rectangular test coupons with dimension of 140 mm × 22 mm were cut from the cured panel using a CNC water-jet cutting machine. The side edges of the tensile coupons were polished to remove debris, notches and any indentations formed during water-jet cutting.

The specimen edges were polished with different grits of sand papers 240, 320, 400, 600 and finally 800. The specimen edges were further polished on disk nap clothing and micron Alumina suspension solution. As shown on the work of O'Brien, polishing specimen edges had no substantial effect on the transverse strength of the laminate [77]. They also showed specimens with polished edges had greater scatter than unpolished specimens [77]. However, in this work, polishing was necessary for the DIC measurement and all specimens were polished at the same level following similar procedure.

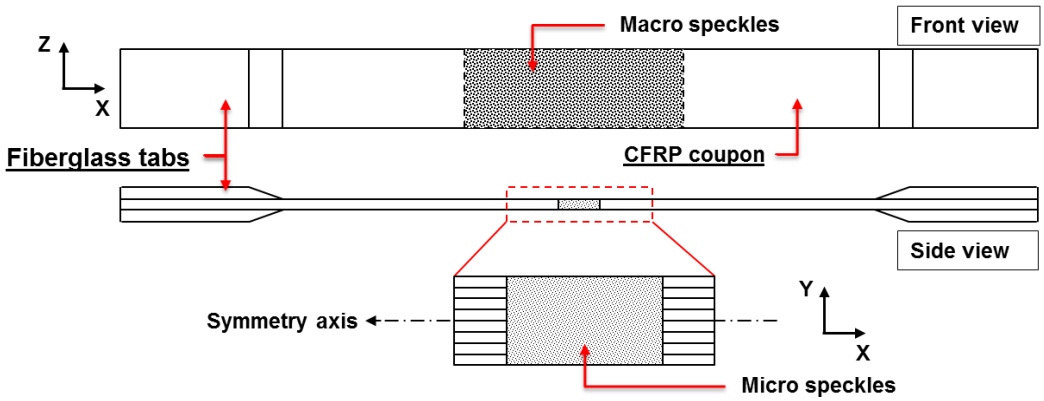

Figure 2.1: The schematic diagram of the coupon sample with macro and micro speckles

The free-edge of the laminates was inspected after polishing and prior to testing using optical microscope. Only specimens without noticeable damage were used in the study. Fiber glass tabs (40×22 mm2) were attached on the width face of the polished coupon at the gripping sides of the specimen as shown in the Figure 2.1. The fiberglass tabs used to protect the damage on the fibers due to the griping pressure during testing. In addition, the tabs facilitate a smooth stress flow and uniform stress distribution over the gauge area.

To facilitate the full field strain measurement using digital image correlation, the surface of the edge and the width of the specimen were speckled with random patterns of two different size; macro scale speckles across the width of the specimen and micro scale speckles across the thickness of the specimen. The macro-speckles were made using conventional spray paint of black speckles over a flat white paint background. On the other hand, the micro-speckles were made by blowing a black toner powder over a flat white paint background. The detail procedure for the micro-speckling technique can be obtained elsewhere [70].The micro scale speckles achieved in this work were about 5-20 μm in size, as measured by microscope with digital scale.

2.4 EXPERIMENTAL SETUP

Displacement controlled quasi-static tensile test was conducted on the coupons using a Material Testing System (MTS 810). The whole experimental setup including the DIC system is shown in the Figure 2.2. The speckled specimen was gripped between the two hydraulic grips and a monotonic uniaxial load was applied at a displacement rate of 0.05 mm/min until the specimen completely failed.

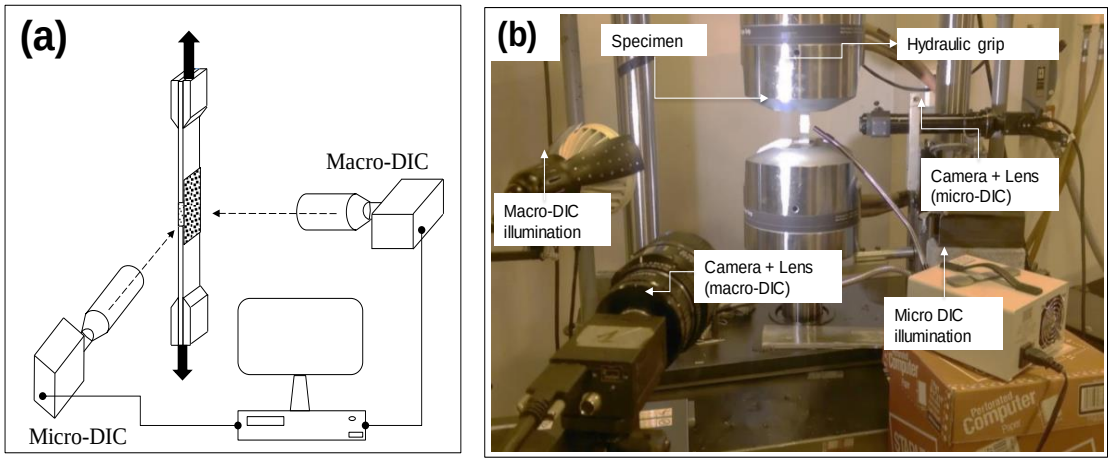

Figure 2.2: Mechanical test setup, MTS 810 testing machine with 2D-DIC (a) Schematic presentation and (b) the actual setup.

The full-field in-plane strains were measured in-situ using 2D DIC (macroscale and meso-scale) setups at the two distinct locations of the specimen. The macroscale setup consisted a 5 MPixels CCD (Grasshopper) with 60 mm Nikon lens directed on the width surface and it was used to acquire the global strain of the specimen. A light emitting diode (LED) lamp was used to illuminate over the speckled surface as shown in Figure 2. The meso-scale setup consisted a 9 MPixels CCD (Grasshopper) camera with 3X magnification Navitar lens focused at the micro-speckled region located on the edge of the specimen. The meso-scale DIC has an approximate field of view 4.15×3.32 mm2 and acquired image at a resolution of 0.9µm/pixel. During the experiment both cameras were controlled by a single

imagining software and triggered together. The images on both sides were recorded simultaneously at the rate of 2 frames per second. After concluding the experiment, the acquired images were post-processed using commercial software VIC-2D (Correlated Solution Inc.). The full-field strain analysis was performed for the macro and micro speckle images separately. The correlation analysis was performed using a subset size of 37 pixels (34μm) and step size of 5 pixels (4.5μm) for micro and subset size of 45 pixels (1mm) and step size of 5 pixels (0.12mm) for the macro region respectively. In both cases, 8 tap optimizing interpolation based on normalized squared difference criterion, with decay filter size of 15 was used.

2.5 RESULTS

2.5.1 Crack initiation and gradual growth

2.5.1.1 Stress-strain

In Figure 2.3 a typical global stress-strain curve of a quasi-isotropic laminate under a monotonic tensile loading is depicted. The global strain was obtained directly from the macro-scale DIC, whereas the stress was calculated from the force data obtained from the load cell. The stress-strain plot had shown a linear trend for the most part of the curve; however, a nonlinear feature had appeared at the final stage of failure. This non-linearity is due to the plastic deformation and emergence of micro damage in the laminate. The laminate had initial strength (S_y) of around 670 MPa and elastic modulus (E_{11}) of 53.6 GPa.

2.5.1.2 Local strain variation

It is noticeable that the stress-strain plot given above doesn't provide a detailed information about the morphological changes appeared in the material structure regarding

to the damage. However, with the help of meso-scale DIC, the gradual development of damage in the laminate as a function of the applied stresses was captured as depicted in the

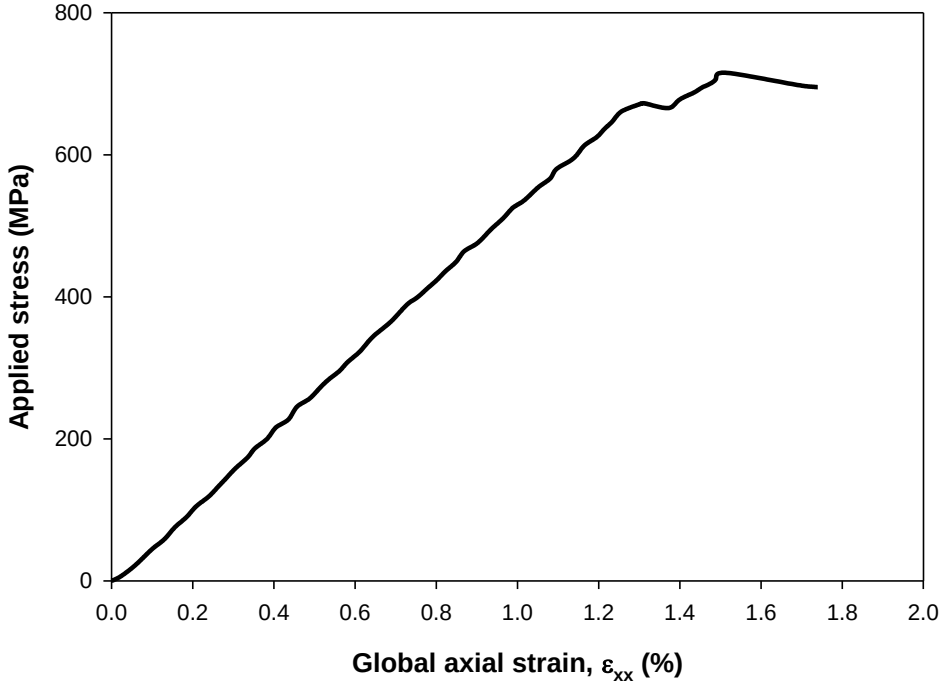

Figure 2.3: A typical global stress-strain diagram for the quasi-isotropic laminate

Figure 4.

Several local strain concentrations are observed at different locations in the 90^o plies, which later turned to be the location where matrix crack was initiated. It was also observed that the formation of multiple matrix cracks was a gradual process; it started from a small crack and developed to rows of multiple cracks as the load increases. From the local axial strain contour shown in the Figure 2.4(a), the first noticeable strain concentration occurred in the 90^o plies when the applied stress is near 204 MPa. It was presumed that the strain concentration occurs at an arbitrary location where the local strength of the laminate was compromised due to a presence of voids or pores in the materials. As the load increases around a stress of 275 MPa, another local strain concentration was sited at a different location which later turned out to be another matrix

cracking in the other 90° ply. Afterwards, numerous matrix cracks started to emerge as the load increases.

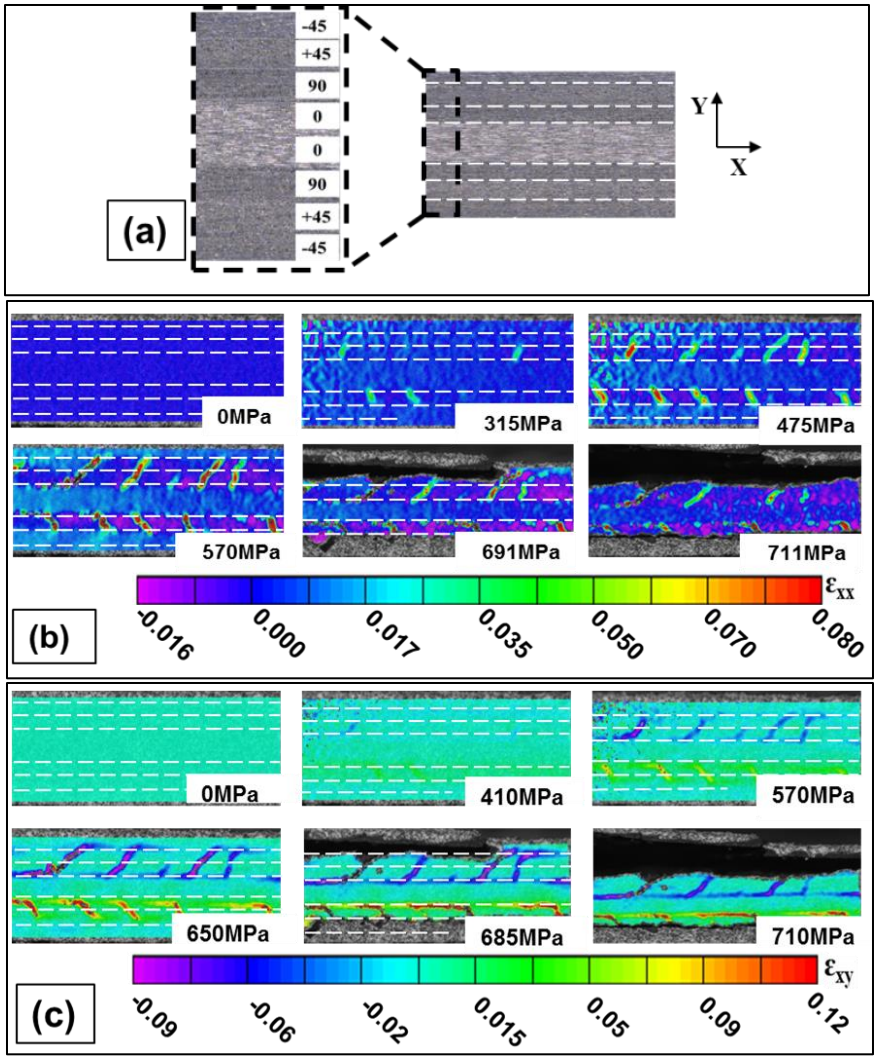

Figure 2.4: (a) Cross section with the ply arrangement (b) Gradual evolution of local axial strain contour and (c) Gradual evolution of local shear strain contour.

As shown in the Figure 2.4, the matrix cracks initiated in the 90° plies propagated in opposite directions towards the neighboring plies (0° and +45°). Once the cracks reached the interface of the neighboring plies, the next path of the cracks was highly dependent on the fiber orientation of the neighboring plies. In the case when a crack tip reached at the 90°/0° interface, the crack did not propagate across the interface. On the other hand, a crack

tip reached at the 90º/+45º interface propagated into the +45º ply. In the first case, the cracks encountered resistance from the fibers in the 0º ply that are oriented perpendicular to the crack direction. Thus, it was difficult for the cracks to propagate into the 0º ply by cutting through the fibers. For this reason, as shown in Figure 4(c), the cracks followed the fiber direction along the interface between 90º ply and 0º ply and caused delamination. On the other hand, when the cracks reached the interface of the +45º ply, the resistance provided by +45º ply was not as tough as that of the 0º ply (the fibers are not perpendicular to the crack direction). The cracks propagated further into the +45º ply by aligning its direction parallel to the fibers' orientation. However, once the crack crosses through the +45º ply, it faces another interface between the +45º/-45º plies. At this moment, the fibers in the -45º ply are perpendicular to the crack direction, which were parallel to fibers in +45º ply. As a result, the crack followed the direction along the interface of -45º/+45º plies and grow as delamination.

It is also interesting to notice the orientation of the matrix cracks in the 90º plies are not perpendicular to the loading direction as it is presumed by most of the theoretical works [21, 33]. As shown in Figure 4 (b and c), the matrix cracks are inclined to the right and they have shown a symmetrical arrangement with respect to the mid-plane. It should be noted that the 90º ply was sandwiched between the 0º and +45º plies. Once damage is occurred, the 0º ply and +45º ply deform differently (the displacement in each ply is not uniform anymore) and that can cause a shear lag. The shear stress developed as a result of shear lag between the neighboring plies could have forced the matrix crack in the 90º ply to rotate accordingly.

2.5.1.3 Discussion: Comparison with the existing models

In most analytical models [58,78], the matrix crack is assumed to be oriented transverse to the loading axis. This assumption might be taken from experimental observation that have focused on identifying damage at the microscopic level [32,33,48]. However, note must be taken that most of the microstructure observation were made ex-situ, the specimen was taken away from the loading and observation was made under an unloaded condition. During unloading, the stress in the material is eliminated and the material retrieved its original undeformed position while it holds the matrix cracks in the plies. In this case there is a great chance the matrix crack appears in vertical position, as there will be no shear stresses that cause the rotation. But our study clearly indicates the matrix crack in the 90^o plies are not perpendicular to the loading direction.

Regarding the delaminating cracks, some analytical models [33,44,50,79] considered delamination initiated at the location where the matrix crack reached the interface, which completely agree with our experimental observation. However, the assumption that delamination will propagate in both directions over the interface of the neighborhood plies, is not observed in our experiment. In our experimental work, as discussed earlier, it is seen that the delaminating crack propagates only in one direction where the shear stress is dominant. This observation is critical in fracture mechanics-based models, where analysis related to fracture energy relies on the crack length and orientation. Likewise, the effective length of the delaminating cracks has a crucial role in predicting degradation in mechanical properties and residual strength, as the interface is considered a load transferring agent between plies.

2.5.2 Matrix crack formation sequence

As shown earlier, the formation of matrix cracks in the 90^o ply is not simultaneous or spontaneous; rather it has a certain form of order. Figure 2.5 shows the local axial strain contour around the matrix crack and the plot of local axial strain of locations close to each crack as a function of applied stress. By considering the sudden change in the strain as an indication of matrix crack initiation, the sequence of the matrix cracks was determined from the plots. Note that the numbers assigned on the axial strain contour (see Figure 2.5 (a)) doesn't represent the order of matrix crack formation; was assigned based on the crack's relative locations.

According to the strain plot (Figure 2.5 (b)), the primary strain jump was observed for the crack #2 at an applied stress of 250 MPa and found in the lower 90^o ply. The second strain jump was observed for matrix crack #6, emanated from the upper 90^o ply, at an applied stress of 290 MPa. Within a small time difference, the third and fourth matrix cracks were initiated in the lower (crack #3) and the upper (crack #9) 90^o plies respectively. Furthermore, matrix cracks #1, #7, #4, #8 and #5 come as fifth, sixth, seventh, eighth and ninth order respectively. As discussed above and shown in the figure, remarkably, the trend of crack formation shown to be alternating by having one crack at a time in each 90^o ply. Nevertheless, the mechanism behind such patterned gradual crack formation is not clear.

2.5.2.1 Discussion: Comparison with the existing numerical results

Based on meso-scale models, the location of the next matrix crack was determined and usually found right in the middle of the two previously developed cracks [50,80]. To validate this observation, in our work, each 90^o ply were considered separately and the

order of matrix cracks formation was evaluated. As shown in figure 2.5(c), for the 90^o ply located below the mid-plane, the first matrix crack to appear was crack #2. Following, the second (#3) and the third (#1) matrix cracks emerged on the right side and the left side of the first crack respectively. The fourth crack (#4) followed just on the right side of the second crack and the fifth crack (#5) comes at the far right.

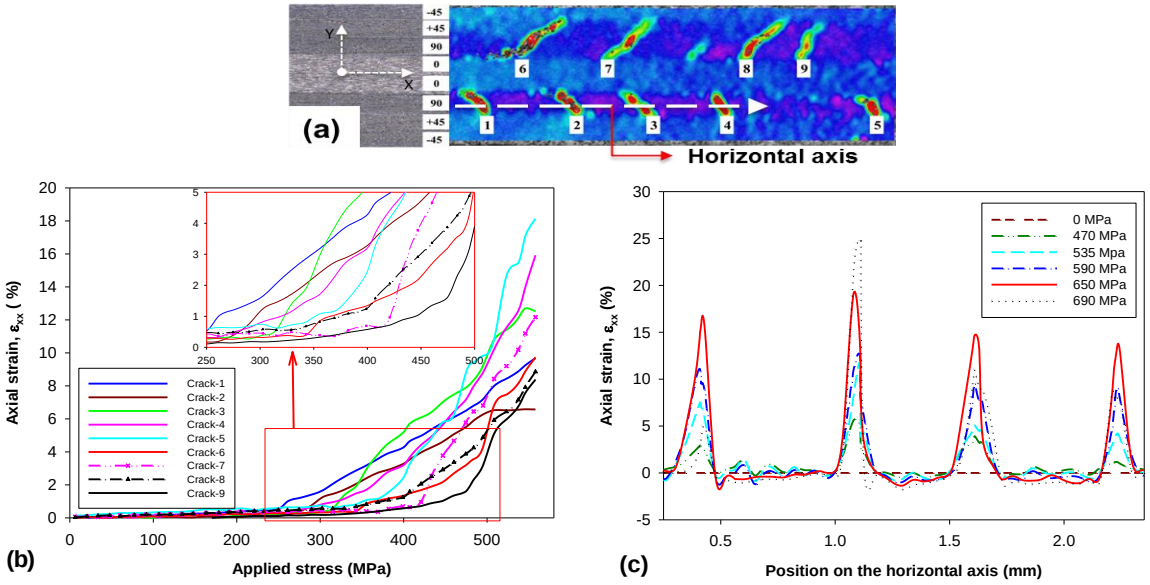

Figure 2.5: (a) Full-filled axial strain contour (b) The axial strain plot for a point near the primary matrix crack (c) The axial strain variation along the horizontal axis.

On the other hand, the order of crack formation on the 90^o ply above the mid-plane was quite different. In this ply, the first crack (#6) was initiated at the far-left side of the field of view and the second crack (#9) followed at the right far end of the window. The third crack (#7) appeared between the two cracks but closer to crack (#6). The fourth crack (#8) also formed in between cracks (#6) and (#9) but close to crack (#9). In this case, the newly emerging crack was seen forming in between two prior cracks, close to the recent formed crack. In both 90^o plies, it was a common trend to obtain a new matrix crack formed very close to the most recent prior matrix, and this trend was similar to the shear lag model presented by Reifsnider [44]. However the theoretical observation or assumption

taking the newly emerging crack appeared right in the middle of the two previously developed cracks [50,80] was not supported in our experimental work.

2.5.2.2 The influence of cracks on the local strain response

The effect of matrix cracks initiation on the local strain response also investigated by extracting the axial and transverse strain at a point between two cracks in the upper 90^o ply. As shown in Figure 2.6, the axial strain continuously increased until the applied stress reached about 400 MPa after which the strain started to decrease. During the increment region, neglecting the initial part (stress below 90 MPa), one can clearly notice a change in the slop of the axial strain at stress about 200 MPa. As previously discussed, at stress around 220 MPa, the primary crack (the crack on the left side of the point as shown in figure 2.6(a)) has initiated and started to propagate. The change in the slope could be associated with the formation of the crack. Though the slope is different, the axial strain remained increasing until it reached a stress around 400 MPa. At this stress, the second crack (on the right had of the point) has initiated causing the region at the vicinity to relax, as indicated in the plot by the decreases in the strain. Once the matrix crack reached the interface and transformed into delamination, the damaged ply becomes isolated from the applied stress, relax further and gradually releases the strain accumulated in it. As shown in the figure, the axial strain goes to negative, which could be due to the relief of thermal residual strain accumulated during curing process.

The shear strain plot also supports the above discussion. As shown in Figure 2.6(c), the shear strain, is observed to increase continuously with the applied stress until it reached maximum stress at around 500 MPa. As expected, the crack formation at 200 MPa at the left and around 400 MPa at the right of the point didn’t affected the shear strain

substantially. However, as soon as delamination is initiated around 500 MPa, the shear strain started to decrease. At the stage of complete delamination around 690 MPa, there is no interface with neighboring plies to provide the shear strength, hence the shear strain drops suddenly.

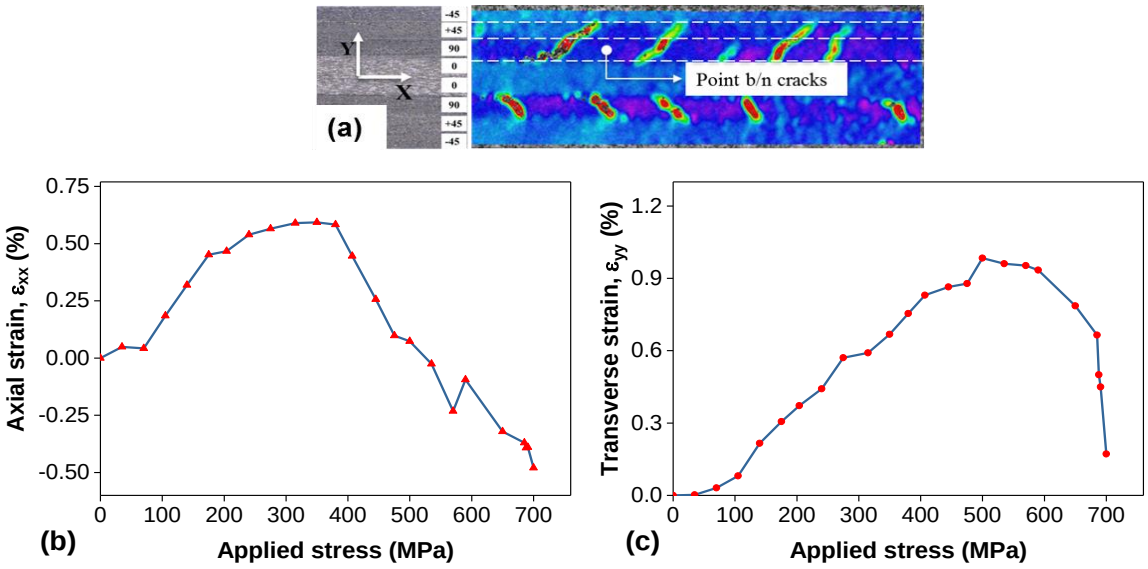

Figure 2.6: (a) The axial strain contour and (b) the axial strain and (c) the shear strain point between two cracks.

2.5.3 Interlaminar shear strain distribution across the inter-ply layers

The shear strain along the interfaces was captured by extracting the strain data over a vertical line across the laminate as shown in Figure 2.7(a). Quantifying the variation in shear strain over each ply is important in formulating the load transfer mechanism and shear lag. Typical shear strain variation along a line across the laminate is shown in Figure 2.7(b). As depicted in Figure 2.7(b), dominant shear strain localizations are encountered on four inter-ply interfaces, two above the mid-plane and two below. Beginning from the top, the first shear stain localization (#1) was observed at the interface layer between -45^o and +45^o plies, the second (#2) was between 90^o and 0^o plies, the third (#3) was at the

interface between 0^o and 90^o plies (below the mid-plane), and the fourth (#4) was at the interface between 90^o and $+45^o$ plies. The peaks in Figure 2.7(b) represent the inter-ply interfaces where a high intensity of localized shear strains occurred.

The shear strain was observed to be dominant in the inter-ply layer where the two plies have a high difference in stiffness. For instance, two of the inter-ply shear strain concentrations appeared on the two $0^o/90^o$ interfaces. It is well known that 0^o ply has the highest stiffness and 90^o ply has the lowest stiffness among the laminate plies. Thus, a difference in stiffness caused a higher gradient of displacement across the interface which induces a much stronger shear lagging, as it was explained by the shear lag theory.

Similar to the trend of the shear strain plot shown in Figure 2.6(c), the shear strain extracted for each interface layer also has shown to increase with the applied stress up to the complete delamination. As depicted in the Figure 2.7(b), though the shear strain was smoothly growing, sudden jumps in shear strain occurred for the stresses from 650 MPa to 690 MPa on the interface layer #3. Such jumps in the strain happen when the delaminating crack in the interface layer #3 approaches the vicinity of the vertical line; however, the shear strain on the other interface layers kept its proportional trend.

2.5.4 Axial and transverse strain response of individual plies

By extracting the axial and transverse strain data on points at each ply (see Figure 2.8), the response of individual plies to externally applied load was examined. At the early stage of loading, stress below around 200 MPa, a similar axial strain response was observed in all plies except the 0^o ply. A moderate and gradual increment trends were experienced in the 0^o ply. The strain trends in the 90^o ply were already discussed in the previous section.

For the -45^o and +45^o plies; the axial strain has increased proportionally up to an applied stress of 550 MPa. Afterwards the strain started to decrease sharply due to the decrease in plies strength because of delamination. Individually, it was found that the magnitude of the axial strains in the + 45^o and -45^o plies are much higher than the 0^o ply. This could be as a result of the increased damage in the off-axis plies (+45 and -45) made them more compliant compared with the 0^o ply.

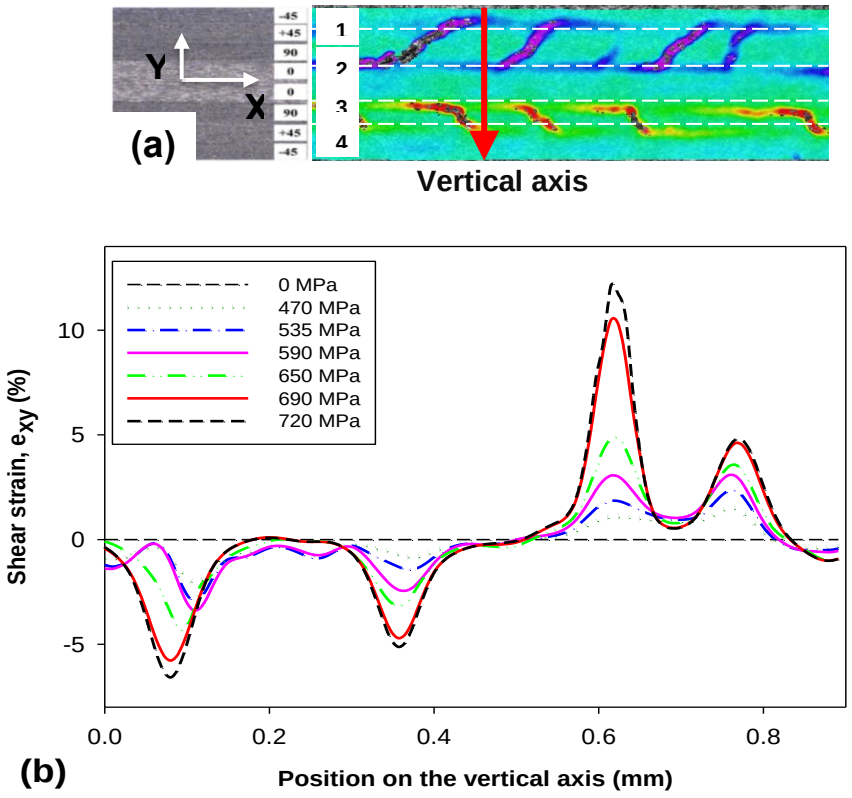

Figure 2.7: (a) The axial strain contour with a vertical axis crossing all the plies (b) The shear strain variation along the vertical axis.

A surprising result was obtained for the transverse strain curve as depicted in Figure 2.8(c). As expected, a compressive transverse strain was observed for the 0^o, +45^o and -45^o plies, however, the 90^o ply showed a tensile transverse strain. The transverse strain for 0^o ply is very small compared to the off-axis plies. This was consistent with the fact that the 0^o ply is stiffer compared to the others. It is unexpected to encounter a compressive

transverse strain for a ply subjected to tensile load. In fact, all plies except 90° ply have, shown transverse contraction due to the Poisson's effect. The contraction of the much stiffer neighboring plies (+45° and 0°) could have put the 90° ply under tension, from both sides. Since the stiffness of the 90° ply is much smaller than the neighboring plies, it could easily expand in the opposite direction. It is anticipated that the compression strain due to Poisson's effect in the 90° ply was overcome by the tension from the contraction of the neighbor ply or formations of free surfaces by the new cracks.

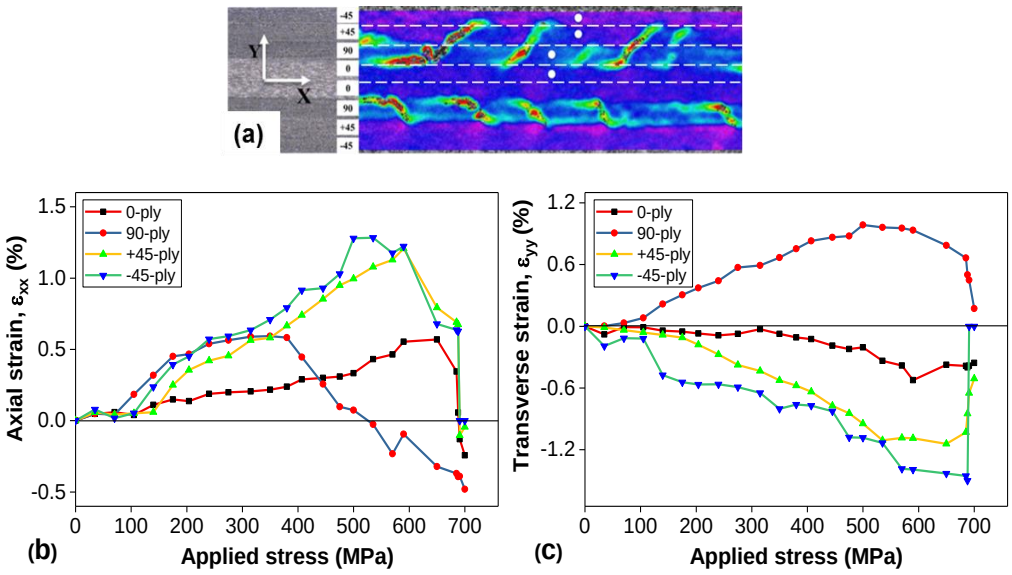

Figure 2.8: The axial strain contour with four points on each distinct ply, (b) the axial strain and (c) the transverse strain variation of the points as a function of the applied load.

2.6 SUMMARY

In this study, a monotonic quasi-static tensile test was performed on a quasi-isotropic laminate composite. A high magnification digital image correlation technique was used to capture the full-field local deformation and failure mechanisms. The findings of the study are summarized as follows:

- The gradual matrix crack initiation and progress across the laminate was captured. The matrix cracks are initiated in the most off-axis ply (90^o ply). The newly formed cracks were observed to appear next to the prior crack and the newest cracks always occur far away from the primary crack.
- Due to the difference in stiffness of the plies in the laminate, a shear lagging between the plies was observed. The direction of matrix crack is observed to be oriented towards the direction of shear stress in the neighboring plies.
- The matrix cracks initiated at 90^o ply propagates towards the 0^o and $+45^o$ plies. The matrix crack reached the 0^o interface didn't cross the interface, rather grow delaminating the $0^o/90^o$ interface.
- The matrix crack reached the -45^o interface propagates further crossing the 90^o /$+45^o$ interface. Later the crack grows delaminating in the -45^o /$+45^o$ interface.
- The presence of matrix cracks on the 90^o and $+45^o$ plies, affects their surroundings by providing free surface and releasing the strain accumulated in the ply.
- Moreover, the matrix cracks in 90^o ply further weaken the ply stiffness and resulted an expansion in a transverse direction, due to tension from the contraction of the neighboring plies.

2.7 LIST OF REFERENCES

[1] Nettles AT. Basic Mechanics of Laminated Composite Plates. NASA Ref Pulication 1994:107.

[2] Kaddour AS, Hinton MJ, Smith PA, Li S. A comparison between the predictive capability of matrix cracking, damage and failure criteria for fibre reinforced composite laminates: Part A of the third world-wide failure exercise. J Compos

Mater 2013;47:2749–79.

[3] Talreja R. Assessment of the fundamentals of failure theories for composite materials. Compos Sci Technol 2014;105:190–201.

[4] Tahani M, Nosier A. Free edge stress analysis of general cross-ply composite laminates under extension and thermal loading. Compos Struct 2003;60:91–103.

[5] Kassapoglou C, Lagace PA. An Efficient Method for the Calculation of Interlaminar Stresses in Composite Materials. J Appl Mech 1986;53:744.

[6] Mittelstedt C, Becker W. Free-Edge Effects in Composite Laminates. Appl Mech Rev 2007;60:217.

[7] Murthy P, Chamis C. Free-edge delamination: laminate width and loading condition effects. Nasa_Tm-100238 1987.

[8] Nailadi CL, Adams DF, Adams DO. An Experimental and Numerical Investigation of the Free Edge Problem in Composite Laminates. J Reinf Plast Compos 2002;21:3–39.

[9] Pagano NJ, Pipes RB. The Influence of Stacking Sequence on Laminate Strength. J Compos Mater 1971;5:50–7.

[10] Buczek MB, Czarnek R. Free edge strain concentrations in real composite laminates: experimental-theoretical correlation. J Appl Mech 1985;52:787.

[11] Mittelstedt C, Becker W. Free-Edge Effects in Composite Laminates. Appl Mech Rev 2007;60:217.

[12] Lecomte-Grosbras P, Réthoré J, Limodin N, Witz JF, Brieu M. Three-Dimensional Investigation of Free-Edge Effects in Laminate Composites Using X-ray Tomography and Digital Volume Correlation. Exp Mech 2015;55:301–11.

[13] Nosier A, Maleki M. Free-edge stresses in general composite laminates. Int J Mech Sci 2008;50:1435–47.

[14] Corporation D. Analysis of the Interlaminar Shear Edge Effect in Laminated Composites * 1971;5:255–9.

[15] Pipes RB. Composite Laminates Under Uniform Axial Extension 2016:538–48.

[16] Joo JWW, Sun CTT. A Failure Criterion for Laminates Governed by Free Edge Interlaminar Shear-Stress. J Compos Mater 1992;26:1510–22.

[17] Whitney JM, Browning CE, Division NM. Free-Edge Delamination of Tensile attributed 1972:300–3.

[18] Riccio A, Mozzillo G, Scaramuzzino F. Stacking sequence effects on fatigue intra-laminar damage progression in composite joints. Appl Compos Mater 2013;20:249–73.

[19] Mittelstedt C, Becker W. Interlaminar Stress Concentrations in Layered Structures: Part I - A Selective Literature Survey on the Free-Edge Effect since 1967. J Compos Mater 2004;38:1037–62.

[20] Pagano J, Pipes RB. The Influence of Stacking Sequence Laminate Strength 2016;5:50–7.

[21] Fenske MT, Vizzini AJ. The Inclusion of In-Plane Stresses in Delamination Criteria. J Compos Mater 2001;35:1325–42.

[22] Crocker LE, Ogin SL, Smith PA, Hill PS. Intra-laminar fracture in angle-ply laminates. Compos Part A Appl Sci Manuf 1997;28:839–46.

[23] Tessema A, Ravindran S, Kidane A. Experimental Study of Residual Plastic Strain and Damages Development in Carbon Fiber Composite. Fract. Fatigue, Fail. Damage Evol. Vol. 8, Springer; 2017, p. 31–6.

[24] Pipes RB. Moire analysis of the interlaminar shear edge effect in laminated composites. J Compos Mater 1971;5:255–9.

[25] Herakovich CT. Free edge effects in laminated composites.Failure in Comp. Vol. 4, 1989, 205-219.

[26] Berthelot J-M. Transverse cracking and delamination in cross-ply glass-fiber and carbon-fiber reinforced plastic laminates: Static and fatigue loading. Appl Mech Rev 2003;56:111–47.

[27] Mortell DJ, Tanner DA, McCarthy CT. An experimental investigation into multi-

scale damage progression in laminated composites in bending. Compos Struct 2016;149:33–40.

[28] París F, Blázquez A, McCartney LN, Barroso A. Characterization and evolution of matrix and interface related damage in [0/90]S laminates under tension. Part II: Experimental evidence. Compos Sci Technol 2010;70:1176–83.

[29] Tong J, Guild FJ, Ogin SL, Smith PA. on Matrix Crack Growth in Quasi-Isotropic Laminates-I. Experimental Investigation. Compos Sci Technol Elsevier Sci Ltd 1997;57:1527–35.

[30] Tessema A, Mymers N, Patel R, Ravindran S, Kidane A. Experimental Investigation on the Correlation between Damage and Thermal Conductivity of CFRP. Proc. Am. Soc. Compos. Thirty-First Tech. Conf., 2016.

[31] Jamison RD, Schulte K, Reifsnider KL, Stinchcomb WW. Characterization and analysis of damage mechanisms in tension-tension fatigue of graphite/epoxy laminates. Eff. defects Compos. Mater., ASTM International; 1984.

[32] Tong J, Guild FJ, Ogin SL, Smith PA. On matrix crack growth in quasi-isotropic laminates—I. Experimental investigation. Compos Sci Technol 1997;57:1527–35.

[33] Berthelot J. Transverse cracking and delamination in cross-ply glass-fiber and carbon-fiber reinforced plastic laminates : Static and fatigue loading 2016:111–47.

[34] Li C, Ellyin F, Wharmby A. On matrix crack saturation in composite laminates. Compos Part B Eng 2003;34:473–80.

[35] Kenneth Reifsnider SC. Damage Tolerance and Durability of Material Systems. 2002.

[36] Masters J, Reifsnider K. An Investigation of Cumulative Damage Development in Quasi-Isotropic Graphite/Epoxy Laminates, Damage in Composite Materials. ASTM STP 1982;775:40–62.

[37] Reifsnider KL, Stinchcomb WW. A critical-element model of the residual strength and life of fatigue-loaded composite coupons. Compos. Mater. Fatigue Fract., ASTM International; 1986.

[38] Singh CV, Talreja R. A synergistic damage mechanics approach for composite laminates with matrix cracks in multiple orientations. Mech Mater 2009;41:954–68.

[39] Varna J, Joffe R, Akshantala N V., Talreja R. Damage in composite laminates with off-axis plies. Compos Sci Technol 1999;59:2139–47.

[40] Tessema A, Zhao D, Kidane A, Kumar SK. Effect of micro-cracks on the thermal conductivity of particulate nanocomposite. Fract. Fatigue, Fail. Damage Evol. Vol. 8, Springer; 2016, p. 89–94.

[41] Samsur R, Rangari VK, Jeelani S, Zhang L, Cheng ZY. Fabrication of carbon nanotubes grown woven carbon fiber/epoxy composites and their electrical and mechanical properties. J Appl Phys 2013;113.

[42] Amrutharaj GS, Lam KY, Cotterell B. Delaminations at the free edge of a composite laminate. Compos Part B Eng 1996;27:475–83.

[43] Alton Highsmith KR. Stiffness-Reduction Mechanisms in Composite Laminates - Damage in Composite Materials: Basic Mechanisms, Accumulation, Tolerance, and Characterization. ASTM STP 1982;775:103–17.

[44] Reifsnider KL, Case SW. Damage tolerance and durability of material systems. WILEY; 2002.

[45] Crossman FW, Warren WJ. Initiation and Growth of Transverse Cracks and Edge Delamination in Composite Laminates Part 2. Experimental Correlation. J Compos Mater Suppl 1980;14:88–108.

[46] Katerelos DTG, Kashtalyan M, Soutis C, Galiotis C. Matrix cracking in polymeric composites laminates: Modelling and experiments. Compos Sci Technol 2008;68:2310–7.

[47] Maimi. P, Camanho PP, Mayugo JA, Turon A. Matrix cracking and delamination in laminated composites. Part II: Evolution of crack density and delamination. Mech Mater 2011;43:194–211.

[48] O'brien T. Analysis of Local Delamination and Their Influence on Composite Laminate Behavior. ASTM STP 1985;876:282–97.

[49] Asadi A, Raghavan J. Model for prediction of simultaneous time-dependent damage evolution in multiple plies of multidirectional polymer composite laminates and its influence on creep. Compos Part B Eng 2015;79:359–73.

[50] Nairn J, Hu S. The initiation and growth of delamination induced by matrix microcracks in laminated composites. Int J Fract 1991;24:1–24.

[51] Liu S, Nairn JA. The Formation and Propagation of Matrix Microcracks in Cross-Ply Laminates during Static Loading 2016;ll:158–78.

[52] O'brien T. Damage in Composite Materials: Basic Mechanisms, Accumulation, Tolerance, and Characterization. ASTM STP 1982;775:140–67.

[53] Alter KW, Regal DM. NASA Contractor Report 4479. Control 2005.

[54] Nairn JA. Fracture mechanics of composites with residual stresses, traction-loaded cracks, and imperfect interfaces. Eur Struct Integr Soc 2000;27:111–21.

[55] Talreja R. A Continuum Mechanics Characterization of Damage in Composite Materials. Proc R Soc A Math Phys Eng Sci 1985;399:195–216.

[56] Varna J, Joffe R, Talreja R. A synergistic damage-mechanics analysis of transverse cracking [±Θ/90_4]s laminates. Compos Sci Technol 2001;61:657–65.

[57] Varna J, Talreja R. Integration of Macro- and MicroDamage Mechanics for the Performance Evaluation of Composite Materials. Mech Compos Mater 2012;48:1–16.

[58] Kashtalyan M, Soutis C. Analysis of local delaminations in composite laminates with angle-ply matrix cracks. Int J Solids Struct 2002;39:1515–37.

[59] Kashtalyan M, Soutis C. Stiffness and fracture analysis of laminated composites with off-axis ply matrix cracking. Compos Part A Appl Sci Manuf 2007;38:1262–9.

[60] Farge L, Ayadi Z, Varna J. Optically measured full-field displacements on the edge of a cracked composite laminate. Compos Part A Appl Sci Manuf 2008;39:1245–52.

[61] Farge L, Varna J, Ayadi Z. Damage characterization of a cross-ply carbon

fiber/epoxy laminate by an optical measurement of the displacement field. Compos Sci Technol 2010;70:94–101.

[62] Liu YM, Mitchell TE, Wadley HNG. Anisotropic damage evolution in a $0^o/90^o$ laminated ceramic-matrix composite. Acta Mater 2000;48:4841–9.

[63] Rask M, Madsen B, Sørensen BF, Fife JL, Martyniuk K, Lauridsen EM. In situ observations of microscale damage evolution in unidirectional natural fibre composites. Compos Part A Appl Sci Manuf 2012;43:1639–49.

[64] Lomov S V., Ivanov DS, Truong TC, Verpoest I, Baudry F, Vanden Bosche K, et al. Experimental methodology of study of damage initiation and development in textile composites in uniaxial tensile test. Compos Sci Technol 2008;68:2340–9.

[65] Koohbor B, Ravindran S, Kidane A. Meso-scale study of non-linear tensile response and fiber trellising mechanisms in woven composites. J Reinf Plast Compos 2016.

[66] Koohbor B, Ravindran S, Kidane A. Meso-scale strain localization and failure response of an orthotropic woven glass–fiber reinforced composite. Compos Part B Eng 2015;78:308–18.

[67] Pollock P, Yu L, Sutton MA, Guo S, Majumdar P, Gresil M. Full-field measurements for determining orthotropic elastic parameters of woven glass-epoxy composites using off-axis tensile specimens. Exp Tech 2014;38:61–71.

[68] Ravindran S, Tessema A, Kidane A. Local Deformation and Failure Mechanisms of Polymer Bonded Energetic Materials Subjected to High Strain Rate Loading. J Dyn Behav Mater 2016:1–11.

[69] Tessema A, Mitchell W, Koohbor B, Ravindra S, Kidane A, Van Tooren M. Effects of Nanoparticles on the Shear Properties of Polymer Composites. Am. Soc. Compos. Tech. Conf., 2015.

[70] Tessema A, Mitchell W, Koohbor B, Ravindran S, Kidane A, Van Tooren M. On the mechanical Response of Polymer fiber Composites reinforced with nanoparticles. Mech. Compos. Multi-functional Mater. Vol. 7, Springer; 2016, p. 125–30.

[71] Sutton MA, Orteu JJ, Schreier H. Image correlation for shape, motion and deformation measurements: basic concepts, theory and applications. Springer Science & Business Media; 2009.

[72] Tamuzs V, Dzelzitis K, Reifsnider K. Prediction of the cyclic durability of woven composite laminates. Compos Sci Technol 2008;68:2717–21.

[73] Ravindran S, Tessema A, Kidane A. Note: Dynamic meso-scale full field surface deformation measurement of heterogeneous materials. Rev Sci Instrum 2016;87:1–4.

[74] Koohbor B, Mallon S, Kidane A, Sutton MA. A DIC-based study of in-plane mechanical response and fracture of orthotropic carbon fiber reinforced composite. Compos Part B Eng 2014;66:388–99.

[75] Wang SD, Palo L. Intiation and growth of transverse cracks and edge delamination in Composite laminates, Part-1. An energy method, J of Comp. Mat. Supplemnt, 2015;14:71–87.

[76] Greenhalgh E. Failure analysis and fractography of polymer composites. Elsevier; 2009.

[77] Bishop SM, McLaughlin KS. Thickness effect and fracture mechanism in notched carbon-fibre composites. 1979.

[78] Siulie Liu, Nairn JA. The Formation and Propagation of Matrix Microcracks in Cross-Ply Laminates during Static Loading. J Reinf Plast Compos 1992;11:158–78.

[79] O'Brien, T. Kevin, Hampton V, Chawan, Arun D., Demarco, Kevin, Blacksburg V, Paris, Isabelle, Hampton V., Influence of Specimen Preparation and Specimen Size on Composite Transverse Tensile Strength and Scatter. Hampton: 2001.

[80] Singh CV, Talreja R. Evolution of ply cracks in multidirectional composite laminates. Int J Solids Struct 2010;47:1338–49.

[81] Potter RT. The notch size effect in carbon fibre, glass fibre and kevlar reinforced plastics laminates. Farnborough, Hants GU146TD: 1981.

[82] Singh CV, Talreja R. International Journal of Solids and Structures Evolution of ply

cracks in multidirectional composite laminates. Int J Solids Struct 2010;47:1338–49.

[83] Naghipour P, Bartsch M, Chernova L, Hausmann J, Voggenreiter H. Effect of fiber angle orientation and stacking sequence on mixed mode fracture toughness of carbon fiber reinforced plastics: Numerical and experimental investigations. Mater Sci Eng A 2010;527:509–17.

[84] Portella EH, Romanzini D, Angrizani CC, Amico SC, Zattera AJ. Influence of Stacking Sequence on the Mechanical and Dynamic Mechanical Properties of Cotton/Glass Fiber Reinforced Polyester Composites. Mater Res 2016;19:542–7.

[85] Ball AJ, Young R, Cervenka A. The Effect of Stacking Sequence Upon the Mechanical Properties of Thermoplastic Composite Laminates. Dev. Sci. Technol. Compos. Mater., Dordrecht: Springer Netherlands; 1990, p. 1031–6.

[86] Tessema A, Ravindran S, Wohlford A, Kidane A. In-Situ Observation of Damage Evolution in Quasi-Isotropic CFRP Laminates. Fract. Fatigue, Fail. Damage Evol. Vol. 7, Springer; 2018, p. 67–72.

[87] Tessema A, Ravindran S, Kidane A. Gradual Damage Evolution and Propagation in Quasi-Isotropic CFRC under Quasi-Static Loading. Compos Struct 2017.

[88] Naik NK, Asmelash A, Kavala VR, Ch V. Interlaminar shear properties of polymer matrix composites : Strain rate effect. Aerosp Eng n.d.

[89] Rebière J-L, Gamby D. Strain Energy Release Rate Analyse of Matrix Micro Cracking in Composite Cross-Ply Laminates. Mater Sci Appl 2011;2:537–45.

[90] Katerelos DTG, Varna J, Galiotis C. Energy criterion for modelling damage evolution in cross-ply composite laminates. Compos Sci Technol 2008;68:2318–24.

[91] Canal LP, González C, Molina-Aldareguía JM, Segurado J, Llorca J. Application of digital image correlation at the microscale in fiber-reinforced composites. Compos Part A Appl Sci Manuf 2012;43:1630–8.

[92] Singh CV, Talreja R. Analysis of multiple off-axis ply cracks in composite laminates. Int J Solids Struct 2008;45:4574–89.

CHAPTER 3
EFFECT OF STACKING SEQUENCE ON THE INTERLAMINAR STRAIN LOCALIZATION AND DAMAGE FORMATION AT THE FREE-EDGE OF CARBON FIBER REINFORCED COMPOSITE LAMINATE

3.1 ABSTRACT

A meso-scale experimental study is performed to elucidate the local strain distribution at the free-edge of CFRC laminates. Rectangular coupon specimens are extracted from four laminates with distinct ply stacking arrangement, and the coupons are subjected to a uniaxial tensile load. The strain distribution across the thickness of the laminate at the free-edge is captured using in-situ DIC setup. The gradual formation of strain localizations and nucleation of matrix cracks are observed at various locations. Moreover, the propagation of cracks and formation of different failure modes are investigated. The significant features in the global mechanical response are correlated with the corresponding damages observed at local scale. Further, the influence of stacking arrangement on the interlaminar strain localization, the damage formation and progressive failure is discussed.

A. Tessema, S. Ravindran and A. Kidane, under preparation.

3.2 INTRODUCTION

Fiber reinforced composites (FRC) have been used for various structural applications due to its high strength to low weight characteristic. Number of studies have been conducted to investigate the mechanical, electrical and hygro-thermal characteristics of the composite laminate. Consequently, different models have been developed to understand the laminate mechanics that facilitate the design of composite structures. In fact, for the last five decades, various analytical, empirical and numerical models have been presented to emphasize the progressive damage and failure mechanisms in FRC. Beginning from the macro scale classical laminate plate theory (CLPT) to meso and micro mechanics models had derived to associate the progressive damages growth with the overall mechanical response of the laminate. The studies have strived to present an efficient way to predict an optimized arrangement of laminate plies for a specific structural application. For this matter, in most composite structures, the laminates are prepared by stacking plies at different fiber orientation to provide reliable reinforcement. For this matter, multi directional (MD) laminates have been successful in obtaining outstanding properties in the different axes of the material structure (orthotropic material property).

During their service time, these laminates are subjected to various forms of loading, such as; tensile, compressive, bending, fatigue, impact, etc. Under a given load, complex stress condition is generated due to the anisotropic property existed at a ply and a laminate level. Such stress conditions lead to the gradual formation and growth of damages within the laminates. Moreover, it is understood that the gradual emergence damage induces permanent change in the material structure, and affects its mechanical response by the degrading the mechanical properties along with the damage quantity and size [32,33,44].

Most failure criteria used in the analysis of structural laminates, are designed based on the stresses/strain obtained from CLPT. As a convenience, the classical laminate plate theory (CLPT) is commonly used to determine the mechanical response of the laminate under a given load. However, there are interesting facts about the CLPT, first, the stacking order of the plies in a given laminate have nearly zero-impact on the stiffness and strength of the laminate [18,20,81–83]. Moreover, due to the assumption made during the preliminary stage of the derivation, CLPT implicate a planar stress condition, and it is proved that such form of stress analysis fail to describe the stress state around the free-edges on the laminate [16,17,19].

The presence of geometrical features (holes, cutouts, edges) within the laminate leads to formation of free-edge/free-surface. As a result, a 3D stresses state (interlaminar axial and shear stress) appear at the vicinity of the free-edge. Such complex stress condition is developed due to the variation in elastic property for the different plies that induce non-uniformity in deformation across the different plies. This discontinuity in transverse deformation led to stress imbalance particularly at the free-edge in between the plies (variation in Poisson's ratio between the plies) [19]. As a result, a 3D stresses state (interlaminar axial and shear stress) appeared at the vicinity of the free-edge.

For this matter, studies have applied the 3D equilibrium condition and inter-ply load transfer to determine the complex stress at the free-edge [16,19,20]. Under a uniaxial tensile loading, additional interlaminar axial and shear stress are witnessed at the free edge of the laminate, beside the applied normal, transverse and in-plane shear stresses (that is stated by the CLPT). Among these stresses, the interlaminar shear stress on the plane of

free-edge is dominant [14–16,18–20] and these interlaminar stresses are suspected to causes the formation of damages at the free edge, particularly delamination between inter-ply or inter-sub laminate interface.

Evidently, various experimental studies have reported that there are different forms of damage that appear in the laminate: fiber splitting, transverse/matrix cracking, fiber buckling (fiber kinking), fiber breakage and delamination, are the well-known[23,30–34]. It is observed that the damage type occurred in the laminate is associated with the form of the load applied and plies stacking arrangement. For instance, under uniaxial tensile loading matrix cracking is the primary for of damage, which followed by delamination and fiber breaking. Whereas, different scenario is observed in the case of compression or bending load conditions. Moreover, the presence of a damage at a certain location in the laminate causes the stress perturbation over the surrounding region; and this led to further growth of the damage. Following, the growth in size and quantity of the damage bring a major degradation in the service life of the laminate [30,35].

In summing up, to date, there is no such experimental work which dealt with the influence of the plies stacking order on the strain or stress distribution/localization and damage formation at the free-edge. With the emergence of Digital image correlation (DIC), which simplified the effort to obtain the full-field strain distribution over a certain region of interest, the demand of obtaining the gradual deformation of any structure is fulfilled [71]. Therefore, by incorporating a high magnification optics system with DIC, it is possible to obtain the gradual strain localization and damage formation over a small area on the free-edge [70,84,85].

Thus, in this study, it is intended to extract the full-filled strain contour over the thickness at the free-edge of the laminate coupon for quasi-static laminates with different stacking arrangements. Using gradually changing strain contours, the effect of stacking sequence on the strain/stress distribution, damage initiation and growth across the laminate thickness are emphasized. Further, the results from the experiment are compared with the theoretical formulations and assumptions developed in the analytical models developed earlier.

3.3 MATERIALS AND METHODS

3.3.1 Material preparation and specimen geometry

In this study quasi-isotropic laminates with four laminates with distinct stacking arrangements are manufactured. The laminates are prepared using pre-impregnated (prepreg) wet fiber laminas. Unidirectional carbon fiber Prepreg (TC350-1) that obtained from Royal Tencate Corporate is selected for this study. For easy handling and improving strand separation, the prepreg roll was stored at -18˚C temperature. From the prepreg roll, 150×150 mm2 size square plies are cut out at angles of 0^o, 45^o and 90^o with respect to the fiber direction. Following, 8 plies are stacked on top of each other in the desired stacking sequences. Four different stacking sequences are chosen based on the merit of convenience in application and fulfillment of the research objective.

By rearranging the relative location of 0^o, 45^o and 90^o plies in four different sequences (-45/+45/90/0)s, (0/-45/+45/90)s , (0/-45/90/+45)s and (0/90/+45/-45)s four groups of laminate are fabricated (see Figure 3.1). The stacked plies are rolled in a special purpose plastic bag which can resist elevated temperature and pressed to a constant pressure of 0.35 MPa. The laminate has curing cycle: temperature of 107.2 ^{o}C for 1 hr, then

the pressed laminate is further subjected to a post curing temperature of 176.7 ºC for 2.5 hrs. Once the curing cycle is completed; the laminate is cooled to a temperature of 48.9 ˚C with forced convection and finally cooled slowly to a room temperature.

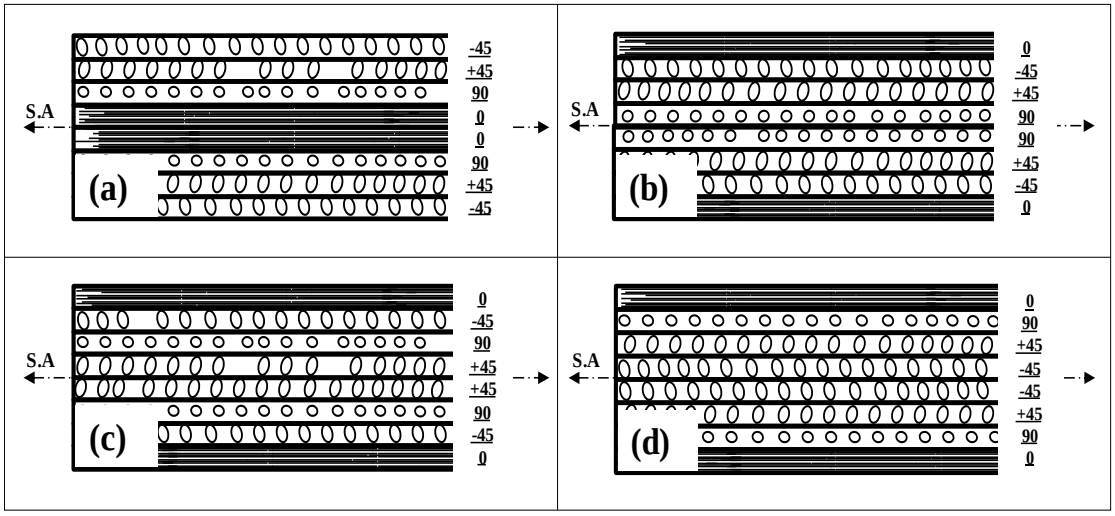

Figure 3.1: The stacking arrangement for the four groups of laminates (a) (-45/+45/90/0)s, (b) (0/-45/+45/90)s, (c) (0/-45/90/+45)$_S$ and (d) (0/90/+45/-45)$_S$.

From the cured laminate panels, 140 mm × 22 mm size rectangular coupons are cut using a CNC water-jet cutting machine. Subsequently, the side edges of the coupons are polished with different grade sandpapers (240, 320, 400, 600 and 800) to remove any kind of flaws, notches and indentations formed during water-jet cutting. As recommended by the test standard, fiberglass tabs are attached on the specimen ends using high strength epoxy glue A 40 mm×22 mm size fiberglass tabs are attached on the width face of the coupon at the two gripping ends as shown in Figure 3.2. These tabs are intended to protect the local damage on the coupon fibers by the pressure induced from the hydraulic grips. The tabs also facilitate the smooth flow of stress and presence of a uniform stress distribution over the gage area.

Since it is intended to use digital image correlation to obtain full-filled strain, black random speckles are patterned over the white background surface of the specimen where the full filled strain is acquired. In this case, two different scale speckles, macro scale and micro scale, are employed on two distinct locations of the coupon specimen. First, the macro scale speckles are made over a certain rectangular region on the outer surface (width of the specimen) by airbrushing black speckles over a flat white background paint. On the other hand, the micro scale speckles are made in a small region (1mm x 4mm) across the free-edge (thickness of the specimen) by blowing a black toner powder over a flat white paint background. Detail procedure of the micro-speckling technique can be obtained elsewhere [70].The micro scale speckles in this work are about 5-20 μm in size. The macro speckles are used to acquire the global strain of the specimen and the micro speckle are employed to obtain the local strain field across the free-edge of the laminate.

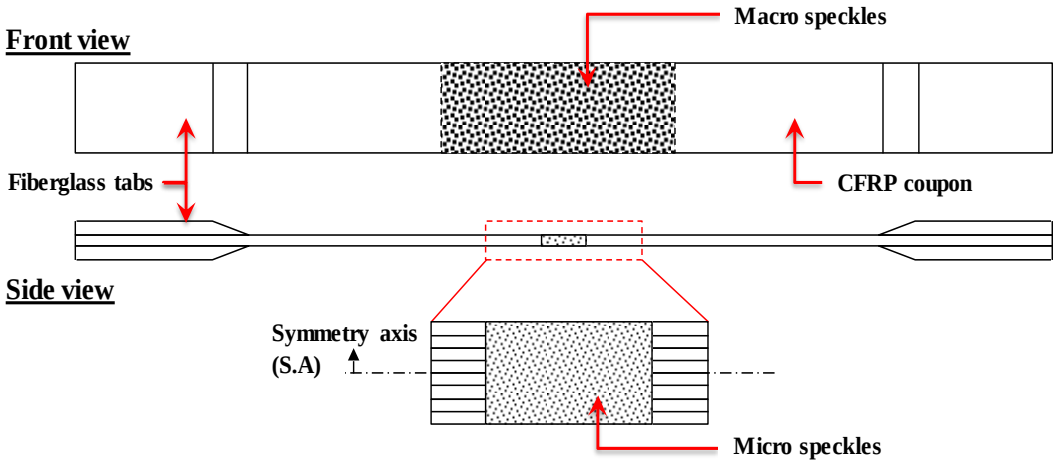

Figure 3.2: The schematic diagram of the tensile coupon sample with macro and micro speckles.

3.3.2 EXPERIMENTAL SETUP

A uniaxial tensile test under quasi-static condition is conducted using a Material Testing System (MTS 810) machine. The schematic representation and the actual image of the experimental setup including the DIC system are shown in Figure 3.3. As seen in the Figure 3.3, the specimen is kept in between the two hydraulic jaws and griped at its fiberglass tabs. A monotonic uniaxial tensile load is applied under displacement-controlled mode at a rate of 0.2 mm/min until the complete failure of the laminate.

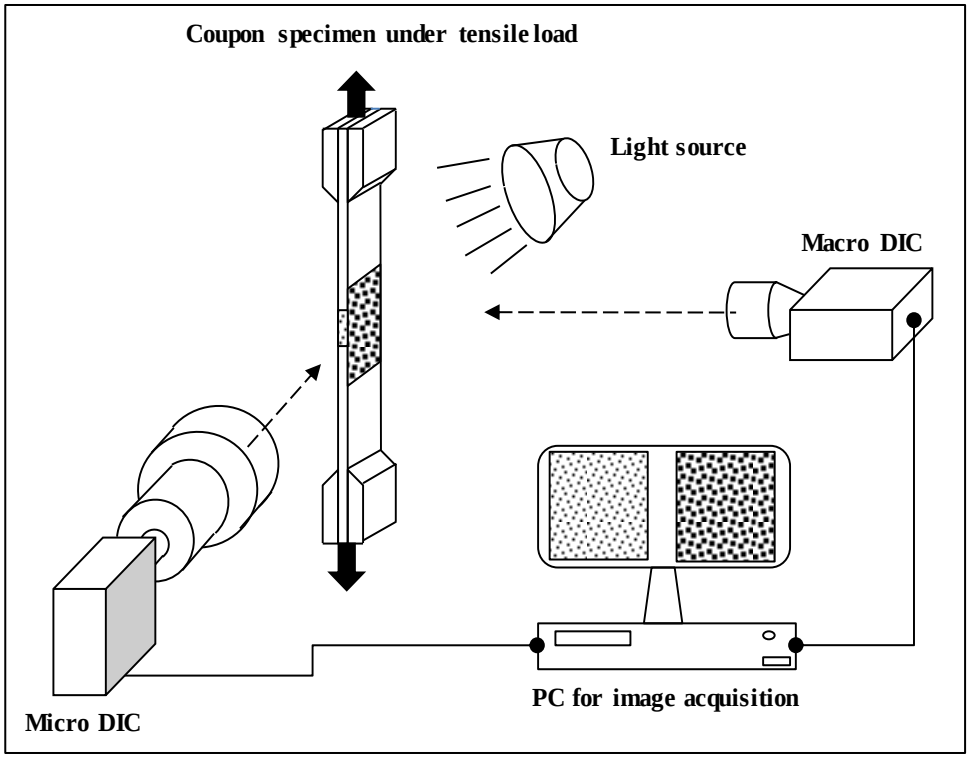

Figure 3.3: The schematic representation of the experimental setup with speckle pattern of AOI.

As shown in the Figure 3.3, two independent cameras focused on the two speckled regions, are used to capture images gradually during loading. The camera setup for the macro scale speckle consists of a 5 MPixels CCD (Grasshopper) camera with 60 mm Nikon

lens and positioned perpendicular to the width face of the coupon. A light emitting diode (LED) lamp is used to illuminate over the speckled surface as shown in Figure 3 (b). The meso-scale setup consists of a high resolution 9 MPixels CCD (Grasshopper) camera incorporated with 3X magnification Navitar lens and focused on the micro-speckled region located on the free-edge of the specimen. The meso-scale DIC has an approximate field of view 4.15×3.32 mm2 and acquired image at a resolution of 0.9µm/pixel. The images are captured for both speckled regions simultaneously at the rate of 2 frames per second.

After the experiment is completed, the acquired images are post-processed using commercial software VIC-2D (Correlated Solution Inc.). The strain analysis for each speckled region is executed separately. The correlation analysis was performed using subset size of 37 pixels (34µm) and step size of 5 pixels (4.5µm) for micro speckle and subset size of 45 pixels (1mm) and step size of 5 pixels (0.12mm) for the macro speckled region. 8 tap optimizing interpolation based on normalized squared difference criterion, with decay filter size of 15 pixels is used for both cases.

3.4 RESULT AND DISCUSSION

3.4.1 Global stress-strain relation and elastic properties

The average global full-field axial strains obtained from the macro scale DIC along with the applied stress for the four distinct groups of laminates are depicted in Figure 3.4. The stress-strain curve for both (0/90/+45/-45)s and the (0/-45/+45/90)s laminates, has shown bilinear trend. However, in the case of the (0/-45/+45/90)s laminate, the first linear section is much smaller compared to the whole curve. On the other hand, the (0/-45/90/+45)s laminate has a single linear trend throughout the whole loading duration with

few irregularities appeared within the curve. The (-45/+45/0/90)s laminate have shown a single linear curve for the large part of loading, and few irregularities are encountered near the last stage of loading. Slight variations in mechanical characteristics, such as strength, elastic modulus and strain at failure, are recorded between the four distinct laminate groups. The highest strength, about 820 MPa, is obtained for the (0/90/+45/-45)s laminate. Whereas, the (0/-45/90/+45)s and (-45/+45/90/0)s laminates have strength of 760 MPa and 715 MPa respectively, However, (0/-45/+45/90)s laminate has the lowest strength which is around 460 MPa.

Regarding the elastic modulus, all the laminates have showed slight variation in the effective elastic modulus. The (0/90/+45/-45)s laminate has the highest effective elastic modulus, around 77.3 GPa. While, the (0/-45/+45/90)s and (0/-45/90/+45)s laminates have an elastic modulus of 70 GPa and 66.8 GPa respectively, and the lowest modulus, 63.8 GPa, is recorded for (+45/-45/90/0)s laminate. Though, the same number of off-axis (90^o, $+45^o$ and -45^o) and on-axis (0^o) plies are used for all groups of laminates, the axial strains at failure are quite different for the diverse group of laminates. As depicted in Figure 3.4, the (0/90/+45/-45)s and (0/-45/90/+45)s laminates have failed at a strain around 1.45%, whereas (-45/+45/90/0)s and (0/-45/+45/90)s laminates have failed at strain of 1.75% and 0.84% respectively.

The basic theoretical formulations of laminate mechanics (i.e. CLPT) described that the relative stacking sequence of plies has no significant influence on the strength, elastic modulus and failure strain of the laminate [33,37,50]. Further, for quasi-isotropic laminate with the same number of individual plies and distinct plies stacking arrangement, the elastic responses are expected to be similar. However, from the macro scale response obtained,

there is slight variation in Elastic Modulus (E), failure strain and ultimate strength between the distinct groups of laminates.

This variation can be due to two reasons, one is because of the loading scheme, where the load is applied directly to the outer ply and transferred to the neighboring plies. In such case the individual plies are subjected to distinct applied load/stress which is quite different from the average stress calculated by using the applied load and cross-sectional area. On the other hand, it could also be due to the strain measurement technique (DIC gives a surface strain measurement). The measured global strain are the surface strains obtained from the outer ply surface, thus, this surface strain will not represent the aggregated response of the overall laminate.

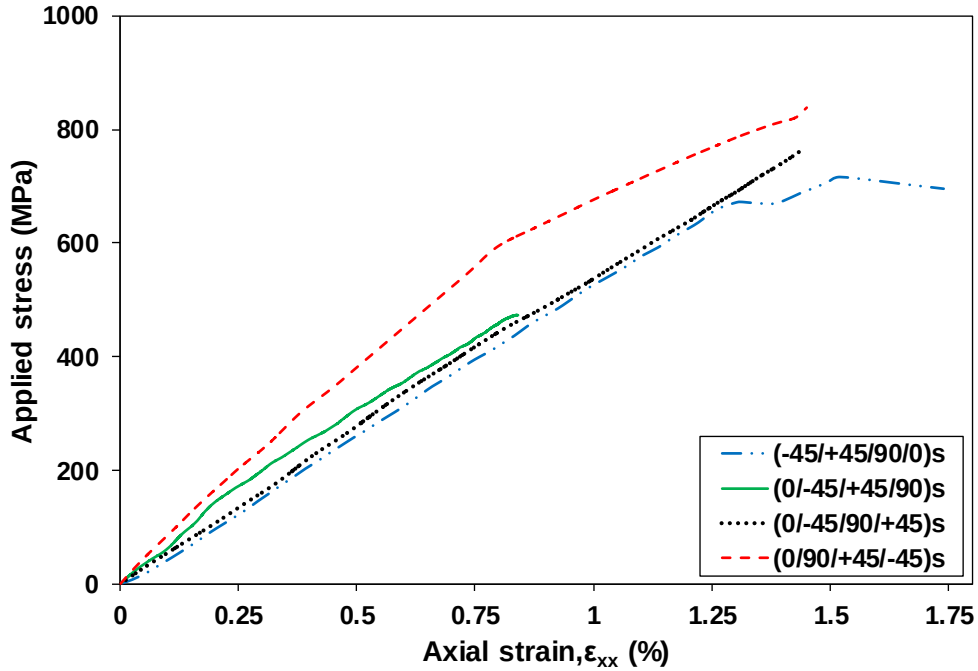

Figure 3.4: A typical stress-strain plot for the three groups of laminates.

3.4.2 Local strain distribution and damage formation

The axial strain contours across the laminate thickness obtained from the micro-scale DIC measurement are depicted in Figure 3.5. To widen the possibility of witnessing

the gradual emergence of distinct strain localizations and damages at the free-edge of the laminate, the strain contours with the gradual transformation at different applied stresses are presented. The initiation of strain localization, crack formation and propagation have shown distinct trends and characteristic for the different group of laminates.

From the strain contour of (-45/+45/90/0)s laminate in Figure 5(a), the strain localization started at the early stage of the loading (around stress of 250 MPa). It is noted that almost all the strain localizations are in the 90^o plies. As the loading advanced these localizations have expanded in quantity and size. In addition, the matrix cracks are seen to initiate from the location where strain localization are spotted and further propagated gradually across the thickness of the 90^o plies.

The matrix cracks on the 90^o ply above the mid-plane, have advanced and crossed to the neighboring $+45^o$ ply and resulted delamination at the interface between $+45^o$ and -45^o plies. On the other hand, for the matrix cracks in the 90^o ply which found below from the mid-plane, the matrix cracks remained in the 90^o ply and initiated delamination as it reached the interface to the $+45^o$ ply. An in-depth elaboration regarding the characteristics and mechanics of progressive damage can be found in the author prior work [86,87].

Figure 3.5(b) depicts the axial strain contour for the (0/-45/+45/90)s laminate as a function of applied stress. In this group, the 90^o plies are located at the middle of the laminate. As in the case of the (-45/+45/90/0)s laminate, the strain localizations have appeared in the 90^o plies and gradually turned to matrix cracking. Only four matrix cracks are observed within the field of view, and these cracks initiated and grown in the 90^o plies but didn't appear to propagate across the neighboring plies. Whereas, in the case of the (0/-45/90/+45)s laminate, high quantity of strain localization spots and matrix cracks are

observed in the 90^o plies (see Figure 3.5(c)). Further, two strain localizations/matrix cracks are noted in the +45^o plies. The strain localization in this laminate started to appear around stress of 400 MPa, which is found to be the highest compared to the other three groups of laminate.

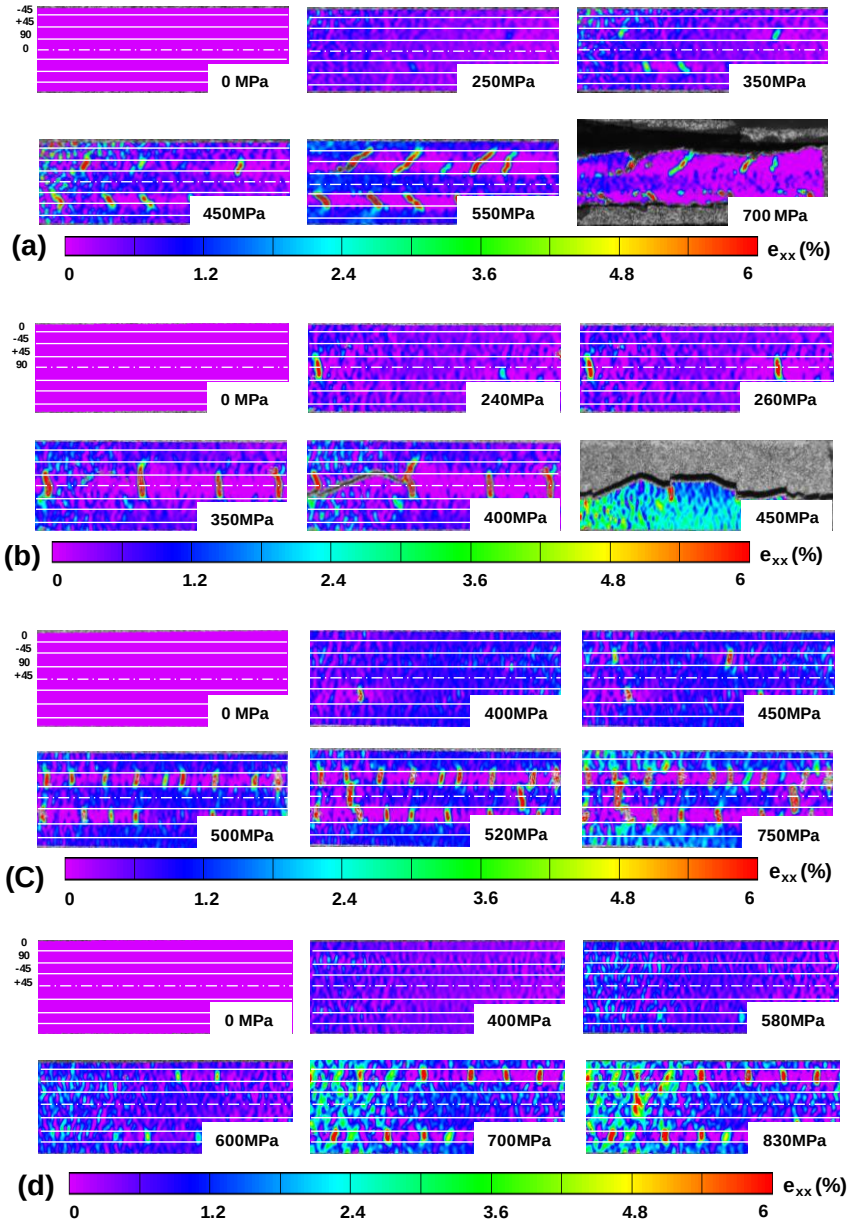

Figure 3.5: The axial strain contour for (a) (-45/+45/90/0)s, (b) (0/-45/+45/90)s, (c) (0/-45/90/+45)s and (d) (0/90/+45/-45) laminates, along the applied stress.

On the other hand, for the (0/90/+45/-45)s laminate (shown on Figure 3.5(d)), strain localizations and matrix cracking appeared in the 90^o plies similar to the other groups of laminates. Highly dense and multiple matrix cracks are observed in the 90^o plies. Moreover, one matrix crack is emerged in the -45^o plies which is located in the middle of the laminate stacking.

Moreover, high interlaminar shear strain localizations sited at the +45^o/-45^o interfaces in all groups of laminates. This phenomenon is well described and supported by theoretical formulations developed by earlier studies [19,22,88]. It is reported that these localizations are induced from an oppositely oriented in-plane shear deformation occurred in the +45^o and -45^o (i.e. due to the rotation of the fiber under tensile loading). In general, it is clearly observed that the stacking arrangement of plies has influenced the initiation and growth of transverse cracks and delamination.

3.4.3 Local axial strain of individual plies in the (0/90/+45/-45)s laminate

To clarify the interaction between the adjacent plies which make up the laminate, it is significant to extract the average strain for all plies near a region close to the primary matrix crack. Thus, by considering a representative region, the axial and transverse strain data of a small area from each ply of the (0/90/+45/-45)s laminate are depicted in Figure 3.6. From the axial strain plot, it seen that the strains in each ply increased continuously at the early stage of loading prior to the emergence of matrix crack within the laminate. As shown on the plot (Figure 3.6(a)), large amount sudden drop is observed for the axial strain plot of the 90^o ply, near applied stress of 600 MPa. At this instance, the strain increment trends have changed for the neighboring +45^o ply, the axial strain in these plies have shown

sharp increment. However, for the 0^o ply, there was no significant interruption/drop in the axial strain during due to the emergence of the matrix crack.

From the transverse strain plot shown in the Figure 3.6 (b), the transverse strain for the 90^o ply is very small up to the stage where matrix crack appeared, afterwards, sudden rise of the strain is noticed. Whereas, in the $+45^o$ and -45^o plies, the transverse strain is observed to change its pace and increased sharply when damages occurred. In the 0^o ply, the transverse strain increased continuously with same rate up to the final failure of the whole laminate. The plot depicted on Figure 3.6 clearly describe that emergence of matrix cracks within a given laminate alter the normal order of stress and strain distribution. Thus, such interruption in the load transfer order will cause stress rise on the undamaged plies. In contrary, when damaged occurred within the 90^o ply the region very close to the damaged surface is relaxed and the strain/stress in this vicinity will be less. However, the area of the 90^o ply much far from the relaxed region is under the normal stressed condition.

From the transverse strain plot shown in the Figure 3.6 (b), the transverse strain for the 90^o ply is very small up to the stage where matrix crack appeared, afterwards, sudden rise of the strain is noticed. Whereas, in the $+45^o$ and -45^o plies, the transverse strain is observed to change its pace and increased sharply when damages occurred. In the 0^o ply, the transverse strain increased continuously with same rate up to the final failure of the whole laminate. This plot depicted on Figure 3.6 clearly describe that emergence of matrix cracks within a given laminate alter the normal order of stress and strain distribution. Thus, such interruption in the load transfer order will cause stress rise on the undamaged plies. In contrary, when damaged occurred within the 90^o ply the region very close to the

damaged surface is relaxed and the strain/stress in this vicinity will be less. However, the area of the 90^o ply much far from the relaxed region is under the normal stressed condition.

3.4.4 Ply strain comparison

Beyond the comparison of the global strain or individual ply strain, it is reasonable to go further and compare the axial strain obtained from the 90^o ply. Thus, the global strain from the outer surface, and the local strains of the 90^o plies (which obtained from damaged and undamaged regions) are depicted on the Figure 3.7(a). These strain data are captured at the instance when significant growth of the first visible matrix crack is observed. In most

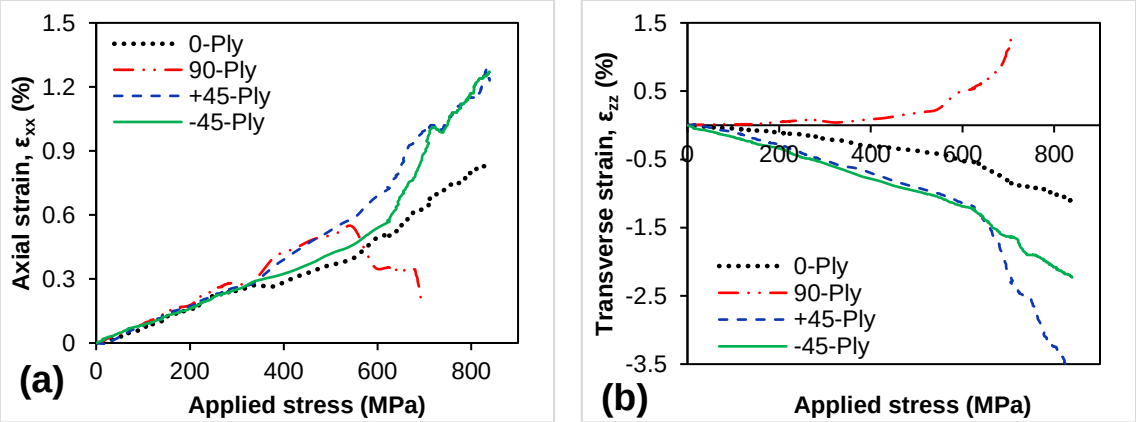

Figure 3.6: (a) The axial strain versus applied load and (b) The transverse strain versus applied load.

of the laminates, the local strain obtained for the damaged region has shown superiority over the undamaged region and global strains. This is acceptable as the presence of damage introduces high stress intensity at the vicinity of the crack. On the other hand, the local strain at the undamaged region is seen to be lower than the global axial strain. Here it should be noted that the undamaged region is neighbor to the location where the

damage/crack occurred. Thus, the reduction in local strain at the undamaged region might be because of the stress/strain relaxation came along with the crack formation.

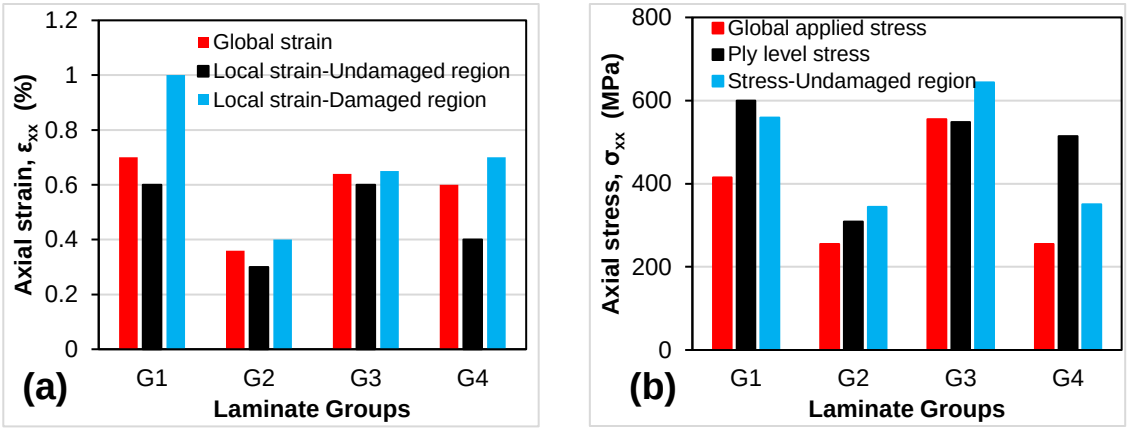

Figure 3.7: (a) The local and global axial strain and (b) The local and applied stresses for the different groups of laminates.

The critical strain (the local strain at damaged region) at which abrupt growth of matrix crack initiated is much higher for (0/-45/90/+45)s (G1) laminate as shown Figure 3.7(a). (-45/+45/90/0)s (G4) and (0/90/+45/-45)s (G3) laminates have shown comparatively moderate critical strain respectively, whereas (0/-45/+45/90)s (G2) laminate has shown the lowest critical strain. The difference in these critical strains is presumed to have association with the variation in stacking arrangement of the laminate groups. To support this argument, three distinct stress values, globally applied stress, the stress sustained by the 90^{o} ply (calculated from the CLPT formulation) and the local stress on undamaged stress evaluated from the free-edge strains are presented on Figure 3.7(b).

In most laminate groups, the local or CLPT based ply-level stresses are higher than the applied global stress. It should be noted that the overall global stress is an average of the individual plies stress, thus higher local stress might be the case in some plies. From the stress data depicted on Figure 3.7(b), the load/stress at which the matrix cracking

initiated is also seems to be influenced by the laminate stacking arrangement (directly relation with variation of the multi-directional free-edge stresses). It is depicted that the lowest matrix crack initiation applied stress is obtained for the (0/-45/+45/90)s and (-45/+45/90/0)s laminates, whereas the highest initiation stress is found in the (0/90/+45/-45)s laminate. Note that in all groups of laminates, there are equal number of off-axis and on-axis plies, however, these laminates encounter the primary matrix crack at different global and local stresses. At the free-edge there is dominant local transverse and shear stresses in addition to the main axial stress as shown on the Figure 3.8. It is critical to investigate the influence of the other multi-axis stress on of the primary matrix crack formation, thus, further exploration is required to provide clear understanding for such variation.

From various studies have explained that there are multi-axis stresses found at the free-edge of the laminate coupon. In this study, taking advantage of the DIC to obtain the full-field strain at the free-edge the multi-axis stresses found at the free-edge are evaluated. The multi-axial stresses at the free-edge are determined from the local strain obtained and by applying the constitutive law. Figure 3.8 show the local axial (along the loading axis), interlaminar transverse (out of the laminate plane) and interlaminar shear stresses. As depicted, the axial stress is much higher than the lateral stresses, nevertheless, significant amount of transverse stress (nearly half of the axial stress) are observed.

The transverse stress for (0/90/+45/-45)s laminate is the highest, followed by the (0/-45/90/+45)s laminate, (0/-45/+45/90)s and (-45/+45/90/0)s respectively. Here, it must be clear that the transverse stress/strain has resistance effect towards the transverse crack propagation. This imply that the higher the interlaminar transverse stress the larger axial stress required to create abrupt transverse crack formation. Thus, it is justifiable to assert that the resistance from the transverse stress is the reason for higher critical axial stresses observed in the (0/90/+45/-45)s and (0/-45/90/+45)s laminates.

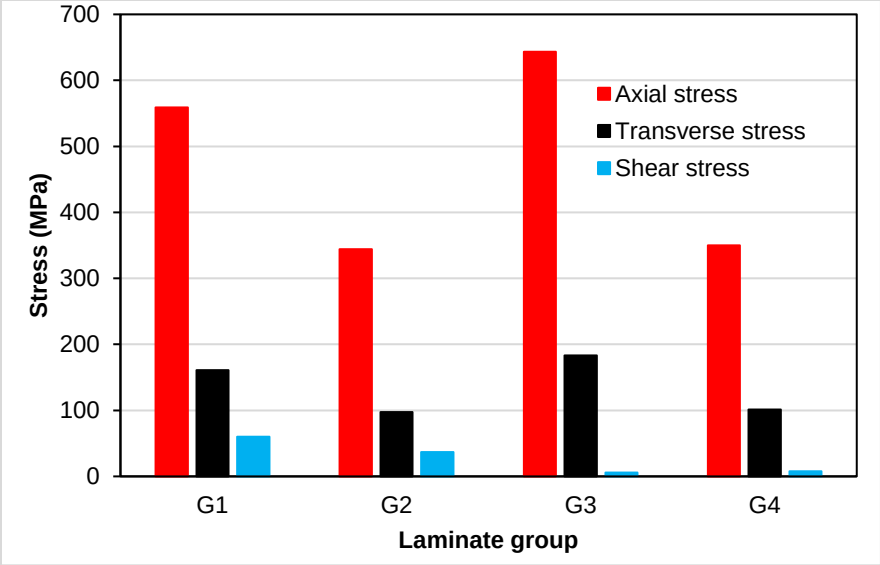

Figure 3.8: (a) Multi-axis local stresses from the free-edge for the different groups of laminates.

In most laminate groups, the local or CLPT based ply-level stresses are higher than the applied global stress. It should be noted that the overall global stress is an average of the individual plies stress, thus higher local stress might be the case in some plies. From the stress data depicted on Figure 3.7(b), the load/stress at which the matrix cracking initiated is also seems to be influenced by the laminate stacking arrangement (directly related with variation of the multi-directional free-edge stresses). It is depicted that the lowest matrix crack initiation applied stress is obtained for the (0/-45/+45/90)s and (-

45/+45/90/0)s laminates, whereas the highest initiation stress is found in the (0/90/+45/-45)s laminate. Note that in all groups of laminates, there are equal number of off-axis and on-axis plies, however, these laminates encounter the primary matrix crack at different global and local stresses. At the free-edge there is dominant local transverse and shear stresses in addition to the main axial stress as shown on the Figure 3.8. It is critical to investigate the influence of the other multi-axis stress on of the primary matrix crack formation, thus, further exploration is required to provide clear understanding for such variation.

3.4.5 Transverse crack density (d) and Energy release rate (ERR)

The overall process of transverse/matrix cracks emergence is gradual along with the applied load. In most of the laminate groups, the primary crack is sited in the 90^{o} plies, somehow, few of them have managed to propagate through the neighboring 45^{o} plies. From Figure 3.9(a), the quantity of matrix cracks, the rate at which the transverse cracks appeared in the laminate and the load at which the primary crack emerged in the free-edge is quite distinct for the different groups of laminates. The highest transverse matrix crack density is observed in the (0/-45/90/+45)s laminate, while (0/90/-45/+45)s and (-45/+45/90/0)s laminates showed the second and third highest crack density and the lowest crack quantity is recorded for the (0/-45/+45/90)s laminate.

The quantity of matrix crack density and the rate at which the cracks appeared in the laminates are higher in the (0/90/+45/-45)s and (0/-45/90/+45)s laminates, whereas, the (-45/+45/90/0)s laminate showed the lowest rate. It is shown that the quantity of matrix crack has sharply grown once after the appearance of the primary matrix crack for the

laminates with higher critical axial stress. It seems that the rate at which these matrix crack appeared in the laminate is influenced by the strain energy release rate within the laminates. This variation has a strong association with the complex stress condition at the free-edge, thus, the energy release rate (ERR) varies with the different stacking arrangement of the laminates.

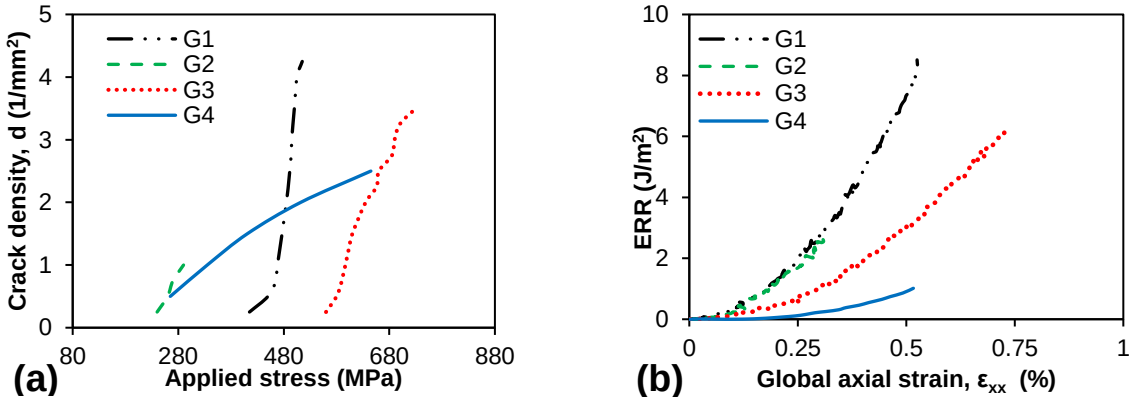

Figure 3.9: (a) The transverse crack density along with applied stress and (b) The ERR up to the primary matrix crack.

Moreover, the plot of energy release rate (ERR) which are evaluated from the free-edge stresses on the 90^{o} plies for mixed mode fracture condition are depicted on Figure 3.9(b). The curves depicted on the Figure 3.9(b) are the ERR up to the emergence of the first matrix crack. It clearly can be seen that the ERR is higher for (0/-45/90/+45)s and (0/90/+45/-45)s laminates while the ERR is lower for the (0/-45/+45/90)s and (-45/+45/90/0)s laminates. Higher ERR is caused by the higher critical stresses. This higher release of stored energy leads to initiation of the other transverse crack within short period of time in the same ply. As a result, sudden rise in transverse matrix quantity will be encountered following the emergence of the first crack.

3.5 SUMMARY

A monotonic quasi-isotropic tension test is performed on four distinct stacking arrangement laminates, and the gradual growth of local strains distribution across the thickness of the laminate is captured with the help of a DIC at high magnification. Variations in the failure stress and the elastic modulus is observed for the different laminates. The arrangement of plies in the laminate has influenced the damage formation, axial and shear strain distribution across the different plies and at the junction the plies.

Regarding the progressive damages, the matrix cracking is observed in the 90o plies for all group laminates, however, the rate at which crack emerged and the quantity of the cracks are affected by the relative position of plies. On the other hand, high interlaminar shear strain localizations are observed at the +45/-45 interface in all laminates. Despite of the shear strain localization, delamination is occurred at the interface where the matrix cracks reached for (-45/+45/90/0)s and (0/-45/+45/90)s laminates. This is unexpected outcome as delamination is assumed to be caused by the interlaminar shear, instead it was initiated due to the presence of matrix crack. Further, the relative arrangement of plies has major influence on the load sustained by the individual plies, thus changing the arrangement of plies directly affect the whole process of gradual damage formation. In overall, the transverse strain/stress developed at the free-edge are seen to be the cause for the variation in the critical stress and quantity of transverse cracks for the different groups of laminate.

3.6 LIST OF REFERENCES

[1] Nettles AT. Basic Mechanics of Laminated Composite Plates. NASA Ref Pulication

1994:107.

[2] Kaddour AS, Hinton MJ, Smith PA, Li S. A comparison between the predictive capability of matrix cracking, damage and failure criteria for fibre reinforced composite laminates: Part A of the third world-wide failure exercise. J Compos Mater 2013;47:2749–79.

[3] Talreja R. Assessment of the fundamentals of failure theories for composite materials. Compos Sci Technol 2014;105:190–201.

[4] Tahani M, Nosier A. Free edge stress analysis of general cross-ply composite laminates under extension and thermal loading. Compos Struct 2003;60:91–103.

[5] Kassapoglou C, Lagace PA. An Efficient Method for the Calculation of Interlaminar Stresses in Composite Materials. J Appl Mech 1986;53:744.

[6] Mittelstedt C, Becker W. Free-Edge Effects in Composite Laminates. Appl Mech Rev 2007;60:217.

[7] Murthy P, Chamis C. Free-edge delamination: laminate width and loading condition effects. Nasa_Tm-100238 1987.

[8] Nailadi CL, Adams DF, Adams DO. An Experimental and Numerical Investigation of the Free Edge Problem in Composite Laminates. J Reinf Plast Compos 2002;21:3–39.

[9] Pagano NJ, Pipes RB. The Influence of Stacking Sequence on Laminate Strength. J Compos Mater 1971;5:50–7.

[10] Buczek MB, Czarnek R. Free edge strain concentrations in real composite laminates: experimental-theoretical correlation. J Appl Mech 1985;52:787.

[11] Mittelstedt C, Becker W. Free-Edge Effects in Composite Laminates. Appl Mech Rev 2007;60:217.

[12] Lecomte-Grosbras P, Réthoré J, Limodin N, Witz JF, Brieu M. Three-Dimensional Investigation of Free-Edge Effects in Laminate Composites Using X-ray Tomography and Digital Volume Correlation. Exp Mech 2015;55:301–11.

[13] Nosier A, Maleki M. Free-edge stresses in general composite laminates. Int J Mech Sci 2008;50:1435–47.

[14] Corporation D. Analysis of the Interlaminar Shear Edge Effect in Laminated Composites * 1971;5:255–9.

[15] Pipes RB. Composite Laminates Under Uniform Axial Extension 2016:538–48.

[16] Joo JWW, Sun CTT. A Failure Criterion for Laminates Governed by Free Edge Interlaminar Shear-Stress. J Compos Mater 1992;26:1510–22.

[17] Whitney JM, Browning CE, Division NM. Free-Edge Delamination of Tensile attributed 1972:300–3.

[18] Riccio A, Mozzillo G, Scaramuzzino F. Stacking sequence effects on fatigue intra-laminar damage progression in composite joints. Appl Compos Mater 2013;20:249–73.

[19] Mittelstedt C, Becker W. Interlaminar Stress Concentrations in Layered Structures: Part I - A Selective Literature Survey on the Free-Edge Effect since 1967. J Compos Mater 2004;38:1037–62.

[20] Pagano J, Pipes RB. The Influence of Stacking Sequence Laminate Strength 2016;5:50–7.

[21] Fenske MT, Vizzini AJ. The Inclusion of In-Plane Stresses in Delamination Criteria. J Compos Mater 2001;35:1325–42.

[22] Crocker LE, Ogin SL, Smith PA, Hill PS. Intra-laminar fracture in angle-ply laminates. Compos Part A Appl Sci Manuf 1997;28:839–46.

[23] Tessema A, Ravindran S, Kidane A. Experimental Study of Residual Plastic Strain and Damages Development in Carbon Fiber Composite. Fract. Fatigue, Fail. Damage Evol. Vol. 8, Springer; 2017, p. 31–6.

[24] Pipes RB. Moire analysis of the interlaminar shear edge effect in laminated composites. J Compos Mater 1971;5:255–9.

[25] Herakovich CT. Free edge effects in laminated composites.Failure in Comp. Vol. 4,

1989, 205-219.

[26] Berthelot J-M. Transverse cracking and delamination in cross-ply glass-fiber and carbon-fiber reinforced plastic laminates: Static and fatigue loading. Appl Mech Rev 2003;56:111–47.

[27] Mortell DJ, Tanner DA, McCarthy CT. An experimental investigation into multi-scale damage progression in laminated composites in bending. Compos Struct 2016;149:33–40.

[28] París F, Blázquez A, McCartney LN, Barroso A. Characterization and evolution of matrix and interface related damage in [0/90]S laminates under tension. Part II: Experimental evidence. Compos Sci Technol 2010;70:1176–83.

[29] Tong J, Guild FJ, Ogin SL, Smith PA. on Matrix Crack Growth in Quasi-Isotropic Laminates-I. Experimental Investigation. Compos Sci Technol Elsevier Sci Ltd 1997;57:1527–35.

[30] Tessema A, Mymers N, Patel R, Ravindran S, Kidane A. Experimental Investigation on the Correlation between Damage and Thermal Conductivity of CFRP. Proc. Am. Soc. Compos. Thirty-First Tech. Conf., 2016.

[31] Jamison RD, Schulte K, Reifsnider KL, Stinchcomb WW. Characterization and analysis of damage mechanisms in tension-tension fatigue of graphite/epoxy laminates. Eff. defects Compos. Mater., ASTM International; 1984.

[32] Tong J, Guild FJ, Ogin SL, Smith PA. On matrix crack growth in quasi-isotropic laminates—I. Experimental investigation. Compos Sci Technol 1997;57:1527–35.

[33] Berthelot J. Transverse cracking and delamination in cross-ply glass-fiber and carbon-fiber reinforced plastic laminates : Static and fatigue loading 2016:111–47.

[34] Li C, Ellyin F, Wharmby A. On matrix crack saturation in composite laminates. Compos Part B Eng 2003;34:473–80.

[35] Kenneth Reifsnider SC. Damage Tolerance and Durability of Material Systems. 2002.

[36] Masters J, Reifsnider K. An Investigation of Cumulative Damage Development in Quasi-Isotropic Graphite/Epoxy Laminates, Damage in Composite Materials. ASTM STP 1982;775:40–62.

[37] Reifsnider KL, Stinchcomb WW. A critical-element model of the residual strength and life of fatigue-loaded composite coupons. Compos. Mater. Fatigue Fract., ASTM International; 1986.

[38] Singh CV, Talreja R. A synergistic damage mechanics approach for composite laminates with matrix cracks in multiple orientations. Mech Mater 2009;41:954–68.

[39] Varna J, Joffe R, Akshantala N V., Talreja R. Damage in composite laminates with off-axis plies. Compos Sci Technol 1999;59:2139–47.

[40] Tessema A, Zhao D, Kidane A, Kumar SK. Effect of micro-cracks on the thermal conductivity of particulate nanocomposite. Fract. Fatigue, Fail. Damage Evol. Vol. 8, Springer; 2016, p. 89–94.

[41] Samsur R, Rangari VK, Jeelani S, Zhang L, Cheng ZY. Fabrication of carbon nanotubes grown woven carbon fiber/epoxy composites and their electrical and mechanical properties. J Appl Phys 2013;113.

[42] Amrutharaj GS, Lam KY, Cotterell B. Delaminations at the free edge of a composite laminate. Compos Part B Eng 1996;27:475–83.

[43] Alton Highsmith KR. Stiffness-Reduction Mechanisms in Composite Laminates - Damage in Composite Materials: Basic Mechanisms, Accumulation, Tolerance, and Characterization. ASTM STP 1982;775:103–17.

[44] Reifsnider KL, Case SW. Damage tolerance and durability of material systems. WILEY; 2002.

[45] Crossman FW, Warren WJ. Initiation and Growth of Transverse Cracks and Edge Delamination in Composite Laminates Part 2. Experimental Correlation. J Compos Mater Suppl 1980;14:88–108.

[46] Katerelos DTG, Kashtalyan M, Soutis C, Galiotis C. Matrix cracking in polymeric

composites laminates: Modelling and experiments. Compos Sci Technol 2008;68:2310–7.

[47] Maimi. P, Camanho PP, Mayugo JA, Turon A. Matrix cracking and delamination in laminated composites. Part II: Evolution of crack density and delamination. Mech Mater 2011;43:194–211.

[48] O'brien T. Analysis of Local Delamination and Their Influence on Composite Laminate Behavior. ASTM STP 1985;876:282–97.

[49] Asadi A, Raghavan J. Model for prediction of simultaneous time-dependent damage evolution in multiple plies of multidirectional polymer composite laminates and its influence on creep. Compos Part B Eng 2015;79:359–73.

[50] Nairn J, Hu S. The initiation and growth of delamination induced by matrix microcracks in laminated composites. Int J Fract 1991;24:1–24.

[51] Liu S, Nairn JA. The Formation and Propagation of Matrix Microcracks in Cross-Ply Laminates during Static Loading 2016;ll:158–78.

[52] O'brien T. Damage in Composite Materials: Basic Mechanisms, Accumulation, Tolerance, and Characterization. ASTM STP 1982;775:140–67.

[53] Alter KW, Regal DM. NASA Contractor Report 4479. Control 2005.

[54] Nairn JA. Fracture mechanics of composites with residual stresses, traction-loaded cracks, and imperfect interfaces. Eur Struct Integr Soc 2000;27:111–21.

[55] Talreja R. A Continuum Mechanics Characterization of Damage in Composite Materials. Proc R Soc A Math Phys Eng Sci 1985;399:195–216.

[56] Varna J, Joffe R, Talreja R. A synergistic damage-mechanics analysis of transverse cracking [±Θ/90_4]s laminates. Compos Sci Technol 2001;61:657–65.

[57] Varna J, Talreja R. Integration of Macro- and MicroDamage Mechanics for the Performance Evaluation of Composite Materials. Mech Compos Mater 2012;48:1–16.

[58] Kashtalyan M, Soutis C. Analysis of local delaminations in composite laminates

with angle-ply matrix cracks. Int J Solids Struct 2002;39:1515–37.

[59] Kashtalyan M, Soutis C. Stiffness and fracture analysis of laminated composites with off-axis ply matrix cracking. Compos Part A Appl Sci Manuf 2007;38:1262–9.

[60] Farge L, Ayadi Z, Varna J. Optically measured full-field displacements on the edge of a cracked composite laminate. Compos Part A Appl Sci Manuf 2008;39:1245–52.

[61] Farge L, Varna J, Ayadi Z. Damage characterization of a cross-ply carbon fiber/epoxy laminate by an optical measurement of the displacement field. Compos Sci Technol 2010;70:94–101.

[62] Liu YM, Mitchell TE, Wadley HNG. Anisotropic damage evolution in a $0^o/90^o$ laminated ceramic-matrix composite. Acta Mater 2000;48:4841–9.

[63] Rask M, Madsen B, Sørensen BF, Fife JL, Martyniuk K, Lauridsen EM. In situ observations of microscale damage evolution in unidirectional natural fibre composites. Compos Part A Appl Sci Manuf 2012;43:1639–49.

[64] Lomov S V., Ivanov DS, Truong TC, Verpoest I, Baudry F, Vanden Bosche K, et al. Experimental methodology of study of damage initiation and development in textile composites in uniaxial tensile test. Compos Sci Technol 2008;68:2340–9.

[65] Koohbor B, Ravindran S, Kidane A. Meso-scale study of non-linear tensile response and fiber trellising mechanisms in woven composites. J Reinf Plast Compos 2016.

[66] Koohbor B, Ravindran S, Kidane A. Meso-scale strain localization and failure response of an orthotropic woven glass–fiber reinforced composite. Compos Part B Eng 2015;78:308–18.

[67] Pollock P, Yu L, Sutton MA, Guo S, Majumdar P, Gresil M. Full-field measurements for determining orthotropic elastic parameters of woven glass-epoxy composites using off-axis tensile specimens. Exp Tech 2014;38:61–71.

[68] Ravindran S, Tessema A, Kidane A. Local Deformation and Failure Mechanisms of

Polymer Bonded Energetic Materials Subjected to High Strain Rate Loading. J Dyn Behav Mater 2016:1–11.

[69] Tessema A, Mitchell W, Koohbor B, Ravindra S, Kidane A, Van Tooren M. Effects of Nanoparticles on the Shear Properties of Polymer Composites. Am. Soc. Compos. Tech. Conf., 2015.

[70] Tessema A, Mitchell W, Koohbor B, Ravindran S, Kidane A, Van Tooren M. On the mechanical Response of Polymer fiber Composites reinforced with nanoparticles. Mech. Compos. Multi-functional Mater. Vol. 7, Springer; 2016, p. 125–30.

[71] Sutton MA, Orteu JJ, Schreier H. Image correlation for shape, motion and deformation measurements: basic concepts, theory and applications. Springer Science & Business Media; 2009.

[72] Tamuzs V, Dzelzitis K, Reifsnider K. Prediction of the cyclic durability of woven composite laminates. Compos Sci Technol 2008;68:2717–21.

[73] Ravindran S, Tessema A, Kidane A. Note: Dynamic meso-scale full field surface deformation measurement of heterogeneous materials. Rev Sci Instrum 2016;87:1–4.

[74] Koohbor B, Mallon S, Kidane A, Sutton MA. A DIC-based study of in-plane mechanical response and fracture of orthotropic carbon fiber reinforced composite. Compos Part B Eng 2014;66:388–99.

[75] Wang SD, Palo L. Intiation and growth of transverse cracks and edge delamination in Composite laminates, Part-1. An energy method, J of Comp. Mat. Supplemnt, 2015;14:71–87.

[76] Greenhalgh E. Failure analysis and fractography of polymer composites. Elsevier; 2009.

[77] Bishop SM, McLaughlin KS. Thickness effect and fracture mechanism in notched carbon-fibre composites. 1979.

[78] Siulie Liu, Nairn JA. The Formation and Propagation of Matrix Microcracks in Cross-Ply Laminates during Static Loading. J Reinf Plast Compos 1992;11:158–78.

[79] O'Brien, T. Kevin, Hampton V, Chawan, Arun D., Demarco, Kevin, Blacksburg V, Paris, Isabelle, Hampton V., Influence of Specimen Preparation and Specimen Size on Composite Transverse Tensile Strength and Scatter. Hampton: 2001.

[80] Singh CV, Talreja R. Evolution of ply cracks in multidirectional composite laminates. Int J Solids Struct 2010;47:1338–49.

[81] Potter RT. The notch size effect in carbon fibre, glass fibre and kevlar reinforced plastics laminates. Farnborough, Hants GU146TD: 1981.

[82] Singh CV, Talreja R. International Journal of Solids and Structures Evolution of ply cracks in multidirectional composite laminates. Int J Solids Struct 2010;47:1338–49.

[83] Naghipour P, Bartsch M, Chernova L, Hausmann J, Voggenreiter H. Effect of fiber angle orientation and stacking sequence on mixed mode fracture toughness of carbon fiber reinforced plastics: Numerical and experimental investigations. Mater Sci Eng A 2010;527:509–17.

[84] Portella EH, Romanzini D, Angrizani CC, Amico SC, Zattera AJ. Influence of Stacking Sequence on the Mechanical and Dynamic Mechanical Properties of Cotton/Glass Fiber Reinforced Polyester Composites. Mater Res 2016;19:542–7.

[85] Ball AJ, Young R, Cervenka A. The Effect of Stacking Sequence Upon the Mechanical Properties of Thermoplastic Composite Laminates. Dev. Sci. Technol. Compos. Mater., Dordrecht: Springer Netherlands; 1990, p. 1031–6.

[86] Tessema A, Ravindran S, Wohlford A, Kidane A. In-Situ Observation of Damage Evolution in Quasi-Isotropic CFRP Laminates. Fract. Fatigue, Fail. Damage Evol. Vol. 7, Springer; 2018, p. 67–72.

[87] Tessema A, Ravindran S, Kidane A. Gradual Damage Evolution and Propagation in Quasi-Isotropic CFRC under Quasi-Static Loading. Compos Struct 2017.

[88] Naik NK, Asmelash A, Kavala VR, Ch V. Interlaminar shear properties of polymer matrix composites : Strain rate effect. Aerosp Eng n.d.

[89] Rebière J-L, Gamby D. Strain Energy Release Rate Analyse of Matrix Micro Cracking in Composite Cross-Ply Laminates. Mater Sci Appl 2011;2:537–45.

[90] Katerelos DTG, Varna J, Galiotis C. Energy criterion for modelling damage evolution in cross-ply composite laminates. Compos Sci Technol 2008;68:2318–24.

[91] Canal LP, González C, Molina-Aldareguía JM, Segurado J, Llorca J. Application of digital image correlation at the microscale in fiber-reinforced composites. Compos Part A Appl Sci Manuf 2012;43:1630–8.

[92] Singh CV, Talreja R. Analysis of multiple off-axis ply cracks in composite laminates. Int J Solids Struct 2008;45:4574–89.

CHAPTER 4
THE EFFECT LAMINA FIBER ORIENTATION ON THE INTERLAMINAR STRAINS OF MULTI-DIRECTIONAL LAMINATE- EXPERIMENTAL INVESTIGATION

4.1 ABSTRACT

Along with highly growing applications of fiber reinforced laminate, the mechanics of laminate plates has advanced tremendously. However, the presence material discontinuity within the laminate structures causes a complexity in the stress condition at the vicinity of the discontinuities (also known as free-edge effect). The demand for an exact or approximate solution for the complex stress condition at the free-edge has been a real concern for more than four decades. Therefore, distinct forms of solutions are derived to address the issue and these solutions are seen to provide a contradicting emphasis. Thus, it is demanding to perform an experimental work that can clarify and verify the stress/strain condition and understand the influence of stress/strain localization on the damage formation. With this motive, an experimental investigation is conducted in this study. A rectangular coupon specimen made from 8 layer laminate with uni-directional (Ɵ)8 and multi-directional laminas with stacking arrangements of (0/-Ɵ/+Ɵ/90)s are used. To evaluate the free-edge strain distribution and damage evolution with the help of Digital Image Correlation (DIC).

A. Tessema, S. Ravindran, A. Wohlford, N. Myers and A. Kidane, Under preparation

From the results, it is found that that a higher interlaminar transverse strain (ε_{zz}) is observed for the 45^o and 30^o laminates and the lowest is recorded for the 15^o laminate. While the highest interlaminar shear strain (ε_{xz}) is found in the 15^o and 30^o laminates, and the lowest is obtained in and 45^o laminates. Further, matrix cracking, the primary and dominant form of damage, is observed in the 90^o ply for all groups of laminates. Interlaminar delamination is noted at the interface of $\Theta/90$ laminas for the laminates with fiber angles of 45^o and 30^o, however, no delamination is found for the fiber angle of 15^o laminate.

4.2 INTRODUCTION

Carbon reinforced polymer composites (CRPC) have wide applications in structural engineering due to its superior high stiffness and strength with relatively light weight. The mechanics of the laminate composites have been under study for more than six decades. In fact, Classical laminate plate theory (CLPT) has served the composite community for the last four decades, CLPT is used to determine the load-deformation correlation [1]. Based on the stress/strain obtained from the CLPT, various failure criteria have been developed to postulate/predict the failure of the laminate structure [2,3]. However, this CLPT model is developed with an assumption of an infinitesimally large laminate, and it is implemented for 2D plane stress condition for a laminate plate.

In actual/real application, laminate plates have finite size and consist of different geometrical features like holes, rectangular cut-outs which induce discontinuity within the laminate. In such situations, the laminate will incorporate traction free surfaces. Thus, due to the traction free boundary condition, the stress state near the free-edges is much complex and completely different from the one described by the CLPT. In fact, with a consideration of the boundary effect at the free-edge and counting the discontinuity of material properties

across the different layers, it is found that there is a 3D stress state is acquired at the free-surfaces [4–9]. The main cause for the formation of 3D-stress state is interrupted the stress equilibrium condition as a result of the stress-free boundary condition (Under the given tension load, the laminas will have difference in transverse deformation, since the layers are bonded together interlaminar stress will be induced in between the laminas). Thus, to acquire and the equilibrium of the system and maintain displacement continuity across the different layers along the thickness, there will be interlaminar axial and shear stresses over the free-edge.

The issues of free-edge have been around for a while and numerous studies have been made over the past few decades. Various analytical models that incorporated distinct boundary conditions and continuity constraints have been implemented to determine the stress/strain at the free-edge. In most cases, the problem is over constrained, and it is very difficult to present an exact solution. Consequently, various analytical and numerical approaches had been applied to exploit the approximate solutions. Based on the theory of elasticity, closed-form solutions are developed by using Lekhnitskii's stress potentials [5,6,9]. From these closed form solutions, it is observed that there is a dominant interlaminar shear stress at the interface of angle laminas.

Moreover, vast number of studies have put efforts to find an accurate closed-form solution using different approaches. A broad review on those works can be found in [6], for brevity we will summarize the general approaches. Most of these works have similarity in their procedures, it starts by providing a displacement or stress function and followed by adjusting the parameters and tune it to fulfil the boundary and continuity conditions. Parts of these works are made based on the consideration of equivalent single-layer theories, in

which the whole laminate is taken as a single layer and a generic displacement or stress function (which is continuous across the thickness) is used. On the other hand, some works have approached the problem from layer wise equilibrium formulations where each layer is considered separately. By regulating the parameters, the continuity of the displacement fields at the interface of the layers will be satisfied. Further, beside the virtual models, few experimental works have been made to evaluate the deformation trends at the free-edge of the laminate [10,24,25]. Herakovich [25] used Moiré interferometry to measure the deformation on the free-edge of +Ɵ/-Ɵ laminates. These experimental works have moved a big step in capturing the sense on how the displacement contour varied across the thickness.

Beyond the concern of obtaining the approximate solutions, the presence of a 3D complex stress condition has led to the initiation of damage on the free-edges. By applying high microscope, the gradual damage evolution is captured in-situ [26,29–31,40]. Post-test microscopic observations have shown that different forms of damage including micro-cracks, transverse/matrix cracks and lamina delamination have initiated at the free-edge [8,26–30]. The formation of these damages is not an instant phenomenon rather it evolves gradually. In a general sense, the damage starts with the emergence of micro-cracks in the most off-axis lamina (90^o lamina in most cases) [69]. These cracks are initiated at a random location within 90^o lamina, it usually appears at the matrix or at the boundary between matrix and fiber [27]. Following, the micro-cracks coalesce and form large cracks that is oriented transverse to the loading orientation. These cracks advance to the neighbor layers across the thickness and expand in to the laminate width direction from the free-edge.

Hence transverse crack encounters a resistance when it reached the interface of the neighboring layers, delaminating cracks are initiated from the spots where the transverse crack touched the interface and propagate through the interface. Further, this delamination does not remain at the free-edge; it advanced in to the whole laminate.

As a result of the matrix cracking and delamination occurrence, degradation in mechanical properties is observed. The degradation is followed by sudden catastrophic failure of the laminate. Thus, the gradual growth of damage from the free-edge has a crucial role on the health and safety of the composite structure. However, there is still a need for a meso-scale experimental study that can show the detail variation of the stress/strain across the different laminas and provide a guideline for the approximate solutions. Further, a clear understanding on the free-edge and emerging damages is required.

Digital Image Correlation (DIC) has been used in the experimental world as a non-contact deformation measurement technique. DIC was found advantageous since it enables to capture the full-field strain contour over a given surface (that could be flat or intricate). Using the images captured consecutively, the deformation and strain on a given surface are calculated by tracking the relative movement of the speckles on the surface. DIC can be used for different size scale range (micro to macro). Particularly, in the DBMML lab at the University of South Carolina, DIC has been used at micro scale to understand the local deformation at the microstructure level [30,68–70].

In this study, DIC is used to obtain the full-field strain localization at meso-scale, it is intended to investigate the strain localizations over the free-edge of a laminate subjected to tensile loading. By changing the fiber angle of the off-axis laminas the effect of fiber angle variation on the free-edge strain/stress will be investigated. From these strain

(axial, transverse and shear) contours, the influence of interlaminar stresses around the free-edge on strain localization and damage formation will be explored. In addition, by using the strain localizations and visual inspection, the evolution of damage will be captured.

4.3 BACKGROUND

According to the CLPT, for a given long and infinite width laminate, there is a generalized plane stress condition. As shown in Figure 4.1, for the laminate subjected to axial strain at the two ends, there will be in-plane axial (σ_{xx}), transverse (σ_{yy}) and shear stress (σ_{xy}) developed. However, the CLPT analysis is reserved only for a very long and large width plate, so that the effect of the boundary condition at the free-edge is neglected. As mentioned earlier, in the structural components where there are boundary edges and different shape cut-outs, the boundary edge effect is crucial.

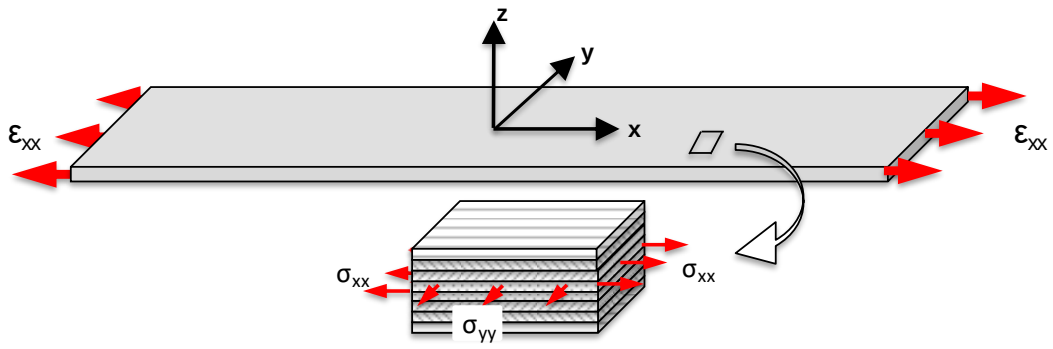

Figure 4.1: The schematic diagram of a laminate coupon under uniaxial tensile strain.

To give more glance to the issue, take a laminate with distinct layers as shown in Figure 4.1, in this laminate there are four different interlaminar interfaces as shown from the edges. These interfaces are the junctions between the off-axis (angled) and the on-axis laminas (0^o/-Θ^o or +Θ^o/90^o laminas), and the interface between the two off-axis laminas (-

$\Theta^o/+\Theta^o$). For the better explanation of the free-edge effect two cases of the $0^o/-\Theta^o$ interface are presented in Figure 4.2(a) where in the first case the two laminas are assumed to be not bonded together. On the second case, the two laminas are bonded together where this represents the actual scenario. In the first case, hence the two laminas have different Poisson's ratio the two laminas will have distinct transverse deformation and the transverse strain for the two laminas is different in magnitude for a given applied axial strain. The 0o lamina has higher transverse strain than the $-\Theta^o$ lamina. Yet in the actual case where the two laminas are bonded at the interface, the deformations of two laminas are constrained, subsequently both laminas are expected to deform transversely with the same amount. Thus, bonding two laminas with distinct transverse deformation together induces a transverse stress (σ_{yy}) at the interface of the two laminas. This stress is tensile on the 0^o laminas while it is compressive on the $-\Theta^o$ laminas.

In addition, for un-boned case, there is an in-plane shear strain in the $-\Theta^o$ lamina case besides the transverse strain due to the angled orientation of the fibers, which is not seen in the 0^o lamina. Due to this relative shear deformation between the two laminas, there is an interlaminar shear stress developed when the two laminas are bonded. In addition, with inclusion of these stresses in the force balance and stress equilibrium analysis, 3D stress state is obtained at the free-edge of the laminate. From the equilibrium condition in the Y and Z-direction, the interlaminar stresses σ_{yz} and σ_{zz} are obtained at the interface. In overall, at the region around the interface of $0^o/-\Theta^o$ or $+\Theta^o/90^o$ laminas three interlaminar stress, σ_{xz}, σ_{yy}, σ_{yz} and σ_{zz} emerge. The two stresses σ_{xz} and σ_{zz} are located on the X-Z plane

and causes delamination. The σ_{zz} is directed out of the laminate plane and tends to open the interface, while the σ_{xz} induces slipping of one lamina over the other.

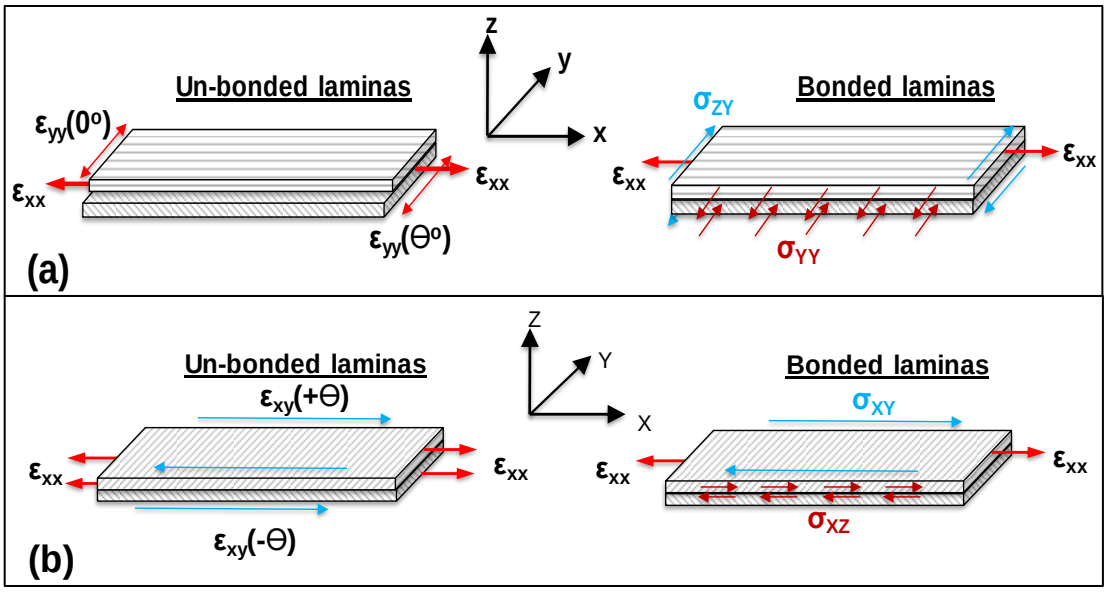

Figure 4.2: The schematic diagram of bonded and un-bonded cases for (a) 0/Θ interface and (b) -Θ/+Θ interface.

On the other hand, for the case of $-\Theta^o/+\Theta^o$ interfaces the issue related with transverse strain doesn't occur as shown in Figure 4.2(b). However, since the two laminas have reversely oriented fibers, they will have in-plane shear strains that oriented oppositely. When the two laminas are bonded, there will be a shear stress concentrated at the interface because of the resistance generated from one lamina on to the other. In this case also, interlaminar shear stress (σ_{xz}) and axial stress (σ_{zz}) are obtained at the free-edge.

From the analytical derivation at the free-edge, both the interlaminar axial and shear stresses are highly dependent on the transverse deformation of the corresponding plies. Thus, the Poisson's ratio of the corresponding plies plays a vital role on the magnitude and orientation of interlaminar stresses. In particular, for the interlaminar axial stress the transverse deformation from the Poisson's effect has a direct influence. While the Poisson

ratio (ν) is a known material parameter for isotropic materials, in a laminate or a single ply the Poisson ratio is highly dependent the orientation of the reinforcing fibers. Laminates or Plies with different fiber orientation angle have distinct Poison's ratio. Hence, the variation in fiber orientation angle of the off-axis plies is expected to put significant effect on the free-edge of the laminate.

4.4 MATERIALS AND METHODS

4.4.1 Material preparation and specimen geometry

This study used Composite laminates made from carbon fiber prepreg with brand name Torayca T-800SC-24K-10E obtained from Toray Composites (America) Inc.. Using automated fiber placement technique, 8 layers of prepregs are stacked in required arrangement (Uni-directional and multi-directional (0/-Θ/+Θ/90)s). For the multi-directional laminates, three separate groups of laminate are stacked with three different fiber orientation angles of the off-axis laminas (Θ=15^{o} (Group-1), 30^{o} (Group-2) and 45^{o} (Group-3)) are prepared. Following, the stacked prepregs are covered with air tight vacuum bag and taken to the oven. The air entrapped in the bagged prepregs is sucked out with assistance of vacuum pump and the autoclave is set to the curing temperature. The curing temperature is set to 107 ^{o}C for 1 hour followed by a post curing temperature of 177 ^{o}C for 2.5 hours at a heating rate of 2 ^{o}C/sec. After the completion of the curing cycle, the specimen is first cooled to a temperature 50 ^{o}C with forced convection and then allowed to cool slowly to a room temperature.

The cured laminate is taken to the CNC waterjet machine where rectangular test coupons with dimension of 160 mm × 23 mm are cut. From the unidirectional laminate,

coupons are cut at different fiber angles (0, 15, 30, 45, 60, 75 and 90 degrees). The edges of tensile coupons are polished using different grades of sandpapers to remove any kind of debris, notches, or indentations formed by the abrasive water-jet cutting. To protect the fibers in the coupon from the gripping pressure during tensile tests, fiberglass tabs (40×22 mm2) are attached on the coupon at the gripping ends as shown in Figure 4.3. These protective tabs have a wedge tip to reduce stress concentration and to enable a smooth stress flow from gripping area to the gage area.

Random speckle patterns (black dots over a white background) are made on the two distinct locations of the test coupons as depicted in Figure 4.3. The first speckle pattern is located on the width side of the coupon and these speckles have macro scale size (one speckle size is 150-300 μm). The second speckle is found on the thickness side (free-edge) of the coupon, these speckles have micro scale size (one speckle size is 5-20 μm). These speckles are used to track the deformation over the surface and calculate the full-field strain over the given region in digital image correlation. The macro scale speckled regions and DIC setups are intended to extract the global full-field strains on the outer surface of the laminate. While the meso-scale speckles are required to collect the local strains across the thickness. The larger speckles (macro size) are made by spattering the black paint over a flat white background using flat black and white spray paints by spattering the black paint over a flat white background. On the other hand, the micro-speckles are produced by blowing a black toner powder over a semi-dried white paint background. Details regarding to the micro-speck preparation can be found elsewhere [70,85].

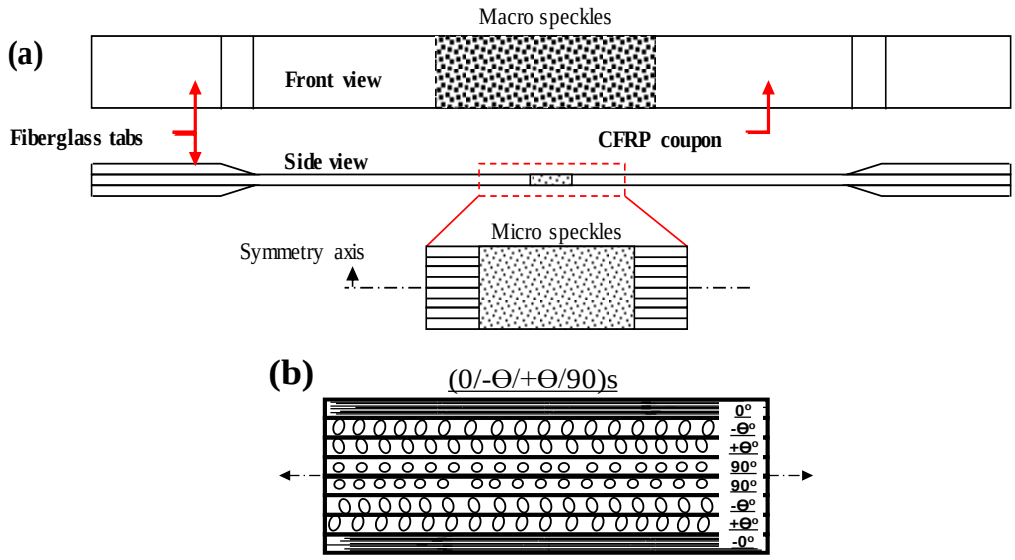

Figure 4.3: The schematic diagram of (a) coupon specimen with macro and micro speckles and (b) stacking arrangement.

4.5 EXPERIMENTAL SETUP

The coupon samples are subjected to tensile loading under displacement-controlled mode. The test is conducted using a Material Testing System (MTS 810). The coupon specimen was gripped from the top and bottom by the two hydraulic grips and a monotonic uniaxial displacement was applied at a rate of 0.05 in/min until the complete failure of the coupon. The experimental setup has included two distinct 2D-DIC systems for the two speckled regions as shown in Figure 4.4.

For this matter, a 5 MPixels CCD (Grasshopper) camera with 60 mm Nikon lens is directed to the macro-scale speckled region. This is used to acquire the surface global strain of the coupon on its wide laminate plane. For the meso-scale, a higher resolution is required thus a 9 MPixels CCD (Grasshopper) camera is paired with 3X magnification Navitar lens directed to the edge of the specimen. The meso-scale 2D-DIC setup has an approximate field of view of 4.15×3.32 mm^2 and an image has a resolution of 0.9µm/pixel. LED based lamp is used as a light source for the macro speckles and a halogen light source is used for

the micro speckled region. For both 2D-DIC setups, the images are acquired simultaneously and recorded at a rate of 1 frame per second.

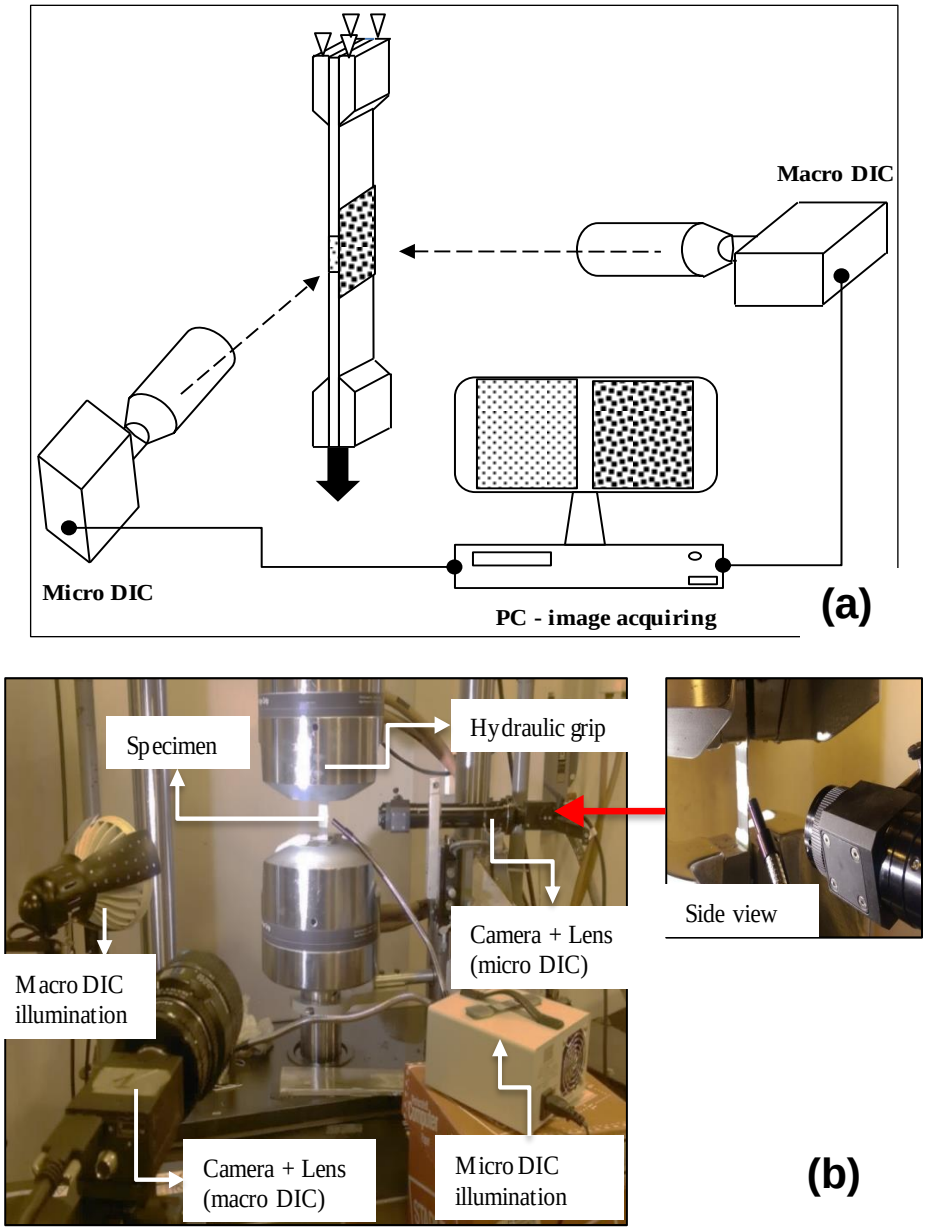

Figure 4.4: (a) The schematic diagram and (b) The actual image of the experimental setup.

Once the experiment is concluded, the images obtained from each setup are post-processed using ©VIC-2D commercial software (Correlated Solution Inc.). The image correlation was performed independently for each speckled region using correlation

parameters with subset size of ~ 37 pixels (34μm) for micro speckle and 45 pixels (1mm) for the macro speckle, and step size of ~ 5 pixels (4.5μm) for micro speckle and 5 pixels (0.12mm) for the macro speckle. Onwards, the strains are extracted over the field of the macro and micro speckle regions independently.

4.6 RESULTS AND DISCUSSION

The experimental works in this study have two groups of tests, the first test group is made on uni-directional laminate coupons with different fiber angle arrangements relative to the applied load. Whereas, the second group of test is made on coupons of multi-axial laminates that have stacking sequence of (0/-Θ/+Θ/90)s, where the off-axis laminas fiber angle (Θ) is varied to 15^o, 30^o and 45^o.

4.6.1 Uni-directional laminates

The first group of tests are explicitly used to understand the mechanical response of the individual lamina that are used to build the laminate. The results from this test are applied to comprehensively explain the free-edge effect and damage formation of the multi-directional laminates. The experimental results from the first group test laminates are depicted in Figures 4.5 & 4.6. From the axial strain-stress plot shown in Figure 4.5(a), the highest failure stress and lowest failure strain is recorded for the 0^o laminate. Since the fibers are the main load carriers in the 0^o laminate, degradation in failure strength is expected. However, in the case of unidirectional laminate with off-axis fiber angle (Θ), some amount of the applied load is carried by the matrix resin. Thus, the strength of the

unidirectional laminate reduced gradually with the fiber orientation angle (Θ) (As a result, the largest failure strain and smallest failure stress is obtained for the 45° laminate.

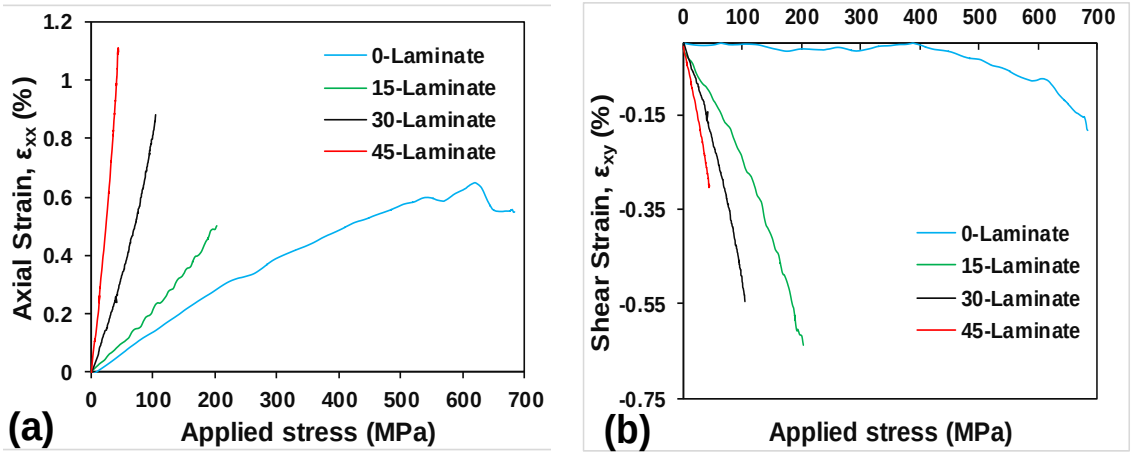

Figure 4.5: (a) Axial strain-stress and (b) Shear strain-stress, for uni-directional laminates with different fiber angle.

On the other hand, for the in-plane shear stress-strain plot as shown in the Figure 4.5(b), distinct in-plane shear strain at failure are observed in the different groups of laminate. In this case, the highest shear strain at failure is recorded for the 15° laminate, while the 30° and 45° laminates have relatively lower in-plane shear strain. Whereas, the 0° laminate possesses the lowest in-plane shear strain. As mentioned earlier, the magnitude of in-plane shear strain is associated with the relative orientation fibers to the applied stress. In fact, from an earlier study on woven composite laminates [68,72] it is found that the highest in-plane shear strain is obtained for the 45° laminate . It is reported that during uniaxial tension test the woven yarns showed a tendency to rotate and adjust its orientation with the loading axis. Such kind of in-plane deformation induces in-plane shear strain. At this instance, the matrix resin accumulated in between the two weave fiber yarns are

squeezed out. However, in the case of the uni-directional laminates, the situation is quite different the highest in-plane shear strain is observed for the 15^{o} laminate.

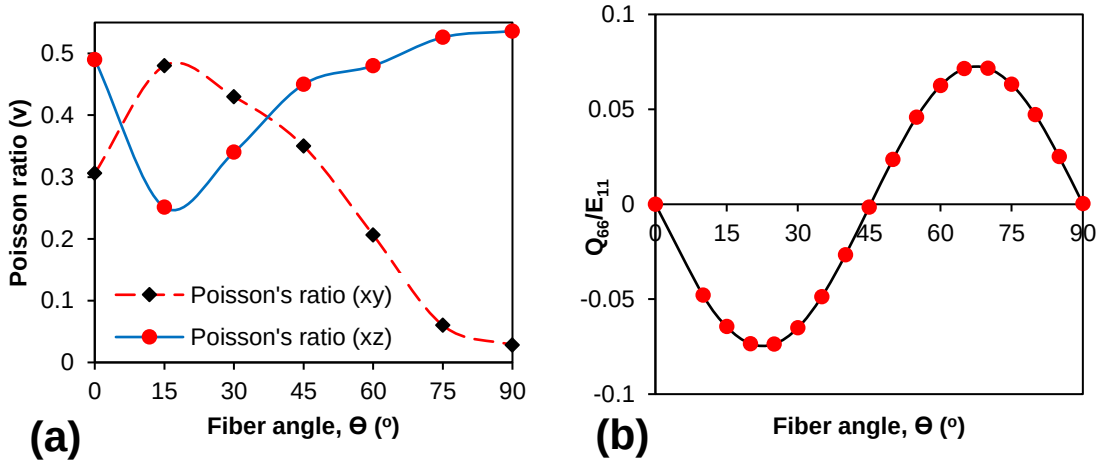

Figure 4.6: (a) The two Poisson ratios (ν) and (b) Normalized Q66, for uni-directional laminates with different fiber angle (θ).

Similarly, the Poisson's ratio (ν) of the unidirectional laminates at different fiber angle are presented in the Figure 4.6. The Poisson's ratio (ν) for the two planes, the laminate plane under the width and length (XY-plane) and the plane across the thickness (XZ-plane), are calculated by averaging the full-field strains (longitudinal and lateral) obtained from the corresponding planes. The Poisson ratio in the XY-plane, which is referred as Poisson ratio-1, has reached the peak for the laminate with fiber angle of 15^{o}, following it gradually decreased for higher fiber angles. Earlier studies also found a similar trend for the Poisson's ratio-1. Rapid decrease in the Poisson's ratio-1 is observed for the laminates with fiber angle (Θ) higher than 45^{o}.

In contrast, for case of the Poisson ratio on the XZ-plane, which is referred as Poisson ratio-2, the smallest value is found in the 15^{o} laminate and it increased with increase in fiber angles. Rapid increment in the Poisson ratio-2 is observed from the fiber

angle 15^o to 45^o. Onwards, the rate has slowdown for higher fiber angles (Θ). At this point, it is difficult to give a firm explanation on how the Poisson ratio-2 is trending this way along with the fiber angle. Nevertheless, it is assumed that the variation of fiber cross sectional geometry (i.e. from circular for 90^o laminate to elliptical for the angled laminas) at the free-edge might cause such variations. Note must be taken that all the strain measurements are made on the outer surfaces and the Poisson ratio results are effective only on these surfaces and might not represent the overall response of the laminate.

The in-plane deformation of off-axis laminate is dominated not only by the in-plane Poisson ratio (ν_{xy}), but also the stiffness matrix constant Q_{66}. The Q_{66} term is associated with the in-plane shear stress-axial strain correlation. The role of Q_{66} is significant in particular case of multi-directional laminate, where the stacked laminas are constrained one to the other. Thus, it is essential to characterize the variation in Q_{66} along with the fiber angle (Θ). The plot on Figure 4.6(b) depicts the variation Q_{66} with the fiber angle (Θ), as it is shown the Q_{66} has continuously varied through all the angles.

4.6.2 Multi-directional laminates

As discussed in the previous section, the variation in fiber orientation angle (Θ) in a lamina has a substantial role in the in-plane mechanical response of the lamina. Moreover, as the angled fiber laminas are used to build laminates, the orientation of the fibers is expected to have sound impact on the overall laminate mechanical response, particularly at the free-edge of the laminate. In this study, three groups of laminate that have the same relative stacking arrangement with different fiber orientation angle (Θ) are tested.

The typical stress-strain for the three laminates groups are depicted in Figure 4.7(a). Nearly a linear relation is noted in the stress-strain plot of all groups of laminates. Higher failure strength is obtained for the laminate with 15^o angle laminas. In contrast, the smallest strength and highest failure strain is recorded for the 45^o laminate. Whereas, the 30^o laminate properties are in between the two laminates. The elastic modulus (E) measured for 15^o, 30^o and 45^o laminates are 80 GPa, 78 GPa and 58 GPa respectively. This hint direct association of the laminas fiber angle (Θ) with the macroscale response of the laminate. In fact, from the uni-directional tests, it is observed that the laminates with higher fiber angle experience a higher failure strain and lower strength, and the reverse is true for the lower fiber angle laminates.

From the micro-speckle DIC, the average of the free-edge strains is obtained for the off-axis layers of the different group laminates. Comparison is made between the different group laminates. This is comparison is relevant in understanding and evaluating how the fiber orientation angle is affecting the strain localization on the angle ply, neighboring plies, and the overall laminate.

Starting from the axial strain plot shown in Figure 4.7(b), linear increment of the axial strains along with the applied stress is featured for all angled laminas. Relatively higher axial strain is attained for the 45^o lamina and lower strain is captured in the 30^o lamina as depicted in Figure 4.7(b). On the other hand, for the transverse strain, the 15^o lamina showed dominance while the 30^o lamina had the lowest strain. The transverse strain (ε_{zz}) result seems quite different from what is expected in accordance with the corresponding Poisson's ratio of the unidirectional laminates. In the case where the lowest Poisson's ratio-2 is obtained for the 15^o fiber angle, thus the smallest transverse strain is

expected in this lamina. Nevertheless, what observed in the transverse strain plot is the reverse, as shown in Figure 4.7(c). This indicate that the whole lateral deformation of the off-axis plies is not only as a result of the axial stretching, rather, there are several undefined factors that influence the transverse deformation. Thus, further investigation is required to clarify this issue.

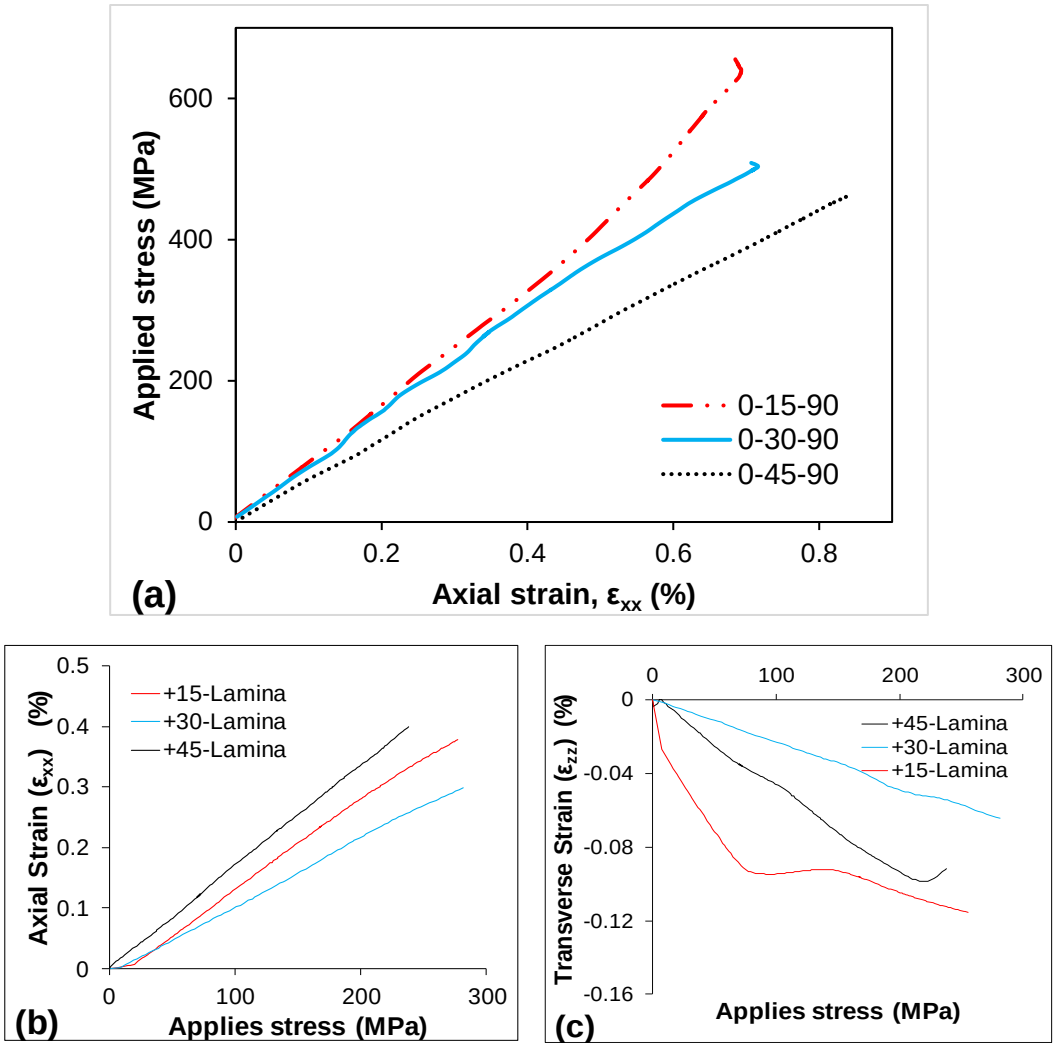

Figure 4.7: (a) The global axial stress-strain, (b) local axial strain (ε_{xx})-stress and (c) local transverse strain (ε_{zz})-stress, for +45, +30 and 15 laminas.

4.6.3 Strains on the individual laminas

To obtain better understanding, investigation on the mechanical response of individual plies at the free-edge (XZ-plane) is required. For this matter, the axial (ε_{xx}), transverse (ε_{zz}) and shear (ε_{xz}) strains for each lamina at the free-edge are plotted separately. It should be noted that these strains are obtained from the thickness plane, thus, this result might not represent the overall response of the whole laminate, and rather, it supports our way to draw much accurate conclusion. Since, the strain trends obtained for the different group of laminates have similarities; only the results for Group-3 laminate is presented in Figure 4.8. As shown in Figure 4.8(a), the axial strain in individual laminas have nearly linear increment and the strain in each lamina is almost the same. This result substantially matched with the assumption made by the CLPT. However, this similarity lasted only up to the initiation of matrix cracks in the 90^o lamina, which induces a sudden drop in axial strain in the lamina.

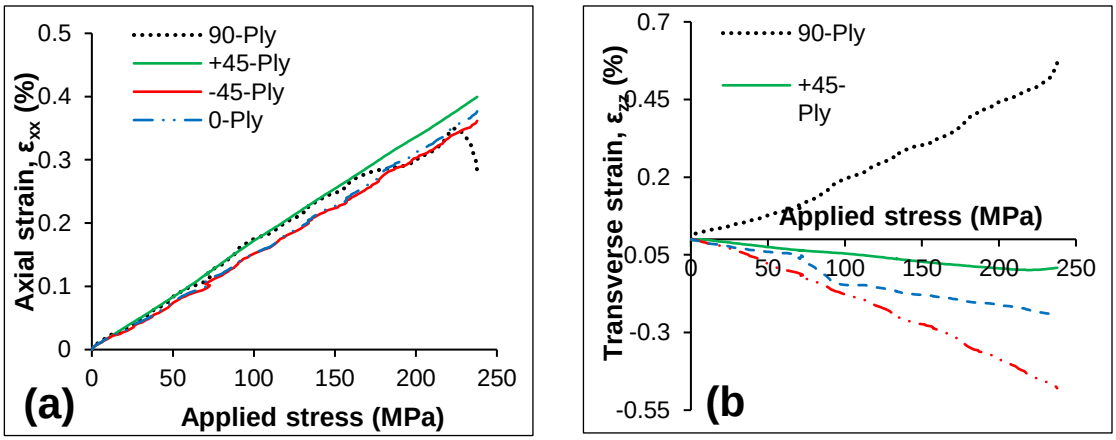

Figure 4.8: (a) Axial strain-stress and (b) Transverse strain-stress

Unlike the axial strain, a significant variation of trend and sign is observed for the transverse strain plots as shown in Figures 4.8(b). Negative transverse strains are noted for the three laminas (0^o, -45^o and +45^o) except the 90^o lamina. It was surprising to see a

positive transverse strain in the 90^o lamina, where a given lamina is subjected to uni-axial tension loading. The magnitude of the transverse strain in the -45^o lamina is much higher, nearly twice that of the other two laminas (0^o and +45^o). On the other hand, the transverse strain in the 90^o and -45^o laminas are nearly the same in magnitude. It is unexpected to see lower shear strain in the +45^o lamina compared to the -45^o lamina. This might be because of the relative location of the +45^o lamina, the two neighbor laminas (90^o and -45^o) has nearly equal but oppositely directed lateral/transverse deformation, thus, the transverse strain in +45^o lamina is much smaller due to the strain cancelation. This result is quite different from the prediction made based on the Poisson's effect (Poisson's ratio-2).

There are two points to mention on the case where the Poisson effect fail to match with the experimental result of the transverse strain (ε_{zz}). First, from the Poisson ratio-2, it is expected that the highest transverse strain appears in the 90^o lamina and it will be lower for the -45^o, +45^o and 0^o laminas, the experimental results are partially agreeing with this prediction (for the case of +45^o and 0^o laminas). However, for the -45^o lamina, it is clearly depicted that the transverse strain is much higher, and this contradicts with the expected Poisson's ratio-2 effect. Secondly, since the Poisson's ratio-2 is positive for all laminas, it is expected that the transverse strain in these laminas is negative, conversely that was not the case for the experimental result for the 90^o lamina.

The positive transverse strain obtained in the 90^o lamina seems out of the context of elastic analysis and it is difficult to explain. Nevertheless, it is assumed that the transverse deformation of the 90^o lamina is influenced not only by the Poisson's ratio effect but also due to the interaction of the transverse deformation by adjacent laminas. In further elaboration, since the 90^o lamina is placed between two -Θ^o laminas, it is subjected to a

pulling from both sides when the constraining neighbor laminas shrink transversely. Thus, the 90^o lamina has expanded instead of transverse shrinking.

4.6.4 Comparison of the interlaminar interfaces

In addition to the individual plies strain observation, it is significant to understand the localized interlaminar strain at the interface. To obtain the full visualization of the strain variation across the different laminas and their interfaces, the strain across half of the laminate thickness is obtained by extracting the strain along a line that cross half of the laminate. As presented in Figure 4.9, there is smooth variation in transverse and shear strains. As shown on the Figure 4.9, the plots have four sections divided by the black-dotted vertical lines, these sections represent each lamina and the lines are located right at the interfaces. The first section on the left side is the 0^o lamina, followed by the $-\Theta^o$ and $+\Theta^o$, and the 90^o lamina is at the far right.

From the plot on Figure 4.9(a), it is seen that there is a positive transverse strain in the 90^o lamina, the strain dropped smoothly near the interface. The transverse strain keeps dropping and became negative in the $+\Theta^o$ and $-\Theta^o$ laminas. The transverse strain is seen to start rising near the interface of the 0o lamina. This oscillating scheme of the transverse strain across the different laminas has consistently appeared in all groups of laminates. The transverse strain for the Group-1 laminate is much lesser, and there was no significant difference observed between Group-2 and Group-3 laminates. As discussed earlier, a positive and much higher transverse strain is noticed in the 90^o lamina; in addition, sharp strain peaks are depicted at the interfaces. Interestingly, for the $+\Theta^o$ the transverse strain is, positive for the region near the interface of the 90^o lamina and negative the region near

the -Θ^o lamina interface. This shows that the +Θ^o/90^o interface is under to oppositely directed transverse deformations, which set this interface as a critical element and vulnerable for delamination to occur.

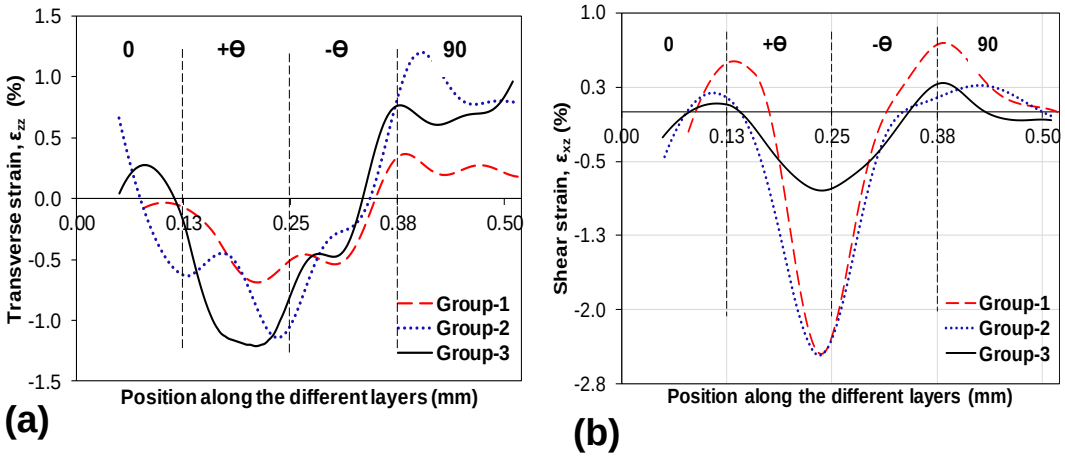

Figure 4.9: (a) Transverse strain-stress and (b) Shear strain-stress, for the vertical axis that cross half of the laminate.

On the other hand, the shear strain variation along the vertical line is depicted in Figure 4.9(b). Like the transverse strain plot, significant peaks and sharp rises are also common at the interlaminar interfaces. The –Θ^o/+Θ^o interface have showed the dominant peak among all the interfaces. The interfaces with -15^o/+15^o and -30^o/+30^o laminas has shown the higher shear strain peaks strain among the different groups of laminates. It is noticeable that the shear strain has flipped in sign at the two interfaces of a given lamina, from negative at one interface to a positive at the other; this leaves a zero-shear strain/stress region in the lamina.

4.6.5 Damage evolution and failure mechanism

Under a complex and intensified stress condition at the free-edge, there is a high probability for the initiation of damage in the laminate coupon from the free-edge. Thus, from gradually captured images of the free-edge along with the loading, the initiation and growth of damages at the free-edge are traced. As depicted in Figure 4.10, the evolution of the axial strain contour at different stage of applied stress is plotted for the three laminates. First, small local strain concentrations are observed to emerge within the 90^o lamina. Later, this strain localizations are turned to transverse/matrix cracking. The emergence and growth matrix cracking are a common feature in all laminates.

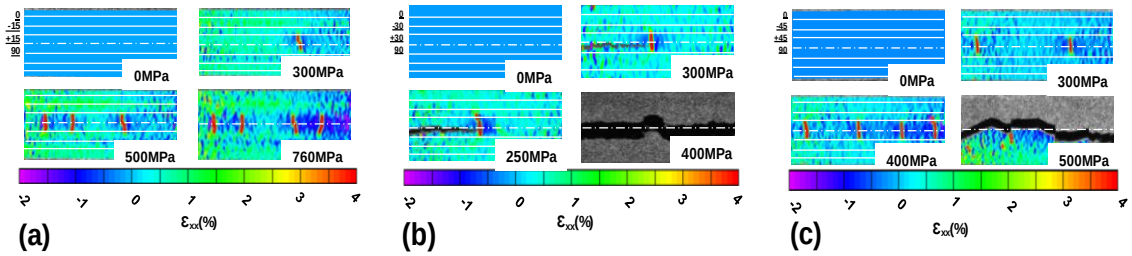

Figure 4.10: The axial strain contour and damage evolution for (a) Group-1(0/-15/+15/90)s, (b) Group-2 (0/-30/+30/90)s and (c) Group-3 (0/-45/+45/90)s laminates.

Once the matrix cracks have initiated in a transverse orientation within the 90^o laminas, it propagated towards the interface of the neighboring laminas. At the instance when the matrix cracks reached the interfaces, it is seen to cause a high stress intensity region around the crack tip. This intensified stress is added to pre-existing interlaminar normal and shear stress that leads to the initiation and growth of delamination at the interface. The delamination is clearly observed for the Group-2 and Group-3 laminates (see Figures 4.10(b) and (c)), however, no sign of delamination is noticed on the Group-1 laminate. One quite causes for the absence of delamination for the Group-1 laminate is lower lateral/transverse strain (ε_{zz}), particularly at the 90^o/+Θ^o interface. The delamination is

observed to propagate across one of the interfaces between $90^o/+\Theta^o$ laminas, and it jumps to the opposite $90^o/+\Theta^o$ interface when it reaches a matrix crack along the way (see Figure 4.10(b) and (c)).

4.7 SUMMARY

Two groups of experiments performed in this study. The first group is uni-directional laminate with different fiber angle, from this study it was found that the maximum in-plane shear and Poisson's ratio over the width plane (XY) are observed for the 15^o laminate. However, for the thickness plane (XZ), the smallest Poisson's ratio is obtained for the 15^o laminate. The second group is the multi-directional laminates, where it is found that a higher transverse strain is observed for Group-2 and Group-3 (laminates with 30^o and 45^o plies) and the lowest is recorded for Group-1 (laminate with 15^o ply) on the thickness plane (XZ). While the highest interlaminar shear strain is found in the Group-1 and Group-2 laminates, the lowest is depicted in the Group-3 laminate.

From the damage evolution, matrix cracking is common in all different group of laminates, however, delamination occurred only in the two laminates where the interlaminar transverse strain is higher. This scenario shows how the delamination is dominated by the transverse strain/stress nor the interlaminar shear; in addition, the presence of stress concentration, due to the matrix cracks tip at the interfaces, has significant on the initiation of delamination. This observation challenges the postulates made based on the approximate solution provided by earlier works. These solutions have found that the transverse stress at the free edge is much smaller compared to the

interlaminar shear stress, following, it was believed that the interlaminar shear failure dominate the failure at the free-edge.

4.8 LIST OF REFERENCES

[1] Nettles AT. Basic Mechanics of Laminated Composite Plates. NASA Ref Pulication 1994:107.

[2] Kaddour AS, Hinton MJ, Smith PA, Li S. A comparison between the predictive capability of matrix cracking, damage and failure criteria for fibre reinforced composite laminates: Part A of the third world-wide failure exercise. J Compos Mater 2013;47:2749–79.

[3] Talreja R. Assessment of the fundamentals of failure theories for composite materials. Compos Sci Technol 2014;105:190–201.

[4] Tahani M, Nosier A. Free edge stress analysis of general cross-ply composite laminates under extension and thermal loading. Compos Struct 2003;60:91–103.

[5] Kassapoglou C, Lagace PA. An Efficient Method for the Calculation of Interlaminar Stresses in Composite Materials. J Appl Mech 1986;53:744.

[6] Mittelstedt C, Becker W. Free-Edge Effects in Composite Laminates. Appl Mech Rev 2007;60:217.

[7] Murthy P, Chamis C. Free-edge delamination: laminate width and loading condition effects. Nasa_Tm-100238 1987.

[8] Nailadi CL, Adams DF, Adams DO. An Experimental and Numerical Investigation of the Free Edge Problem in Composite Laminates. J Reinf Plast Compos 2002;21:3–39.

[9] Pagano NJ, Pipes RB. The Influence of Stacking Sequence on Laminate Strength. J Compos Mater 1971;5:50–7.

[10] Buczek MB, Czarnek R. Free edge strain concentrations in real composite laminates: experimental-theoretical correlation. J Appl Mech 1985;52:787.

[11] Mittelstedt C, Becker W. Free-Edge Effects in Composite Laminates. Appl Mech Rev 2007;60:217.

[12] Lecomte-Grosbras P, Réthoré J, Limodin N, Witz JF, Brieu M. Three-Dimensional Investigation of Free-Edge Effects in Laminate Composites Using X-ray Tomography and Digital Volume Correlation. Exp Mech 2015;55:301–11.

[13] Nosier A, Maleki M. Free-edge stresses in general composite laminates. Int J Mech Sci 2008;50:1435–47.

[14] Corporation D. Analysis of the Interlaminar Shear Edge Effect in Laminated Composites * 1971;5:255–9.

[15] Pipes RB. Composite Laminates Under Uniform Axial Extension 2016:538–48.

[16] Joo JWW, Sun CTT. A Failure Criterion for Laminates Governed by Free Edge Interlaminar Shear-Stress. J Compos Mater 1992;26:1510–22.

[17] Whitney JM, Browning CE, Division NM. Free-Edge Delamination of Tensile attributed 1972:300–3.

[18] Riccio A, Mozzillo G, Scaramuzzino F. Stacking sequence effects on fatigue intra-laminar damage progression in composite joints. Appl Compos Mater 2013;20:249–73.

[19] Mittelstedt C, Becker W. Interlaminar Stress Concentrations in Layered Structures: Part I - A Selective Literature Survey on the Free-Edge Effect since 1967. J Compos Mater 2004;38:1037–62.

[20] Pagano J, Pipes RB. The Influence of Stacking Sequence Laminate Strength 2016;5:50–7.

[21] Fenske MT, Vizzini AJ. The Inclusion of In-Plane Stresses in Delamination Criteria. J Compos Mater 2001;35:1325–42.

[22] Crocker LE, Ogin SL, Smith PA, Hill PS. Intra-laminar fracture in angle-ply laminates. Compos Part A Appl Sci Manuf 1997;28:839–46.

[23] Tessema A, Ravindran S, Kidane A. Experimental Study of Residual Plastic Strain and Damages Development in Carbon Fiber Composite. Fract. Fatigue, Fail.

Damage Evol. Vol. 8, Springer; 2017, p. 31–6.

[24] Pipes RB. Moire analysis of the interlaminar shear edge effect in laminated composites. J Compos Mater 1971;5:255–9.

[25] Herakovich CT. Free edge effects in laminated composites.Failure in Comp. Vol. 4, 1989, 205-219.

[26] Berthelot J-M. Transverse cracking and delamination in cross-ply glass-fiber and carbon-fiber reinforced plastic laminates: Static and fatigue loading. Appl Mech Rev 2003;56:111–47.

[27] Mortell DJ, Tanner DA, McCarthy CT. An experimental investigation into multi-scale damage progression in laminated composites in bending. Compos Struct 2016;149:33–40.

[28] París F, Blázquez A, McCartney LN, Barroso A. Characterization and evolution of matrix and interface related damage in [0/90]S laminates under tension. Part II: Experimental evidence. Compos Sci Technol 2010;70:1176–83.

[29] Tong J, Guild FJ, Ogin SL, Smith PA. on Matrix Crack Growth in Quasi-Isotropic Laminates-I. Experimental Investigation. Compos Sci Technol Elsevier Sci Ltd 1997;57:1527–35.

[30] Tessema A, Mymers N, Patel R, Ravindran S, Kidane A. Experimental Investigation on the Correlation between Damage and Thermal Conductivity of CFRP. Proc. Am. Soc. Compos. Thirty-First Tech. Conf., 2016.

[31] Jamison RD, Schulte K, Reifsnider KL, Stinchcomb WW. Characterization and analysis of damage mechanisms in tension-tension fatigue of graphite/epoxy laminates. Eff. defects Compos. Mater., ASTM International; 1984.

[32] Tong J, Guild FJ, Ogin SL, Smith PA. On matrix crack growth in quasi-isotropic laminates—I. Experimental investigation. Compos Sci Technol 1997;57:1527–35.

[33] Berthelot J. Transverse cracking and delamination in cross-ply glass-fiber and carbon-fiber reinforced plastic laminates : Static and fatigue loading 2016:111–47.

[34] Li C, Ellyin F, Wharmby A. On matrix crack saturation in composite laminates.

Compos Part B Eng 2003;34:473–80.

[35] Kenneth Reifsnider SC. Damage Tolerance and Durability of Material Systems. 2002.

[36] Masters J, Reifsnider K. An Investigation of Cumulative Damage Development in Quasi-Isotropic Graphite/Epoxy Laminates, Damage in Composite Materials. ASTM STP 1982;775:40–62.

[37] Reifsnider KL, Stinchcomb WW. A critical-element model of the residual strength and life of fatigue-loaded composite coupons. Compos. Mater. Fatigue Fract., ASTM International; 1986.

[38] Singh CV, Talreja R. A synergistic damage mechanics approach for composite laminates with matrix cracks in multiple orientations. Mech Mater 2009;41:954–68.

[39] Varna J, Joffe R, Akshantala N V., Talreja R. Damage in composite laminates with off-axis plies. Compos Sci Technol 1999;59:2139–47.

[40] Tessema A, Zhao D, Kidane A, Kumar SK. Effect of micro-cracks on the thermal conductivity of particulate nanocomposite. Fract. Fatigue, Fail. Damage Evol. Vol. 8, Springer; 2016, p. 89–94.

[41] Samsur R, Rangari VK, Jeelani S, Zhang L, Cheng ZY. Fabrication of carbon nanotubes grown woven carbon fiber/epoxy composites and their electrical and mechanical properties. J Appl Phys 2013;113.

[42] Amrutharaj GS, Lam KY, Cotterell B. Delaminations at the free edge of a composite laminate. Compos Part B Eng 1996;27:475–83.

[43] Alton Highsmith KR. Stiffness-Reduction Mechanisms in Composite Laminates - Damage in Composite Materials: Basic Mechanisms, Accumulation, Tolerance, and Characterization. ASTM STP 1982;775:103–17.

[44] Reifsnider KL, Case SW. Damage tolerance and durability of material systems. WILEY; 2002.

[45] Crossman FW, Warren WJ. Initiation and Growth of Transverse Cracks and Edge Delamination in Composite Laminates Part 2. Experimental Correlation. J Compos

Mater Suppl 1980;14:88–108.

[46] Katerelos DTG, Kashtalyan M, Soutis C, Galiotis C. Matrix cracking in polymeric composites laminates: Modelling and experiments. Compos Sci Technol 2008;68:2310–7.

[47] Maimi. P, Camanho PP, Mayugo JA, Turon A. Matrix cracking and delamination in laminated composites. Part II: Evolution of crack density and delamination. Mech Mater 2011;43:194–211.

[48] O'brien T. Analysis of Local Delamination and Their Influence on Composite Laminate Behavior. ASTM STP 1985;876:282–97.

[49] Asadi A, Raghavan J. Model for prediction of simultaneous time-dependent damage evolution in multiple plies of multidirectional polymer composite laminates and its influence on creep. Compos Part B Eng 2015;79:359–73.

[50] Nairn J, Hu S. The initiation and growth of delamination induced by matrix microcracks in laminated composites. Int J Fract 1991;24:1–24.

[51] Liu S, Nairn JA. The Formation and Propagation of Matrix Microcracks in Cross-Ply Laminates during Static Loading 2016;ll:158–78.

[52] O'brien T. Damage in Composite Materials: Basic Mechanisms, Accumulation, Tolerance, and Characterization. ASTM STP 1982;775:140–67.

[53] Alter KW, Regal DM. NASA Contractor Report 4479. Control 2005.

[54] Nairn JA. Fracture mechanics of composites with residual stresses, traction-loaded cracks, and imperfect interfaces. Eur Struct Integr Soc 2000;27:111–21.

[55] Talreja R. A Continuum Mechanics Characterization of Damage in Composite Materials. Proc R Soc A Math Phys Eng Sci 1985;399:195–216.

[56] Varna J, Joffe R, Talreja R. A synergistic damage-mechanics analysis of transverse cracking [±Θ/90_4]s laminates. Compos Sci Technol 2001;61:657–65.

[57] Varna J, Talreja R. Integration of Macro- and MicroDamage Mechanics for the Performance Evaluation of Composite Materials. Mech Compos Mater 2012;48:1–16.

[58] Kashtalyan M, Soutis C. Analysis of local delaminations in composite laminates with angle-ply matrix cracks. Int J Solids Struct 2002;39:1515–37.

[59] Kashtalyan M, Soutis C. Stiffness and fracture analysis of laminated composites with off-axis ply matrix cracking. Compos Part A Appl Sci Manuf 2007;38:1262–9.

[60] Farge L, Ayadi Z, Varna J. Optically measured full-field displacements on the edge of a cracked composite laminate. Compos Part A Appl Sci Manuf 2008;39:1245–52.

[61] Farge L, Varna J, Ayadi Z. Damage characterization of a cross-ply carbon fiber/epoxy laminate by an optical measurement of the displacement field. Compos Sci Technol 2010;70:94–101.

[62] Liu YM, Mitchell TE, Wadley HNG. Anisotropic damage evolution in a $0^o/90^o$ laminated ceramic-matrix composite. Acta Mater 2000;48:4841–9.

[63] Rask M, Madsen B, Sørensen BF, Fife JL, Martyniuk K, Lauridsen EM. In situ observations of microscale damage evolution in unidirectional natural fibre composites. Compos Part A Appl Sci Manuf 2012;43:1639–49.

[64] Lomov S V., Ivanov DS, Truong TC, Verpoest I, Baudry F, Vanden Bosche K, et al. Experimental methodology of study of damage initiation and development in textile composites in uniaxial tensile test. Compos Sci Technol 2008;68:2340–9.

[65] Koohbor B, Ravindran S, Kidane A. Meso-scale study of non-linear tensile response and fiber trellising mechanisms in woven composites. J Reinf Plast Compos 2016.

[66] Koohbor B, Ravindran S, Kidane A. Meso-scale strain localization and failure response of an orthotropic woven glass–fiber reinforced composite. Compos Part B Eng 2015;78:308–18.

[67] Pollock P, Yu L, Sutton MA, Guo S, Majumdar P, Gresil M. Full-field measurements for determining orthotropic elastic parameters of woven glass-epoxy composites using off-axis tensile specimens. Exp Tech 2014;38:61–71.

[68] Ravindran S, Tessema A, Kidane A. Local Deformation and Failure Mechanisms of

Polymer Bonded Energetic Materials Subjected to High Strain Rate Loading. J Dyn Behav Mater 2016:1–11.

[69] Tessema A, Mitchell W, Koohbor B, Ravindra S, Kidane A, Van Tooren M. Effects of Nanoparticles on the Shear Properties of Polymer Composites. Am. Soc. Compos. Tech. Conf., 2015.

[70] Tessema A, Mitchell W, Koohbor B, Ravindran S, Kidane A, Van Tooren M. On the mechanical Response of Polymer fiber Composites reinforced with nanoparticles. Mech. Compos. Multi-functional Mater. Vol. 7, Springer; 2016, p. 125–30.

[71] Sutton MA, Orteu JJ, Schreier H. Image correlation for shape, motion and deformation measurements: basic concepts, theory and applications. Springer Science & Business Media; 2009.

[72] Tamuzs V, Dzelzitis K, Reifsnider K. Prediction of the cyclic durability of woven composite laminates. Compos Sci Technol 2008;68:2717–21.

[73] Ravindran S, Tessema A, Kidane A. Note: Dynamic meso-scale full field surface deformation measurement of heterogeneous materials. Rev Sci Instrum 2016;87:1–4.

[74] Koohbor B, Mallon S, Kidane A, Sutton MA. A DIC-based study of in-plane mechanical response and fracture of orthotropic carbon fiber reinforced composite. Compos Part B Eng 2014;66:388–99.

[75] Wang SD, Palo L. Intiation and growth of transverse cracks and edge delamination in Composite laminates, Part-1. An energy method, J of Comp. Mat. Supplemnt, 2015;14:71–87.

[76] Greenhalgh E. Failure analysis and fractography of polymer composites. Elsevier; 2009.

[77] Bishop SM, McLaughlin KS. Thickness effect and fracture mechanism in notched carbon-fibre composites. 1979.

[78] Siulie Liu, Nairn JA. The Formation and Propagation of Matrix Microcracks in

Cross-Ply Laminates during Static Loading. J Reinf Plast Compos 1992;11:158–78.

[79] O'Brien, T. Kevin, Hampton V, Chawan, Arun D., Demarco, Kevin, Blacksburg V, Paris, Isabelle, Hampton V., Influence of Specimen Preparation and Specimen Size on Composite Transverse Tensile Strength and Scatter. Hampton: 2001.

[80] Singh CV, Talreja R. Evolution of ply cracks in multidirectional composite laminates. Int J Solids Struct 2010;47:1338–49.

[81] Potter RT. The notch size effect in carbon fibre, glass fibre and kevlar reinforced plastics laminates. Farnborough, Hants GU146TD: 1981.

[82] Singh CV, Talreja R. International Journal of Solids and Structures Evolution of ply cracks in multidirectional composite laminates. Int J Solids Struct 2010;47:1338–49.

[83] Naghipour P, Bartsch M, Chernova L, Hausmann J, Voggenreiter H. Effect of fiber angle orientation and stacking sequence on mixed mode fracture toughness of carbon fiber reinforced plastics: Numerical and experimental investigations. Mater Sci Eng A 2010;527:509–17.

[84] Portella EH, Romanzini D, Angrizani CC, Amico SC, Zattera AJ. Influence of Stacking Sequence on the Mechanical and Dynamic Mechanical Properties of Cotton/Glass Fiber Reinforced Polyester Composites. Mater Res 2016;19:542–7.

[85] Ball AJ, Young R, Cervenka A. The Effect of Stacking Sequence Upon the Mechanical Properties of Thermoplastic Composite Laminates. Dev. Sci. Technol. Compos. Mater., Dordrecht: Springer Netherlands; 1990, p. 1031–6.

[86] Tessema A, Ravindran S, Wohlford A, Kidane A. In-Situ Observation of Damage Evolution in Quasi-Isotropic CFRP Laminates. Fract. Fatigue, Fail. Damage Evol. Vol. 7, Springer; 2018, p. 67–72.

[87] Tessema A, Ravindran S, Kidane A. Gradual Damage Evolution and Propagation in Quasi-Isotropic CFRC under Quasi-Static Loading. Compos Struct 2017.

[88] Naik NK, Asmelash A, Kavala VR, Ch V. Interlaminar shear properties of polymer matrix composites : Strain rate effect. Aerosp Eng n.d.

[89] Rebière J-L, Gamby D. Strain Energy Release Rate Analyse of Matrix Micro Cracking in Composite Cross-Ply Laminates. Mater Sci Appl 2011;2:537–45.

[90] Katerelos DTG, Varna J, Galiotis C. Energy criterion for modelling damage evolution in cross-ply composite laminates. Compos Sci Technol 2008;68:2318–24.

[91] Canal LP, González C, Molina-Aldareguía JM, Segurado J, Llorca J. Application of digital image correlation at the microscale in fiber-reinforced composites. Compos Part A Appl Sci Manuf 2012;43:1630–8.

[92] Singh CV, Talreja R. Analysis of multiple off-axis ply cracks in composite laminates. Int J Solids Struct 2008;45:4574–89.

CHAPTER 5
EXPERIMENTAL STUDY OF RESIDUAL PLASTIC STRAIN AND DAMAGES DEVELOPMENT IN CARBON FIBER COMPOSITE

5.1 ABSTRACT

In this work, experimental study is conducted to investigate the correlation between local damage, material residual stiffness and thermal conductivity in the carbon fiber composite. The study presents an explicit interaction between the damage mechanism developed and the global response of the laminate. The finding from this study is expected to fill the gap in visualizing the actual phenomenon during analytical or FEA modeling. A quasi-isotropic carbon reinforced composites is subjected to tension–tension fatigue loading and an in-situ digital image correlation (DIC) technique at high magnification is used to capture the initiation and propagation of micro cracks at different cycles. The thermal conductivity is measured using a modified transient plane source technique. During the test, images of a speckled surface of the specimen are captured at specified number of loading cycles.

The gradual growth of local plastic deformation as a function of loading cycle is acquired and different damage modes as a function of loading cycle is explored.

A. Tessema, S. Ravindran and A. Kidane, Proceedings of the American Society for Composites 2016, 31st Technical Conference on Composite Materials

Further, the study has elucidated the gradual growth of matrix cracking and the formation of inter-ply debonding. The gradual growth of local cracks and its corresponding influence on the change in thermal conductivity of the laminate at different fatigue cycles are acquired. Thereby, the effect of local damages on the heat flow and thermal conductivity of the laminate is understood. Similarly, the change in modulus of elasticity with the crack growth is elaborated. Finally, an explicit correlation between the degradation of thermal conductivity and modulus of elasticity is described.

5.2 INTRODUCTION

In composite design, the orientation of the dominant stresses' guides and tailor the arrangement and stacking of fibers/plies within the laminate structures. In most designs, the plies arranged in a fashion that it is favored to sustain the anticipated major loads efficiently. For instance, fibers are aligned in a direction where the major tensile load is oriented, and in some cases, fibers are arranged at a certain angle deviated from the given load to provide the necessary shear and transverse stiffness within a laminate. In current industries, it has become convenient to manufacture laminates with a multi-direction fiber orientation such as cross-ply and quasi-isotropic laminates. Even though multi-directional laminates have their own advantage, for the plies which the fibers are oriented in deviation from the major loading directions, will be susceptible to loading transverse to the fiber axis and this easily induce damage within the laminate.

Intensive studies have been made to investigate how the damage is caused, under what conditions and the mechanism the damage evolve. It is found that there are various types of damages appeared in laminates; transverse cracking, ply delamination, fiber

splitting and fiber breaking, are the dominant one. Usually two or more forms of damage are seen to appear in the laminate for a given loading. In a certain case, one form of damage leads to the formation of the other one. In general, the form, the size and quantity of damage are mainly influenced by the type of loading scheme, thickness of laminate, the geometry of the structure, ply orientation and stacking sequence [29,35].

Numerous theoretical formulations and analytical models have been developed to understand the initiation and growth of damages within the laminate. Further, studies have been applied to elaborate the relation between the damage type, size and quantity with mechanical properties of the laminate. Moreover, the models have shown the influence of damage type, density and location, on the change/degradation in the mechanical properties. These theories are based on, classical laminate theory [35], fracture mechanics [59,89], energy method [46,90]and constitutive/elasticity model [50,76].However, these models lacks depicting the actual phenomenon and has reservations in predicting and simulating the damage initiation and evolution. Thus, experimental works are required to understanding the damage evolution. In addition, experimental verification is required on the correlation between the damage growth and the degradation of mechanical and thermal properties of the laminate.

For this matter, numerous experimental works [32,45,46,59,89] have been established to recognize the initiation and evolution of damages from micro level to the final failure of the composite. However, due to inadequate experimental techniques that enable to capture the gradual development of damage in-situ and its influence on the mechanical response of the material is not well understood. Recently, digital image correlation technique (DIC) has been applied in understanding material deformation at

different length scale from macro to nano-scale[68–70,85]. Most recently, DIC has been effectively used to get the strain localization in composites at meso [65,66,91] and micro [65,70,92] scales. These small-scale strain localizations have been helpful in establishing and clarifying the correlation between the very small microstructural element and its displacement with macro scale deformation. High magnification imaging apparatus, such as optical microscope and Scanning Electron Microscopes (SEM) has been used to capture consecutive images during deformation.

The main objective of this study is to evaluate the gradual evolution of damage in composites during fatigue loading using in-situ DIC technique at high magnification. The initiation and propagation of micro cracks at different cycle will be captured. In parallel, by measuring the corresponding elastic modulus and thermal conductivity degradation at a certain interval of cycles, the correlation between the damage and the change in material property is examined. Further, the explicit relation between the thermal conductivity and modulus of elasticity with progressively growing damage is investigated.

5.3 MATERIALS AND EXPERIMENTAL METHODS

5.3.1 Material preparation and specimen geometry

As manufactured unidirectional carbon Prepregs (TC350-1) purchased from Royal TenCate Cooperate are used to prepare laminate panels. The Prepregs are cut in square of 150mmX150mm size at 0^o and 45^o fiber angle orientation using a scissor. The Prepreg cut outs are stacked in the required sequence (±45/90/0)s by arranging the orientation of the prepregs. Following, the stack is placed in the plastic bag and kept in between two steel mold plates. The mold is placed in a hot press machine and clamped between two heating

platens at a pressure of 0.35 tons and set to the curing temperatures recommended by the manufacturer. The curing cycle has three stages, first the platens are heated up to temperature of 225^{o}F at rate of 2^{o}F/min and kept for 1 hour, then it is further heated to temperature of 350^{o}F at the same rate and kept for 2.5 hours, and the machine is cooled to a temperature of 120^{o}F at the rate of 5^{o}F/min. Finally, the cured laminate is taken out of the hot press and let to cool down to room temperature by the natural convection.

Rectangular samples (140mmX22mm) are cut from the cured laminate using CNC water jet in accordance to ASTM D3930 standard. Following, the side edges of the coupons are polished with different grade of sandpaper to remove any form of debris and notches formed during the abrasive water jet cutting. Further, Fiberglass tabs are glued on the two ends of the specimen to protect the damage on the fiber from the grip pressure during the experiment (see Figure 5.1). For the convenience of applying digital image correlation, black and white speckle patterns are applied on the specimen surface where full-field strain is required. The specimen is speckled at two distinct regions, one is on the thickness edge side and the other is on the width side of the samples. The speckles on edge side are micro scale approximately 6~16 μm in size and these speckles are used to capture the local residual strain concentration and damage formation across the thickness. On the other hand, the speckles on the width side had an approximate size of 250~300 μm and it is used to obtain the laminate global average strain.

5.3.2 Experimental method

5.3.2.1 Mechanical test

Tension-tension fatigue experiment is conducted using Material Testing System (MTS 810) machine in accordance with ASTM D3479 standard as shown in Figure 5.1. The MTS machine is adjusted to perform two distinct loading schemes alternatively, monotonic quasi-static tension and fatigue loading schemes. The monotonic quasi-static loading is performed to determine the modulus of elasticity of the laminate in between certain fatigue cycles. The quasi-static load is applied in displacement-controlled mode at the rate of 0.01mm/min up to stress of 200MPa (i.e. 30% of the failure stress). Conversely, the fatigue test is executed in load-controlled mode with mean stress of 165MPa and amplitude stress of 135MPa at a frequency of 5Hz. The two tests are performed independently at different fatigue cycles intervals.

The experimental setup with two 2D digital image correlation (2D-DIC) set at speckled regions is shown on Figure 5.1 (a). The two DIC setups are designated for the corresponding speckled regions, for the micro speckled region (on the side of the laminate) a 9MPixels CCD (Grasshopper) camera and a 3X magnification lens is used to capture the images with area of interest approximately (i.e. 3.5mmX1mm) at an object distance of 20mm. Images of the micro speckle region are captured by stopping the fatigue cycle and unloaded the coupon at a certain interval cycles. On the other side, the macro speckled region is used for the quasi-isotropic loading scheme, thus the images are acquired simultaneously with the loading at a framing rate of 1fps using 9MPixel CCD camera incorporated with 60mm Nikon lenses. The acquired images from both DIC setups are post

processed using VIC-2D commercial software. Thereby, the full-field axial, transverse and shear strain data are obtained at local and global levels.

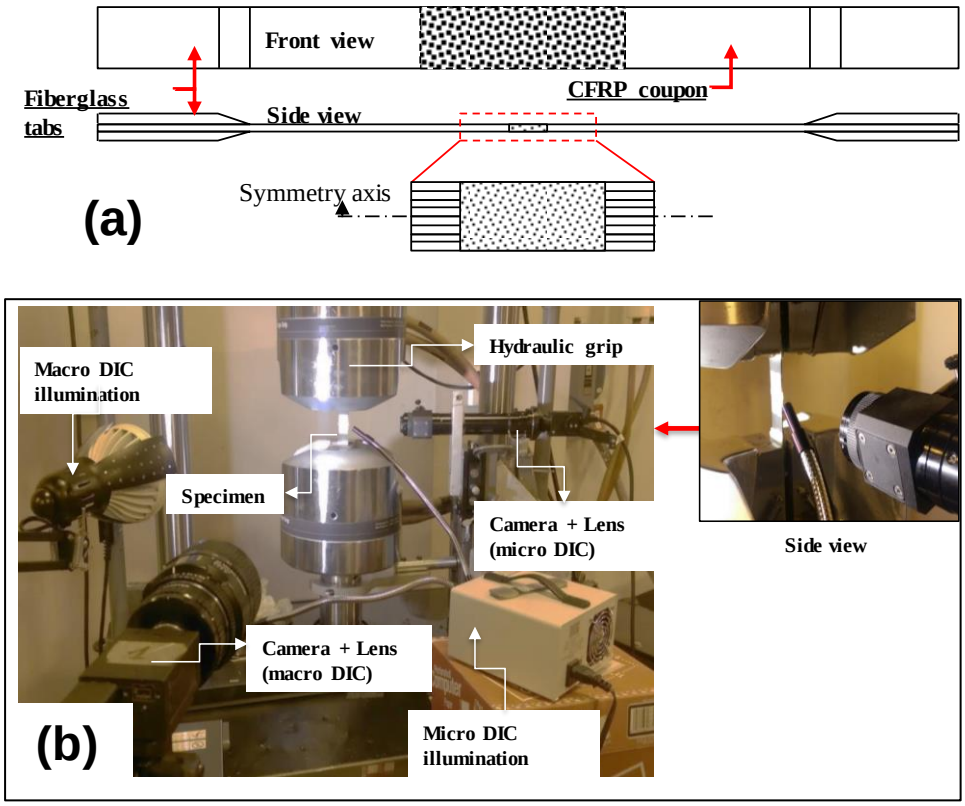

Figure 5.1: (a) Test coupon sample with macro speckles and side view with micro speckles and (b) Mechanical test setup.

5.3.2.2 Thermal conductivity test

The thermal conductivity (across the thickness) of the laminate is measured by applying a modified transient plane source (MTPS) technique using C-Thermal TCi Thermal Conductivity Analyzer. The experimental setup is depicted in the Figure 5.2, the C-thermal device has incorporated controlling unit, a user interface laptop and plane heating stage. The specimen is placed on the top of the cylindrical plane heating stage. During the test a 200-gm weight is placed on the top of the specimen to create an air sealed

contact between the specimen and the heating surface. Based on the manufacturer recommendation, water is used as a contact agent between the laminate and the heating surface. A spiral heating coil is used to supply heat to the specimen, and it is also used as a sensor to capture the temperature change on the heating surface during test. The thermal conductivity is calculated based on the amount of heat effused from heating surface to the specimen. The thermal conductivity test is performed at different fatigue cycle intervals corresponding to the quasi-static tension test.

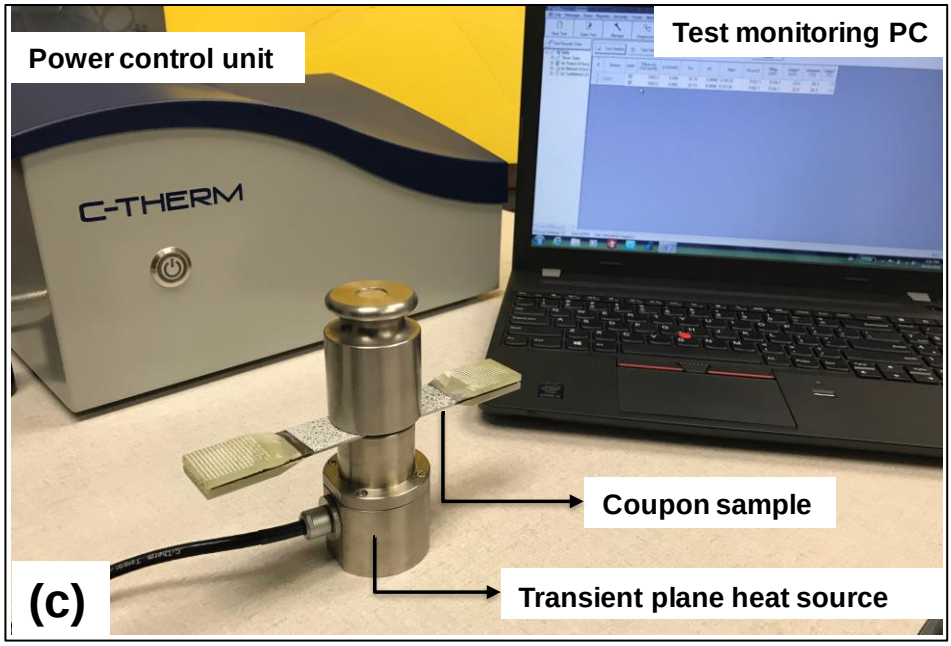

Figure 5.2: Thermal conductivity measurement test setup.

5.4 RESULT AND DISCUSSION

5.4.1 Damage evolution

The local residual axial strain contours across the thickness plane of the coupon laminate at different stage of fatigue cycle is depicted in Figure 5.3. From the strain

contours, small strain localizations are noticed starting from the early stage of the fatigue cycle, these localizations are observed to multiply so quickly and spread throughout the 90^o ply within our field of view. Later on, these strain localizations are turned to spots where the matrix/transverse cracks are initiated. The primary matrix cracks are initiated in the 90^o plies, where the fibers are oriented off-axis from the loading and the ply is the weakest among the plies. The primary matrix cracks are initiated around couple of hundreds of cycles. As the fatigue cycle advances more cracks are observed to emerge in the 90^o ply and the adjacent $+45^o$ plies. Most of the matrix cracks are initiated at the middle of the 90^o plies and advanced to the interfaces of the adjacent neighboring plies in the two vertical directions. Once it reached the interfaces, further growth of the crack is influenced by the relative alignment of the fibers in the neighboring plies relative to the crack direction. In most instances, the crack is deflected its direction and followed the inter-ply interface by delaminating the adjacent plies.

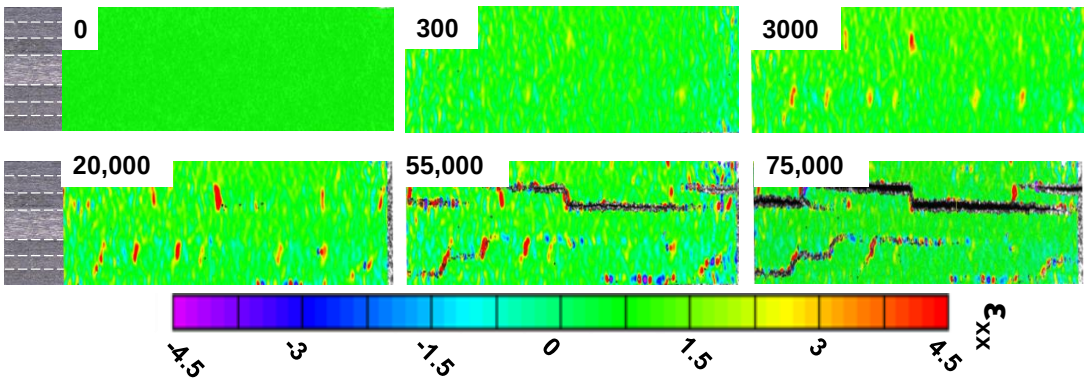

Figure 5.3: Residual axial strain contour and gradual micro damage evolution at different fatigue cycles.

5.4.2 Crack Density (d) and Elastic Modulus (E) degradation

The matrix crack density (d) variation along with the fatigue cycles are shown in the Figure 4. The crack density is measured based on the matrix crack counts within the field of view at different cycles. The field of view is approximately 3.5 mmX1mm in size, and this area covers the whole thickness section of the laminate. As it is shown in the Figure 5.4, the crack density (d) sharply increased starting from the early stage to 750 cycles. Afterwards, the crack density increments relatively slowed down and after a while it became stable/constant which is show the saturation of matrix crack formation.

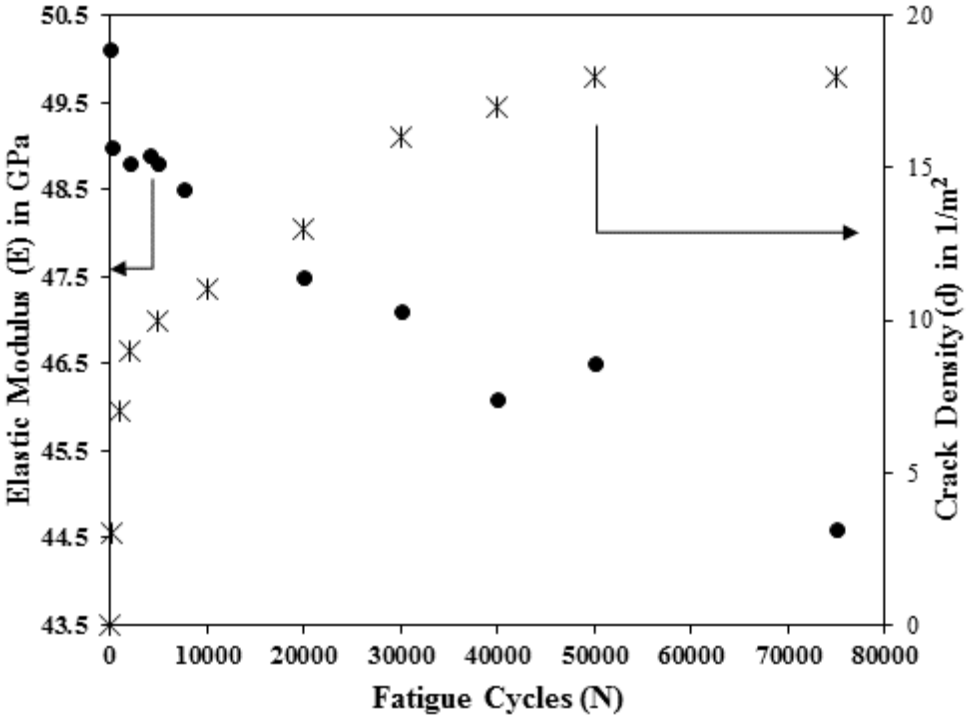

Figure 5.4: Variation in crack density (d) and modulus of elasticity (E) at different fatigue cycles (N).

In parallel to the crack density, the effective elastic modulus (E) is measured at certain interval of fatigue cycle and the laminate is observed to degrade with the fatigue cycle (see Figure 5.4). Various degradation trends are observed, at the early stage of the fatigue cycle

the modulus of elasticity dropped suddenly, and as the fatigue cycle advances the modulus decreased at a nearly constant rate. The trend and rate of degradation is seen to correspond with the quantity and form of cracks generated within the laminate. The initial large drop in elastic modulus is followed the emergence of immense matrix cracks. Further, with the decrease in matrix crack formation rate and growth in matrix cracks size a slower rate of degradation is recorded. Finally, with the emergence of delamination further decrease in the modulus elasticity is encountered.

5.4.3 Thermal conductivity degradation

The thermal conductivity (K) results obtained from the experiment along with the fatigue cycle are depicted in the Figure 5.5. Similar to the plot of elastic modulus, the thermal conductivity has shown a sharp drop in the first few hundreds of cycles. As seen in the Figure 5.5, the sudden drop in thermal conductivity is occurred at the instances where there is higher increment in matrix crack density. For further with increasing in fatigue cycle, the rate at which the thermal conductivity degrade is very small where the emergence of new crack formation is relatively slow. At the instant where the delamination started (around 30,000-40,000 cycles), the thermal conductivity showed another sudden drop and keeps declining further to the rest of the cycles. Here it should be noticed that in most polymer composite, the heat energy is carried by the molecular chain vibration which known as Phonons. Whereas it is obvious that the formation and growth of cracks break and dismantle the molecular bonds within the polymer chains, in such it induces discontinuities within the material/resin network. Those discontinuities cause interruption in the chained phonon vibration and have direct influence on the reduction of thermal

conductivity. Thus, the quantity and size of matrix cracking presented in the material have a sound interaction with the degradation rate of thermal conductivity. Particularly, due to the emergence of delaminating cracks the adjacent plies separated, and this separation induces absence of a direct contact between the two adjacent plies. Therefore, the transverse phonon vibration, which carry and channel the heat across the plies, is hindered by the discontinuity found in the material network due to delamination.

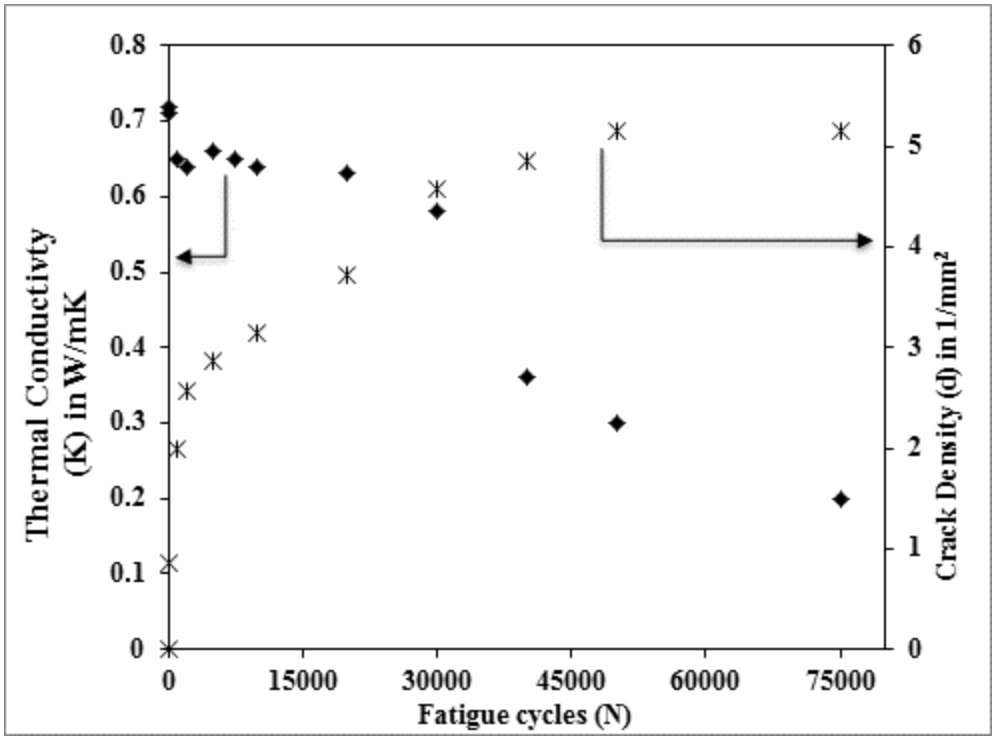

Figure 5.5: Combined plot of Thermal conductivity degradation and crack density growth.

5.4.4 Thermal conductivity and Modulus of Elasticity

For comparing and relating the two material properties Figure 5.6 has depicted both the elastic modulus and thermal conductivity degradation, and a noticeable similarity in trend is seen between the two properties. Features such as sudden drops at an early stage

of the fatigue, a relatively slower rate of degradation near matrix cracks saturation and higher rate of degradation when delamination is initiated, are common in both trends. Thus, presence of damage in the laminate is the basic phenomenon that influence the properties commonly and it can be used to correlate the degradation of the thermal conductivity and the elastic modulus. The contributions of the damaged plies on the mechanical and thermal response of the laminate is gradual, in the other way, it is possible to explicitly interrelate the mechanical response with damage characteristics and thermal response of the laminate. This in turn can facilitate the way to determine very inconvenient laminate properties with

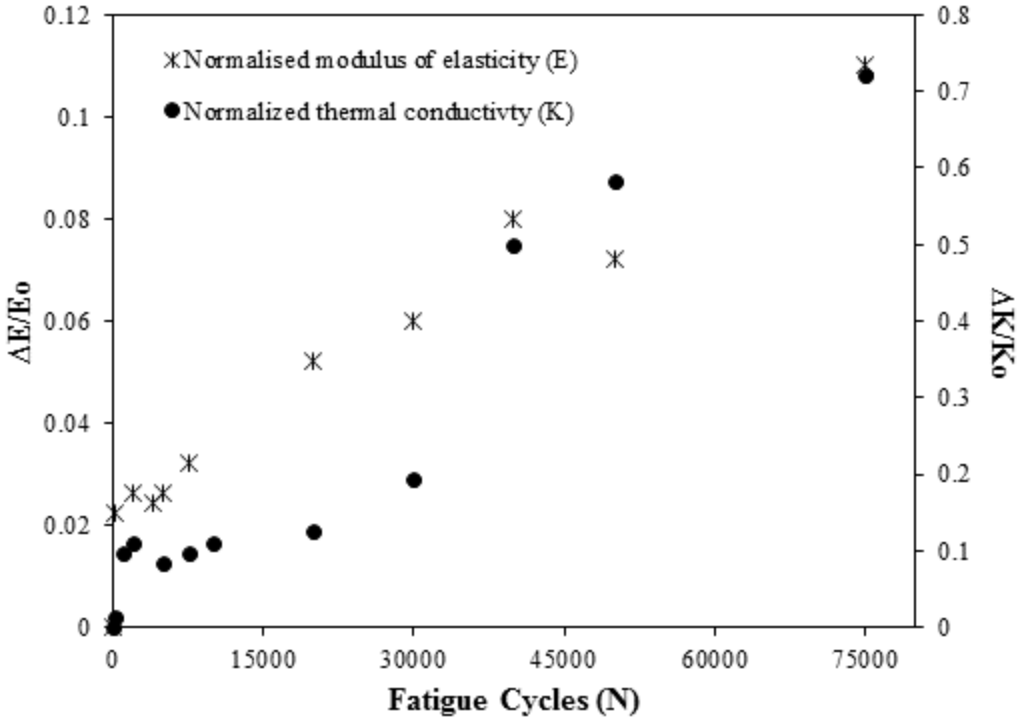

Figure 5.6: The combined plot of the thermal conductivity (K) and elastic modulus (E) degradation.

other one which convenient to measure.

5.5 SUMMARY

Using a high magnification optical digital image correlation technique, the local residual strain distribution in composites is analyzed. The progressive growth of damages within the quasi-isotropic laminate is captured along with degradation in modulus of elasticity at different fatigue cycles. In parallel to the damage growth, the change in thermal conductivity of the laminate is measured. The corresponding influence of damage types (matrix cracking and delamination) on the degradation of modulus of elasticity and thermal conductivity is emphasized. It is found that, matrix cracking and delamination has an almost the same effect on the degradation of the modulus. On the other hand, the thermal conductivity is observed to deteriorate at higher rates during delamination than matrix cracking stages. In sum up, both properties have shown a similar degradation trend, an appreciable explicit correlation between the properties is obtained.

5.6 LIST OF REFERENCES

[1] Nettles AT. Basic Mechanics of Laminated Composite Plates. NASA Ref Pulication 1994:107.

[2] Kaddour AS, Hinton MJ, Smith PA, Li S. A comparison between the predictive capability of matrix cracking, damage and failure criteria for fibre reinforced composite laminates: Part A of the third world-wide failure exercise. J Compos Mater 2013;47:2749–79.

[3] Talreja R. Assessment of the fundamentals of failure theories for composite materials. Compos Sci Technol 2014;105:190–201.

[4] Tahani M, Nosier A. Free edge stress analysis of general cross-ply composite laminates under extension and thermal loading. Compos Struct 2003;60:91–103.

[5] Kassapoglou C, Lagace PA. An Efficient Method for the Calculation of Interlaminar

Stresses in Composite Materials. J Appl Mech 1986;53:744.

[6] Mittelstedt C, Becker W. Free-Edge Effects in Composite Laminates. Appl Mech Rev 2007;60:217.

[7] Murthy P, Chamis C. Free-edge delamination: laminate width and loading condition effects. Nasa_Tm-100238 1987.

[8] Nailadi CL, Adams DF, Adams DO. An Experimental and Numerical Investigation of the Free Edge Problem in Composite Laminates. J Reinf Plast Compos 2002;21:3–39.

[9] Pagano NJ, Pipes RB. The Influence of Stacking Sequence on Laminate Strength. J Compos Mater 1971;5:50–7.

[10] Buczek MB, Czarnek R. Free edge strain concentrations in real composite laminates: experimental-theoretical correlation. J Appl Mech 1985;52:787.

[11] Mittelstedt C, Becker W. Free-Edge Effects in Composite Laminates. Appl Mech Rev 2007;60:217.

[12] Lecomte-Grosbras P, Réthoré J, Limodin N, Witz JF, Brieu M. Three-Dimensional Investigation of Free-Edge Effects in Laminate Composites Using X-ray Tomography and Digital Volume Correlation. Exp Mech 2015;55:301–11.

[13] Nosier A, Maleki M. Free-edge stresses in general composite laminates. Int J Mech Sci 2008;50:1435–47.

[14] Corporation D. Analysis of the Interlaminar Shear Edge Effect in Laminated Composites * 1971;5:255–9.

[15] Pipes RB. Composite Laminates Under Uniform Axial Extension 2016:538–48.

[16] Joo JWW, Sun CTT. A Failure Criterion for Laminates Governed by Free Edge Interlaminar Shear-Stress. J Compos Mater 1992;26:1510–22.

[17] Whitney JM, Browning CE, Division NM. Free-Edge Delamination of Tensile attributed 1972:300–3.

[18] Riccio A, Mozzillo G, Scaramuzzino F. Stacking sequence effects on fatigue intra-

laminar damage progression in composite joints. Appl Compos Mater 2013;20:249–73.

[19] Mittelstedt C, Becker W. Interlaminar Stress Concentrations in Layered Structures: Part I - A Selective Literature Survey on the Free-Edge Effect since 1967. J Compos Mater 2004;38:1037–62.

[20] Pagano J, Pipes RB. The Influence of Stacking Sequence Laminate Strength 2016;5:50–7.

[21] Fenske MT, Vizzini AJ. The Inclusion of In-Plane Stresses in Delamination Criteria. J Compos Mater 2001;35:1325–42.

[22] Crocker LE, Ogin SL, Smith PA, Hill PS. Intra-laminar fracture in angle-ply laminates. Compos Part A Appl Sci Manuf 1997;28:839–46.

[23] Tessema A, Ravindran S, Kidane A. Experimental Study of Residual Plastic Strain and Damages Development in Carbon Fiber Composite. Fract. Fatigue, Fail. Damage Evol. Vol. 8, Springer; 2017, p. 31–6.

[24] Pipes RB. Moire analysis of the interlaminar shear edge effect in laminated composites. J Compos Mater 1971;5:255–9.

[25] Herakovich CT. Free edge effects in laminated composites.Failure in Comp. Vol. 4, 1989, 205-219.

[26] Berthelot J-M. Transverse cracking and delamination in cross-ply glass-fiber and carbon-fiber reinforced plastic laminates: Static and fatigue loading. Appl Mech Rev 2003;56:111–47.

[27] Mortell DJ, Tanner DA, McCarthy CT. An experimental investigation into multi-scale damage progression in laminated composites in bending. Compos Struct 2016;149:33–40.

[28] París F, Blázquez A, McCartney LN, Barroso A. Characterization and evolution of matrix and interface related damage in [0/90]S laminates under tension. Part II: Experimental evidence. Compos Sci Technol 2010;70:1176–83.

[29] Tong J, Guild FJ, Ogin SL, Smith PA. On Matrix Crack Growth in Quasi-Isotropic Laminates-I. Experimental Investigation. Compos Sci Technol Elsevier Sci Ltd 1997;57:1527–35.

[30] Tessema A, Mymers N, Patel R, Ravindran S, Kidane A. Experimental Investigation on the Correlation between Damage and Thermal Conductivity of CFRP. Proc. Am. Soc. Compos. Thirty-First Tech. Conf., 2016.

[31] Jamison RD, Schulte K, Reifsnider KL, Stinchcomb WW. Characterization and analysis of damage mechanisms in tension-tension fatigue of graphite/epoxy laminates. Eff. defects Compos. Mater., ASTM International; 1984.

[32] Tong J, Guild FJ, Ogin SL, Smith PA. On matrix crack growth in quasi-isotropic laminates—I. Experimental investigation. Compos Sci Technol 1997;57:1527–35.

[33] Berthelot J. Transverse cracking and delamination in cross-ply glass-fiber and carbon-fiber reinforced plastic laminates : Static and fatigue loading 2016:111–47.

[34] Li C, Ellyin F, Wharmby A. On matrix crack saturation in composite laminates. Compos Part B Eng 2003;34:473–80.

[35] Kenneth Reifsnider SC. Damage Tolerance and Durability of Material Systems. 2002.

[36] Masters J, Reifsnider K. An Investigation of Cumulative Damage Development in Quasi-Isotropic Graphite/Epoxy Laminates, Damage in Composite Materials. ASTM STP 1982;775:40–62.

[37] Reifsnider KL, Stinchcomb WW. A critical-element model of the residual strength and life of fatigue-loaded composite coupons. Compos. Mater. Fatigue Fract., ASTM International; 1986.

[38] Singh CV, Talreja R. A synergistic damage mechanics approach for composite laminates with matrix cracks in multiple orientations. Mech Mater 2009;41:954–68.

[39] Varna J, Joffe R, Akshantala N V., Talreja R. Damage in composite laminates with off-axis plies. Compos Sci Technol 1999;59:2139–47.

[40] Tessema A, Zhao D, Kidane A, Kumar SK. Effect of micro-cracks on the thermal conductivity of particulate nanocomposite. Fract. Fatigue, Fail. Damage Evol. Vol. 8, Springer; 2016, p. 89–94.

[41] Samsur R, Rangari VK, Jeelani S, Zhang L, Cheng ZY. Fabrication of carbon nanotubes grown woven carbon fiber/epoxy composites and their electrical and mechanical properties. J Appl Phys 2013;113.

[42] Amrutharaj GS, Lam KY, Cotterell B. Delaminations at the free edge of a composite laminate. Compos Part B Eng 1996;27:475–83.

[43] Alton Highsmith KR. Stiffness-Reduction Mechanisms in Composite Laminates - Damage in Composite Materials: Basic Mechanisms, Accumulation, Tolerance, and Characterization. ASTM STP 1982;775:103–17.

[44] Reifsnider KL, Case SW. Damage tolerance and durability of material systems. WILEY; 2002.

[45] Crossman FW, Warren WJ. Initiation and Growth of Transverse Cracks and Edge Delamination in Composite Laminates Part 2. Experimental Correlation. J Compos Mater Suppl 1980;14:88–108.

[46] Katerelos DTG, Kashtalyan M, Soutis C, Galiotis C. Matrix cracking in polymeric composites laminates: Modelling and experiments. Compos Sci Technol 2008;68:2310–7.

[47] Maimi. P, Camanho PP, Mayugo JA, Turon A. Matrix cracking and delamination in laminated composites. Part II: Evolution of crack density and delamination. Mech Mater 2011;43:194–211.

[48] O'brien T. Analysis of Local Delamination and Their Influence on Composite Laminate Behavior. ASTM STP 1985;876:282–97.

[49] Asadi A, Raghavan J. Model for prediction of simultaneous time-dependent damage evolution in multiple plies of multidirectional polymer composite laminates and its influence on creep. Compos Part B Eng 2015;79:359–73.

[50] Nairn J, Hu S. The initiation and growth of delamination induced by matrix microcracks in laminated composites. Int J Fract 1991;24:1–24.

[51] Liu S, Nairn JA. The Formation and Propagation of Matrix Microcracks in Cross-Ply Laminates during Static Loading 2016;ll:158–78.

[52] O'brien T. Damage in Composite Materials: Basic Mechanisms, Accumulation, Tolerance, and Characterization. ASTM STP 1982;775:140–67.

[53] Alter KW, Regal DM. NASA Contractor Report 4479. Control 2005.

[54] Nairn JA. Fracture mechanics of composites with residual stresses, traction-loaded cracks, and imperfect interfaces. Eur Struct Integr Soc 2000;27:111–21.

[55] Talreja R. A Continuum Mechanics Characterization of Damage in Composite Materials. Proc R Soc A Math Phys Eng Sci 1985;399:195–216.

[56] Varna J, Joffe R, Talreja R. A synergistic damage-mechanics analysis of transverse cracking [±Θ/90_4]s laminates. Compos Sci Technol 2001;61:657–65.

[57] Varna J, Talreja R. Integration of Macro- and MicroDamage Mechanics for the Performance Evaluation of Composite Materials. Mech Compos Mater 2012;48:1–16.

[58] Kashtalyan M, Soutis C. Analysis of local delaminations in composite laminates with angle-ply matrix cracks. Int J Solids Struct 2002;39:1515–37.

[59] Kashtalyan M, Soutis C. Stiffness and fracture analysis of laminated composites with off-axis ply matrix cracking. Compos Part A Appl Sci Manuf 2007;38:1262–9.

[60] Farge L, Ayadi Z, Varna J. Optically measured full-field displacements on the edge of a cracked composite laminate. Compos Part A Appl Sci Manuf 2008;39:1245–52.

[61] Farge L, Varna J, Ayadi Z. Damage characterization of a cross-ply carbon fiber/epoxy laminate by an optical measurement of the displacement field. Compos Sci Technol 2010;70:94–101.

[62] Liu YM, Mitchell TE, Wadley HNG. Anisotropic damage evolution in a $0^o/90^o$ laminated ceramic-matrix composite. Acta Mater 2000;48:4841–9.

[63] Rask M, Madsen B, Sørensen BF, Fife JL, Martyniuk K, Lauridsen EM. In situ observations of microscale damage evolution in unidirectional natural fibre composites. Compos Part A Appl Sci Manuf 2012;43:1639–49.

[64] Lomov S V., Ivanov DS, Truong TC, Verpoest I, Baudry F, Vanden Bosche K, et al. Experimental methodology of study of damage initiation and development in textile composites in uniaxial tensile test. Compos Sci Technol 2008;68:2340–9.

[65] Koohbor B, Ravindran S, Kidane A. Meso-scale study of non-linear tensile response and fiber trellising mechanisms in woven composites. J Reinf Plast Compos 2016.

[66] Koohbor B, Ravindran S, Kidane A. Meso-scale strain localization and failure response of an orthotropic woven glass–fiber reinforced composite. Compos Part B Eng 2015;78:308–18.

[67] Pollock P, Yu L, Sutton MA, Guo S, Majumdar P, Gresil M. Full-field measurements for determining orthotropic elastic parameters of woven glass-epoxy composites using off-axis tensile specimens. Exp Tech 2014;38:61–71.

[68] Ravindran S, Tessema A, Kidane A. Local Deformation and Failure Mechanisms of Polymer Bonded Energetic Materials Subjected to High Strain Rate Loading. J Dyn Behav Mater 2016:1–11.

[69] Tessema A, Mitchell W, Koohbor B, Ravindra S, Kidane A, Van Tooren M. Effects of Nanoparticles on the Shear Properties of Polymer Composites. Am. Soc. Compos. Tech. Conf., 2015.

[70] Tessema A, Mitchell W, Koohbor B, Ravindran S, Kidane A, Van Tooren M. On the mechanical Response of Polymer fiber Composites reinforced with nanoparticles. Mech. Compos. Multi-functional Mater. Vol. 7, Springer; 2016, p. 125–30.

[71] Sutton MA, Orteu JJ, Schreier H. Image correlation for shape, motion and deformation measurements: basic concepts, theory and applications. Springer

Science & Business Media; 2009.

[72] Tamuzs V, Dzelzitis K, Reifsnider K. Prediction of the cyclic durability of woven composite laminates. Compos Sci Technol 2008;68:2717–21.

[73] Ravindran S, Tessema A, Kidane A. Note: Dynamic meso-scale full field surface deformation measurement of heterogeneous materials. Rev Sci Instrum 2016;87:1–4.

[74] Koohbor B, Mallon S, Kidane A, Sutton MA. A DIC-based study of in-plane mechanical response and fracture of orthotropic carbon fiber reinforced composite. Compos Part B Eng 2014;66:388–99.

[75] Wang SD, Palo L. Intiation and growth of transverse cracks and edge delamination in Composite laminates, Part-1. An energy method, J of Comp. Mat. Supplemnt, 2015;14:71–87.

[76] Greenhalgh E. Failure analysis and fractography of polymer composites. Elsevier; 2009.

[77] Bishop SM, McLaughlin KS. Thickness effect and fracture mechanism in notched carbon-fibre composites. 1979.

[78] Siulie Liu, Nairn JA. The Formation and Propagation of Matrix Microcracks in Cross-Ply Laminates during Static Loading. J Reinf Plast Compos 1992;11:158–78.

[79] O'Brien, T. Kevin, Hampton V, Chawan, Arun D., Demarco, Kevin, Blacksburg V, Paris, Isabelle, Hampton V., Influence of Specimen Preparation and Specimen Size on Composite Transverse Tensile Strength and Scatter. Hampton: 2001.

[80] Singh CV, Talreja R. Evolution of ply cracks in multidirectional composite laminates. Int J Solids Struct 2010;47:1338–49.

[81] Potter RT. The notch size effect in carbon fibre, glass fibre and kevlar reinforced plastics laminates. Farnborough, Hants GU146TD: 1981.

[82] Singh CV, Talreja R. International Journal of Solids and Structures Evolution of ply cracks in multidirectional composite laminates. Int J Solids Struct 2010;47:1338–

49.

[83] Naghipour P, Bartsch M, Chernova L, Hausmann J, Voggenreiter H. Effect of fiber angle orientation and stacking sequence on mixed mode fracture toughness of carbon fiber reinforced plastics: Numerical and experimental investigations. Mater Sci Eng A 2010;527:509–17.

[84] Portella EH, Romanzini D, Angrizani CC, Amico SC, Zattera AJ. Influence of Stacking Sequence on the Mechanical and Dynamic Mechanical Properties of Cotton/Glass Fiber Reinforced Polyester Composites. Mater Res 2016;19:542–7.

[85] Ball AJ, Young R, Cervenka A. The Effect of Stacking Sequence Upon the Mechanical Properties of Thermoplastic Composite Laminates. Dev. Sci. Technol. Compos. Mater., Dordrecht: Springer Netherlands; 1990, p. 1031–6.

[86] Tessema A, Ravindran S, Wohlford A, Kidane A. In-Situ Observation of Damage Evolution in Quasi-Isotropic CFRP Laminates. Fract. Fatigue, Fail. Damage Evol. Vol. 7, Springer; 2018, p. 67–72.

[87] Tessema A, Ravindran S, Kidane A. Gradual Damage Evolution and Propagation in Quasi-Isotropic CFRC under Quasi-Static Loading. Compos Struct 2017.

[88] Naik NK, Asmelash A, Kavala VR, Ch V. Interlaminar shear properties of polymer matrix composites : Strain rate effect. Aerosp Eng n.d.

[89] Rebière J-L, Gamby D. Strain Energy Release Rate Analyse of Matrix Micro Cracking in Composite Cross-Ply Laminates. Mater Sci Appl 2011;2:537–45.

[90] Katerelos DTG, Varna J, Galiotis C. Energy criterion for modelling damage evolution in cross-ply composite laminates. Compos Sci Technol 2008;68:2318–24.

[91] Canal LP, González C, Molina-Aldareguía JM, Segurado J, Llorca J. Application of digital image correlation at the microscale in fiber-reinforced composites. Compos Part A Appl Sci Manuf 2012;43:1630–8.

[92] Singh CV, Talreja R. Analysis of multiple off-axis ply cracks in composite laminates. Int J Solids Struct 2008;45:4574–89.

CHAPTER 6

SUMMARY AND RECOMMENDATIONS

6.1 SUMMARY

Digital Image Correlation (DIC) technique is successfully implemented to obtain the full-field strain contour during uniaxial tension and fatigue tests. In this experimental setup, two distinct digital imaging sets are applied at two different region of coupon laminate sample. These two DIC sets have incorporated gray scale cameras and different scale magnification lenses. This technique has provided an adequate means to evaluate the strains on two distinct surfaces of the laminate coupons and the technique is advantageous in its capability to capture and quantify the full-field in-plane displacement and strain contours for a given surface. Further, it enables to provide a visual observation of the deforming body and fracturing spot. In particular, the study focused to capture the strain localization observed at the free-edge of the coupon sample using DIC. It is applied to verify the strain localization and the gradual damage evolution at the free-edge.

When it come to the experimental results, there are four group of test sets. The first set of experiment is performed on quasi-isotropic laminate with stacking arrangement of (-45/+45/90/0)s. A high magnification digital image correlation technique was used to capture the full-field local deformation and failure mechanisms at the free-edge of the coupon. Several valuable findings are obtained from this experiment. To mention few; at the early stage of loading a shear lagging between the plies were observed, which is

assumed to be due to the difference in stiffness of the plies in the laminate. Moreover, small strain localizations are seen to emerge gradually and spotted in the 90^o plies. Later on, these strain localizations spots are turned to matrix cracks which initiated and grown in the laminate. Most of the matrix cracks are initiated in the most off-axis ply (90^o plies) and the formation crack has a trend where a newly formed crack is observed to appear next to the one emerged prior to it, thus, the newest cracks occur far away from the primary crack. In addition, it is observed that the matrix cracks are oriented where it is directed towards the interlaminar shear stress. The matrix cracks initiated from the 90^o ply propagated towards the neighboring (0^o and $+45^o$) plies. After the matrix crack reached the 0^o ply interface, it hindered from crossing over the interface, rather it grows delaminating the $0^o/90^o$ interface. However, the crack tip that reached the $+45^o$ interface propagated further crossing the $90^o/+45^o$ interface, later, these crack tip grow to delamination in the $-45^o/+45^o$ interface. This phenomenon showed that the relative fiber orientation of neighboring plies has major influence on the growth and propagation of cracks in the laminate. The presence of matrix cracks in the 90^o and $+45^o$ plies affected the integrity of the material structure which induce degradation in stiffness of the laminate.

In the second group of experiment sets, a monotonic quasi-isotropic tension test is performed on laminates with four distinct stacking arrangements. The gradual growth of local strains distribution across the thickness of the laminate is captured with the help of a DIC at high magnification. Variation in failure stress and elastic modulus (E) is observed for the distinct groups of laminates. The arrangement of plies in the laminate has influence on the axial, transverse, shear strain distribution and the damage formation, in the individual plies and at the interfaces between the plies.

Regarding the progressive damage growth, the matrix cracking is observed in the 90^o plies for all group laminates, however, the rate at which crack emerged and the quantity of the cracks are seen to be affected by the relative position of plies. On the other hand, high interlaminar shear strain localizations are observed at the $+45^o/-45^o$ interface in all laminates and at the $0^o/90^o$ interfaces for some of the laminates. Despite of the shear strain localization, delamination is occurred at the interface where the matrix cracks reached for (-45/+45/90/0)s and (0/-45/+45/90)s laminates. This is unexpected outcome as delamination is presumed to be as a result of the interlaminar shear localized at the free-edge, instead, it was initiated due to the presence of matrix crack. In general, the deformation trend of plies and the loading scenario are not as simplified by the basic assumption of CLPT, rather it is much complex phenomenon. Further, the relative arrangement of plies has major influence on the load sustained by the individual plies, thus changing the arrangement of plies directly affect the entire process of gradual damage formation.

In the third group of the study, there are two groups of experiments performed. The first group is uni-directional laminate with different fiber angle, from this set of tests it was found that the maximum in-plane shear and Poisson's ratio (over the width plane (XY)) is obtained for the 15^o laminate. However, for the thickness plane (XZ), the smallest Poisson's ratio is obtained for the 15^o laminate. The second group experiment is performed on the multi-directional laminates, where it is found that a higher transverse strain is observed for the 30^o laminate and the lowest is recorded for the 15^o laminate for the thickness plane (XZ). Whereas, the highest interlaminar shear strain is found in the 15^o laminate, the lowest is depicted in the 30^o and 45^o laminates.

From the damage evolution, matrix cracking is common in all different laminates, however delamination occurred only in two laminates (laminates with 30^o and 45^o plies) where the interlaminar shear is relatively lower. Out of these two laminates, the delamination occurred earlier in the laminate where the transverse interlaminar strain is negative and much higher. This scenario showed how the delamination is dominated by neither the transverse strain/stress nor the interlaminar shear; rather it is guided by the presence of stress concentration created due to the tip of a matrix crack. This observation challenges the postulates made based on the approximate solutions provided by earlier works, where the approximate solutions have found that the transverse stress at the free edge is much smaller compared to the interlaminar shear stress. Thus, it was suggested that the failure at the free-edge is dominated by the interlaminar shear failure.

In the last group of the study, the local residual strain accumulated at the free-edge of a composite coupon is analyzed at the different stage of fatigue cycles. The progressive growth of damages within the quasi-isotropic laminate is captured along with degradation in modulus of elasticity at different fatigue cycles using a high magnification optical digital image correlation (DIC) technique. In parallel to the damage growth, the change in thermal conductivity of the laminate is measured. The corresponding influence of damage types (matrix cracking and delamination) on the degradation of modulus of elasticity and thermal conductivity is emphasized. It is found that, matrix cracking and delamination has an almost the same effect on the degradation of the elastic modulus. On the other hand, the thermal conductivity is observed to deteriorate at higher rates during delamination than matrix cracking stages. In sum up, both properties have shown a similarity in degradation trend, an appreciable explicit correlation between the properties is obtained.

6.2 RECOMMENDATIONS

After the conclusion of this study and obtained such significant findings, there are further works that must be performed to completely understand the free-edge effect. Thus, the author would like give recommendation on the work that should extend from this study in the future. As is mentioned in this work, the 2D-DIC technique applied provide only the full-filled displacement and strain on the given surface. However, the damage that initiated from the free-edge is seen to propagate in to the laminate width. This growth of damage is a 3D phenomenon which is difficult to capture the full sense of damage propagation using the 2D-DIC setup. Therefore, it is necessary to upgrade the 2D-DIC setup to Digital Volume Correlation (DVC).

In order to use DVC, the 3D volumetric images must be acquired using X-ray Computed Tomography system (X-ray CT) or Magnetic Resonance Imaging (MRI) systems. These imaging techniques allow to evaluate the deformations across the different layers of the laminate in a volumetric scale. The changes in material contrast due to voids, fibers or defect can be used in the place of randomly patterned speckles. Further, it is discovered that the stress singularity from the free-edge phase-out as it goes in to the laminate width, and this phenomenon was not justified by the 2D-DIC and this volumetric technique can be used to clarify and evaluate the volumetric strain across the width.

In addition to the DVC, acoustic emission technique can used to describe the 3D damage progress within the laminate. This technique might not give precise and clear picture of the gradual damage progress, nevertheless, it helps to capture the general sense of damage growth.

APPENDIX A: COPYRIGHT RELEASE LETTERS

1. CHAPTER-1: GRADUAL DAMAGE EVOLUTION AND PROPAGATION IN QUASI-ISOTROPIC CFRC UNDER QUASI-STATIC LOADING

6/11/2018 RightsLink® by Copyright Clearance Center

Copyright Clearance Center RightsLink®

Home | Create Account | Help

Title: Gradual damage evolution and propagation in quasi-isotropic CFRC under quasi-static loading

Author: Addis Tessema,Suraj Ravindran,Addis Kidane

Publication: Composite Structures

Publisher: Elsevier

Date: 1 February 2018

LOGIN

If you're a copyright.com user, you can login to RightsLink using your copyright.com credentials.

Already a RightsLink user or want to learn more?

Please note that, as the author of this Elsevier article, you retain the right to include it in a thesis or dissertation, provided it is not published commercially. Permission is not required, but please ensure that you reference the journal as the original source. For more information on this and on your other retained rights, please visit: https://www.elsevier.com/about/our-business/policies/copyright#Author-rights

BACK | CLOSE WINDOW

https://s100.copyright.com/AppDispatchServlet#formTop 1/1

2. CHAPTER-5: EXPERIMENTAL STUDY OF RESIDUAL PLASTIC STRAIN AND DAMAGES DEVELOPMENT IN CARBON FIBER COMPOSITE

RE: Copyright release

Tony Deraco <aderaco@destechpub.com>
Fri 2/15/2019 3:31 PM
To: TESSEMA, ADDIS T <atessema@email.sc.edu>
Dear Addis Tessem:

We grant you permission to use the material you requested for your dissertation and ask that you list credit with the paper used from the Proceedings. The wording should include:

This article appeared in the *Proceedings of the American Society for Composites: Thirty-first Technical Conference*, 2016. Lancaster, PA: DEStech Publications, Inc.

Best Regards,

Anthony A. Deraco
President
DEStech Publications, Inc.
439 North Duke Street
Lancaster, PA 17602-4967
Toll Free: 877-500-4337
Tel: 717-290-1660
Fax: 717-509-6100
E-Mail: aderaco@destechpub.com
Website: www.destechpub.com

From: TESSEMA, ADDIS T [mailto:atessema@email.sc.edu]
Sent: Friday, February 15, 2019 1:27 PM
To: info <info@destechpub.com>
Subject: Copyright release

Dear Sir/Madam

My name is Addis Tessema, I have published a paper on the ASC proceeding of the 31st Technical conference on Composite material under the title of **"Experimental Investigation on the Correlation between Damage and Thermal Conductivity of CFRP".** Now I am planning to include that paper on my dissertation as a chapter and I need your copyright permission. Can you help me with allowing me to use the material as a part of my dissertation? or Can you help me how I can get permission from the publishers?

Regards,
Addis Tessem